PYRIMIDINE NUCLEOTIDE DE NOVO BIOSYNTHESIS

AS A MODEL OF METABOLIC CONTROL

A Dissertation

by

MAURICIO RODRIGUEZ RODRIGUEZ

Submitted to the Office of Graduate Studies of
Texas A&M University
in partial fulfillment of the requirements for the degree of

DOCTOR OF PHILOSOPHY

August 2005

Major Subject: Biochemistry

PYRIMIDINE NUCLEOTIDE DE NOVO BIOSYNTHESIS

AS A MODEL OF METABOLIC CONTROL

A Dissertation

by

MAURICIO RODRIGUEZ RODRIGUEZ

Submitted to the Office of Graduate Studies of
Texas A&M University
in partial fulfillment of the requirements for the degree of

DOCTOR OF PHILOSOPHY

Approved by:

Chair of Committee,	James R. Wild
Committee Members,	Theresa Good
	Michael Manson
	C. Nick Pace
	Melinda E. Wales
Head of Department,	Gregory Reinhart

August 2005

Major Subject: Biochemistry

ABSTRACT

Pyrimidine Nucleotide de novo Biosynthesis as a Model

of Metabolic Control. (August 2005)

Mauricio Rodríguez Rodríguez, B.S., Pontificia Universidad Javeriana

Chair of Advisory Committee: Dr. James R. Wild

This manuscript presents a thorough investigation and description of metabolic control dynamics in vivo and in silico using as a model de novo pyrimidine biosynthesis. Metabolic networks have been studied intensely for decades, helping develop a detailed understanding of the way cells carry out their biosynthetic and catabolic functions. Biochemical reactions have been defined, pathway structures have been proposed, networks of genetic control have been examined, and mechanisms of enzymatic activity and regulation have been elucidated. In parallel with these types of traditional biochemical analysis, there has been increasing interest in engineering cellular metabolism for commercial and medical applications. Several different mathematical approaches have been developed to model biochemical pathways by combining stoichiometric and/or kinetic information with probabilistic analysis, or deciphering the comparative logic of metabolic networks using genomic-derived data. However, most of the research performed to date has relied on theoretical analyses and non-dynamic physiological states. The studies described in this dissertation provide a unique effort toward combining mathematical analysis with dynamic transition experimental data. Most importantly these studies emphasize the significance of providing a quantitative

framework for understanding metabolic control. The pathway of de novo biosynthesis of pyrimidines in *Escherichia coli* provides an ideal model for the study of metabolic control, as there is extensive documentation available on each gene and enzyme involved as well as on their corresponding mechanisms of regulation. Biochemical flux through the pathway was analyzed under dynamic conditions using middle-exponential growth and steady state cultures. The fluctuations of the biochemical pathway intermediates and end products transitions were quantified in response to physiological perturbation. Different growth rates allowed the comparison of rapid versus long-term equilibrium shifts in metabolic adaptation. Finally, monitoring enzymatic activity levels during metabolic transitions provided insight into the interaction of genetic and biochemical mechanisms of regulation. Thus, it was possible to construct a robust mathematical model that faithfully represented, with a remarkable predictability, the nature of the metabolic response to specific environmental perturbations. These studies constitute a significant contribution to the fields of quantitative biochemistry and metabolic control, which can be extended to other cellular processes as well as different organisms.

DEDICATION

To my family.

ACKNOWLEDGMENTS

These studies have been partially funded by a fellowship from the Fulbright Commission, in association with The Colombian Institute for the Advancement of Science and Technology - Colciencias, the Institute of International Education and the United States Information Agency.

Additional support has also been granted from the National Science Foundation and the Robert A. Welch Foundation.

Most importantly, each member of the Advisory Committee has greatly contributed to the success of this research. Drs. Melinda Wales, Theresa Good, Nicholas Pace, Michael Manson and James Wild have participated with teachings, advice, information, ideas and helpful discussions that have enriched the significance and quality of my education.

TABLE OF CONTENTS

Page

CHAPTER

LIST OF FIGURES

Page

Page

Page

LIST OF TABLES

Page

CHAPTER I

INTRODUCTION

METABOLISM AND ITS CONTROL

A complete understanding of cellular metabolism requires, in addition to a description of its architecture, a thorough analysis of the inherent network of biochemical signals and genetic mechanisms controlling it. The physiological responses of the cell associated with changes in environmental conditions are far from simple and understanding them is of exceptional importance for the advancement of basic science as well as in medical and biotechnological applications.

The current paradigm of metabolic control describes cellular homeostasis as a state of intracellular equilibrium in which the macromolecular machinery thrives in a chaotic world that continually opposes its need for equilibrium. According to this view, the whole organization of the cell, structural and functional, is intended to maintain the cell's internal environment in equilibrium. In fact, cellular metabolism teaches us that living organisms are dynamic systems in constant flow and readjustment.

This dissertation follows the style of Journal of Bacteriology.

As an organism progresses through its life cycle, metabolism balances both provision and consumption of the energy it needs to function. As such, metabolism is the collective name for all the chemical reactions, both anabolic and catabolic, carried out inside and on the surface of a cell, coupling the exergonic oxidation of nutrients with the endergonic transformation and biosynthetic processes needed for life. Metabolic balance is thus managed by an extremely intricate and efficient (often overlapping) system of regulatory controls. In practice, the different mechanisms of metabolic control can be generally grouped as genetic and biochemical. Although most of these mechanisms are present throughout the evolutionary scale, the scope of this manuscript will be limited to the description of those in prokaryotic organisms.

Genetic Mechanisms of Control

The term genetic is applied in this context to distinguish those cellular responses acting at the level of gene expression; these responses are typically transcriptional controls that regulate the activity of certain genes. In the case of prokaryotes, this type of control is largely applied through functionally distinct groups of genes called operons, in which polycistronic sequences can be jointly regulated. If multiple operons are regulated by the same mechanism they are described as a regulon, or a modulon if grouping seemingly unrelated operons. These different levels of regulation ensure the coordinated interplay of related cellular functions. The actual mechanisms involve the control of expression of genes through their promoters and adjacent sequences. Gene expression promoters are,

in certain cases, responsive to the concentration of certain metabolites inside the cell via cis-acting DNA control elements that bind trans-acting regulatory proteins. The regulatory proteins binding DNA operators can act either as activators or as repressors of gene expression and their activity can be modulated by the concentration of effector metabolites (54). A different strategy of metabolic regulation at the transcriptional level affects not initiation but elongation and termination steps. It was thought initially that once the transcription complex left the promoter region it could continue uninterrupted until it reached the termination structures, but specific regions along the DNA have been identified that serve as sites of transcriptional pausing and premature termination. In such cases, mechanisms of attenuation and antitermination act to bring about metabolic regulation (26).

Enzymatic Mechanisms of Metabolic Control

Transcriptional level control provides a relatively slow metabolic response to environmental changes, as there can be a lag as genes are turned on or induced and enzyme levels are adjusted. This lag can be even more dramatic in the case of repression as levels of already present proteins drop. A more immediate response is achieved by controlling the flux through active biochemical reactions. These additional responses are not redundant or energetically inefficient mechanisms as they are, in fact, complementary signals that help fine-tune the cellular response to rapid perturbations in the external milieu. There are three recognized mechanisms of fine-tuning the metabolic

response at the enzyme level: allosteric regulation, covalent modification and substrate cycles. Allosteric regulation involves the conformational change of key enzymes in a pathway that bring about variation in the catalytic activity and, therefore, overall metabolic flux. The key enzyme is usually the first step unique to a specific pathway and its activity can be feedback-inhibited by one or more of the end products of that pathway. Allosteric effectors can also act as activators of enzymatic activity, although these are typically not metabolites of the same pathway, but rather products of a parallel or dependent pathway that can signal the need for more product of the activated pathway. Covalent modification of proteins can also affect metabolism by controlling the activities of a wide variety of enzymes in the cell (54). Although covalent modification includes phosphorylation, uridylylation and adenylylation, protein phosphorylation is probably the most frequent posttranslational control mechanism and acts as a more global mechanism of regulation. Substrate cycling is important in enzymes with low activity coefficients such as allosteric enzymes and it serves to bypass the thermodynamically unfavorable reverse reaction and diminish the flow through a pathway.

PYRIMIDINE BIOSYNTHESIS AS A MODEL TO STUDY METABOLIC CONTROL

De novo pyrimidine nucleotide metabolism is a central component of all free-living cells, occupying an essential position relative to metabolic processes involved in the macromolecular synthesis of nucleic acids. Pyrimidine nucleotide biosynthesis is typically initiated de novo in a ubiquitous biosynthetic pathway that is managed through a complex system of regulatory signals. The pivotal position of this pathway requires that it be carefully regulated to provide for maintenance of the stable, intracellular nucleotide pools necessary for cell survival. In the *Enterobacteriaceae*, this regulatory network involves genetic, allosteric, and physiological control systems that need to be integrated into a coordinated set of metabolic checks and balances. Over the years a repertoire of mechanisms that can modify flux in this pathway have been discovered. These important discoveries have resulted largely from a reductionism approach and integration of the molecular details of regulation with the complex portrait of cell function has proven challenging. However, over the past ten years both technical and theoretical tools have been developed such that the global picture is emerging. The theoretical framework allows for a mathematical description of each of the individual molecular mechanisms and their potential to contribute to the control of metabolic flux. The new sciences of genomics, proteomics, transcriptomics and metabolomics provide us with the most detailed picture yet of metabolism, identifying complex networks of genes with coordinated regulation. As biology integrates these new technologies, and

moves from the study of one protein in a pathway to the study of networks of proteins, a molecular understanding of how living cells operate as systems is closer than ever before.

Figure 1 illustrates how intricate the network of reactions is which sustains life. All of these reactions occur in a cell that is less that 1 mm in diameter, and each requires an enzyme that is itself the product of a series of information-transfer and protein synthesis reactions. For each metabolite produced there can be multiple enzymes that are required not just for synthesis, but also those that can chemically modify it in a variety of ways. For example, uridine-5′-triphosphate (UTP) is produced in *Escherichia coli* by the sequential reaction of eight independent enzymatic steps. Once produced it serves as a substrate for RNA polymerase, responsible for the RNA synthesis essential for cell growth. However, UTP can also be aminated in an ATP requiring reaction to yield cytidine-5′-triphosphate (CTP), dephosphorylated to uridine-5′-diphosphate (UDP) and reduced to 2′-deoxyuridine-5′-triphosphate (dUTP). Similar to these UTP reactions, competitions for thousands of other metabolites are occurring simultaneously. It would be easy to imagine that the network of metabolism is so finely balanced that any perturbation would be disastrous. Yet, the cell is amazingly resilient. Environmental perturbations are countered with responses directed at maintaining homeostasis, and this is achieved by an elaborate network of mechanisms that control and regulate each reaction. In addition to environmental signals, cells respond to internal signals that allow them to evaluate their physiological state and coordinate their biosynthetic capabilities.

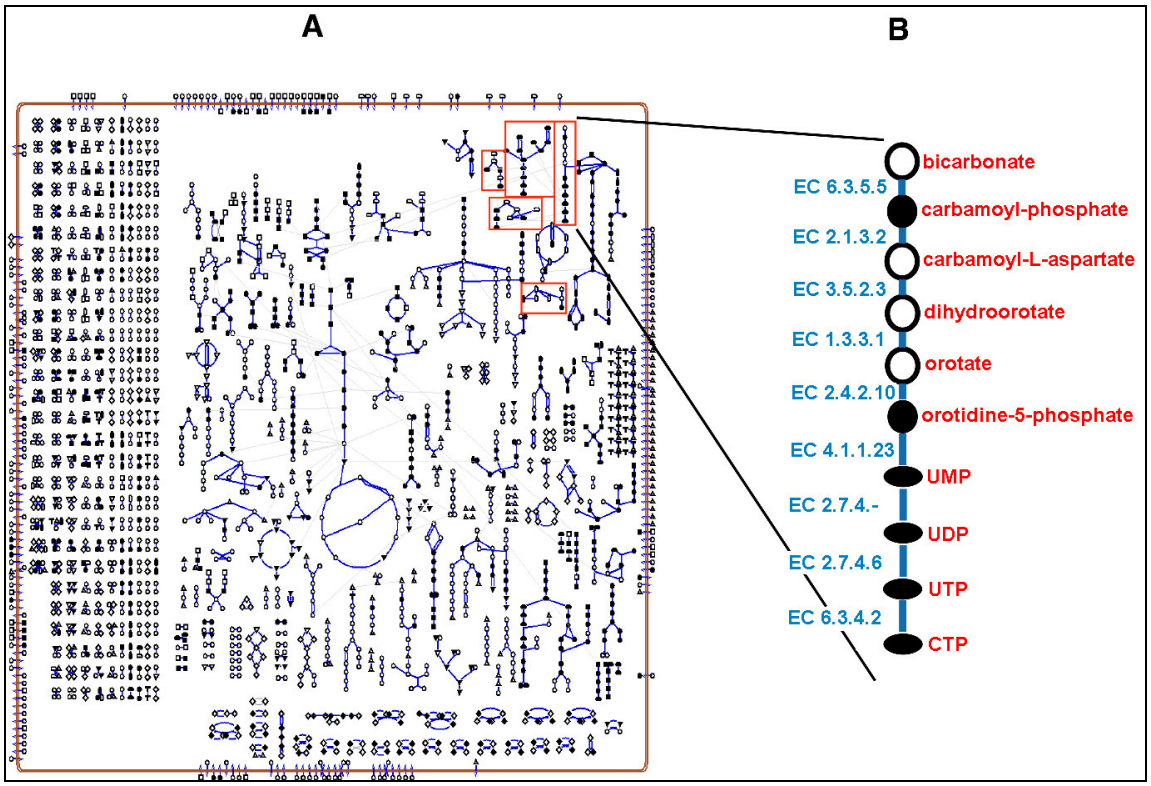

Figure 1. Overview of the biochemical network in *E. coli*. A) Schematic representation of a cell and its metabolic network and pools of metabolites; circles represent metabolites and lines represent reactions; all other symbols represent pools of intracellular metabolites. B) Detail of the pathway of de novo biosynthesis of pyrimidine nucleotides (47).

As pathways of reactions intersect or branch, multiple control points responsive to different metabolites have developed to handle the competing demands. Traditional biology tells us that by regulating a few enzymes at key points in a metabolic network, a cell can effect large-scale changes in its general metabolism. For pyrimidine biosynthesis, this controlling enzyme is aspartate transcarbamoylase, and the de novo pathway is an ideal system for the testing of these traditional regulatory concepts. Although ubiquitous in nature, it has been adapted by the acquisition of a variety of different regulatory controls and pathway organizations. Fifty years of research on the

pathways and enzymes of pyrimidine biosynthesis provide a detail of information essential for the testing the regulatory paradigms.

Overview of Pyrimidine Biosynthesis in *Escherichia coli*

In *Escherichia coli*, de novo pyrimidine biosynthesis starts with the condensation of ammonia or glutamine with bicarbonate in the presence of ATP (Figure 2). This initial reaction of the *de novo* pathway is catalyzed by the enzyme carbamoyl phosphate synthase, CPSase (EC 6.3.5.5) (62). The carbamoyl phosphate produced by this reaction is combined with aspartate in a subsequent reaction catalyzed by aspartate transcarbamoylase (ATCase, EC 2.1.3.2). This reaction marks the first step unique to pyrimidine biosynthesis and, as such, is traditionally considered to be the rate-limiting step for flux through the pathway. This is consistent with its characterization as an allosterically regulated enzyme responsive to the pathway's end products. The amino-acid derivative that is produced, carbamoyl aspartate, is then cyclized by dihydroorotase (DHOase, EC 3.5.2.3) to form dihydroorotate. This cyclic amide is subsequently oxidized to orotate by dihydroorotate dehydrogenase (DHOdeHase, EC 1.3.3.1). The ribose ring from PRPP is transferred to the pyrimidine ring by orotate phosphoribosyltransferase (OPRTase, EC 2.4.2.10). The orotidine-5'-phosphate produced is then decarboxylated by ODCase (EC 4.1.1.23) to form uridine monophosphate (UMP), the end product of the de novo pathway. As seen in Figure 2, this is only the beginning as ultimately the pyrimidine requirement for DNA and RNA

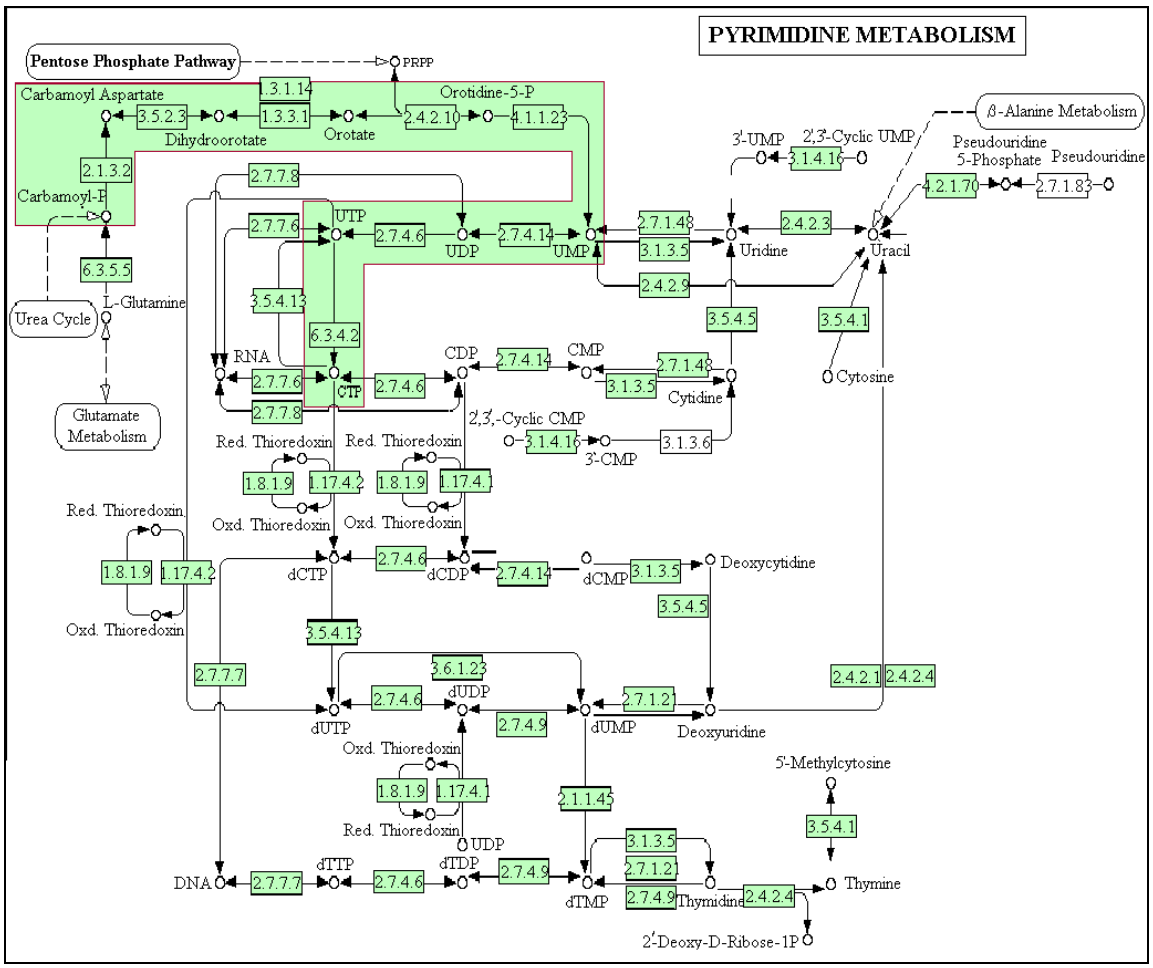

Figure 2. Pyrimidine metabolism. Schematic map of pyrimidine metabolic reactions in *E. coli*. De novo reactions are highlighted. The enzymes are represented by their IUPAC-IUBMB enzyme classification nomenclature (68).

synthesis is fulfilled by interconversion of nucleotides. For this purpose, the UMP is phosphorylated by uridylate kinase (EC 2.7.4.-) and UDP kinase (EC 2.7.4.6) to provide UDP and UTP, which is ultimately converted into CTP by CTP synthetase (EC 6.3.4.2). The formation of the deoxyribonucleotides dUDP and dCDP from the corresponding ribonucleotides is controlled by ribonucleotide reductase (EC 1.17.4.1). Thymidylate synthase (EC 2.1.1.45), another important enzyme of the pyrimidine nucleotide pathway,

catalyzes the conversion of dUMP into dTMP. The deoxynucleoside triphosphates dTTP and dCTP eventually provide the pyrimidine nucleotide substrates for DNA polymerization.

The Network of Regulatory Genetic Interactions

Carbamoyl Phosphate Synthase. The genes and operons encoding for the pyrimidine de novo enzymes are led by sequences responsive to the intracellular concentrations of UTP and CTP as summarized in Table 1.

Table 1. Genetic regulation of metabolic flux through de novo pyrimidine biosynthesis

Gene (Enzyme)	Regulation	Reference
carAB (CPSase)	UTP and CTP	Lu *et al*., 1989 Piérard *et al*., 1976
pyrBI (ATCase)	UTP	Turnbough, 1983
pyrC (DHOase)	CTP	Turnbough, 1993
pyrD (DHOdeHase)	CTP	Wilson and Turnbough, 1990
pyrE (OPRTase)	UTP	Poulsen and Jensen,, 1987
pyrF (ODCase)	UTP	Turnbough *et al*., 1987

Expression of the *carAB* operon, which encodes the two subunits of CPSase, is regulated at two tandem promoters, P1 and P2, by the cumulative repression of the end products of the arginine and pyrimidine biosynthetic pathways. Initiation of transcription of this operon at P1 can be negatively regulated by

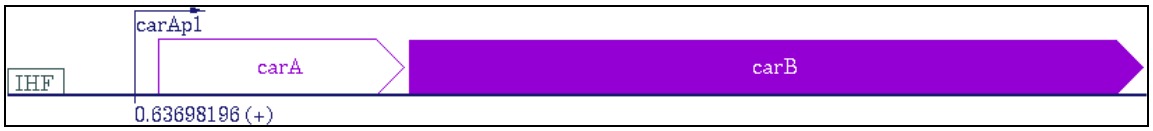

Figure 3. Schematic organization of the *carAB* operon (47).

the intracellular availability of pyrimidine nucleotides (Figure 3). This regulation requires the upstream binding of trans-acting factors CarP and IHF (integration host factor). Binding of these proteins is believed to induce structural modifications (bending) of the DNA and facilitate the recruitment of other regulatory factors (8, 12-14, 71). Another mechanism that appears to act independently from CarP/IHF-mediated regulation involves UTP-sensitive reiterative transcription at the 3'-end of the transcript, due to transcript-template slippage (28). At the P2 promoter, initiation is regulated by ArgR, the arginine repressor. Binding of the hexameric ArgR to the two operator sequences (ARG boxes) flanking the start site for transcription, prevents binding of the transcriptional machinery (8, 71, 104). The regulatory activity of ArgR over the P2 promoter, however, does not appear to affect initiation of transcription at the P1 promoter.

Aspartate Transcarbamoylase. The organization of the *pyrLBI* operon includes two tandem promoters, P1 and P2, followed by an open reading frame that encodes a "leader" polypeptide with 44 amino acids in length (Figure 4). The catalytic chains are

encoded by the *pyrB* gene, while *pyrI* encodes the regulatory chains. Of the two promoters, P_2 has been identified as the physiologically significant promoter (56).

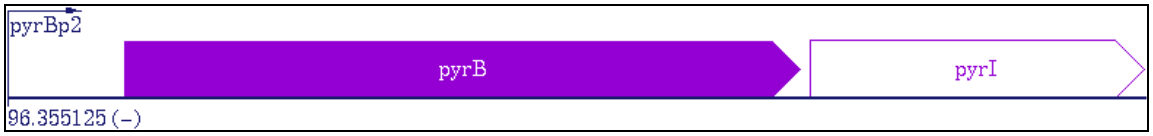

Figure 4. Schematic organization of the *pyrBI* operon (47).

The *pyrLBI* operon is located at 97 minutes on the chromosome map, away from the genes encoding the other six enzymes involved in pyrimidine biosynthesis. The expression of this operon is regulated by the intracellular levels of uridine or cytidine nucleotides. Most of this regulation occurs through an UTP-sensitive attenuation control mechanism (Figure 5). Attenuator-independent mechanisms, including a pyrimidine-sensitive transcriptional initiation mechanism and stringent control by ppGpp, account for a smaller range of regulation (56). Transcriptional termination at the *pyrBI* attenuator (a ρ-independent transcriptional terminator) is regulated by the relative rates of transcription and translation within the *pyrBI* leader region. When intracellular levels of UTP are low, they cause RNA polymerase to pause at the uridine-rich region in the leader transcript, which allows time for the ribosome initiating translation to catch up to the stalled RNA polymerase before it transcribes the attenuator region. As RNA polymerase makes its way through the attenuator, the adjacent translating ribosome blocks formation of the terminator hairpin. This permits RNA polymerase to read through into the *pyrBI* structural genes, with translation terminating before the *pyrB*

initiation codon. At high intracellular levels of UTP, RNA polymerase does not pause during transcription of *pyrL*. Without this pausing, the ribosomes cannot catch up to RNA polymerase before it transcribes the attenuator. This allows formation of the RNA hairpin, thus terminating transcription prior to the structural genes (21).

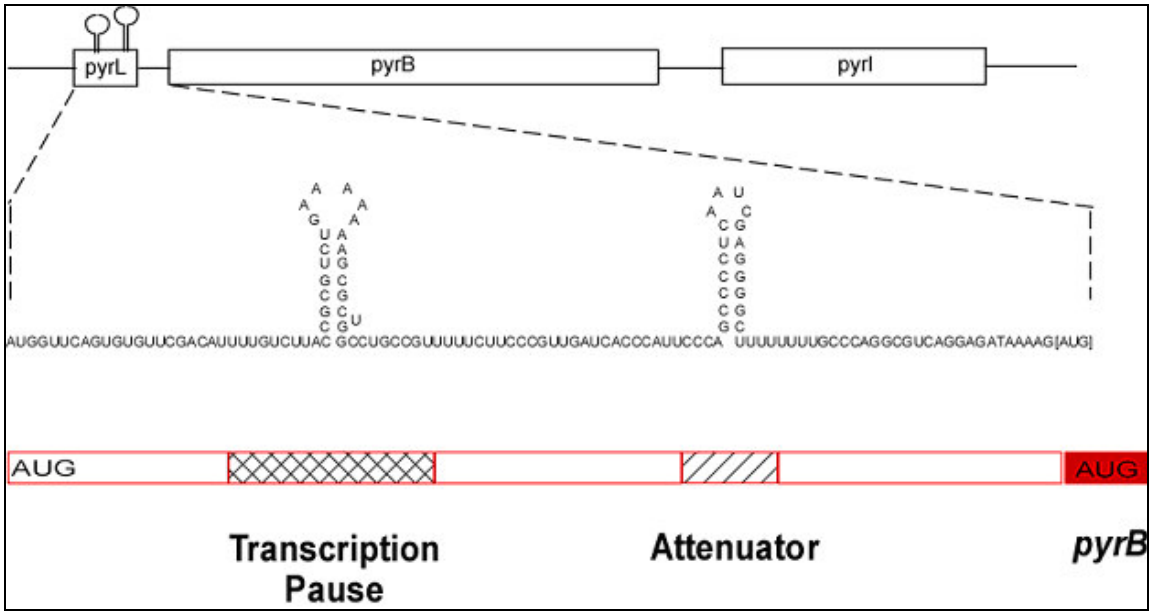

Figure 5. Transcriptional control of *pyrBI* (101).

Dihydroorotase. The transcriptional start site of *pyrC* is located 36 base-pairs upstream of the structural gene. Regulation of the *pyrC* gene of *Escherichia coli* appears to respond coordinately to pyrimidine limitation. The mechanism of regulation of gene expression involves attenuation, as in the case of ATCase. A regulatory region between the promoter and the beginning of the *pyrC* transcriptional initiation region has been shown to form a hairpin at the 5'-end of the transcript. This hairpin structure, which

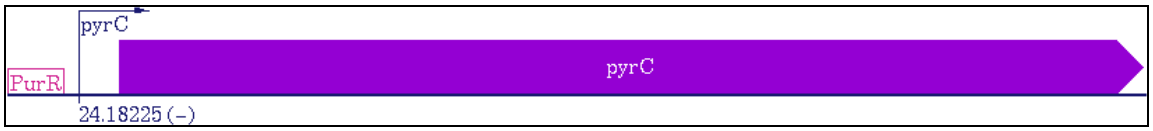

Figure 6. Schematic organization of *pyrC* (47).

overlaps the functional ribosome-binding site SD1 (the Shine-Dalgarno sequence 1), is controlled by a nucleotide-sensitive selection of the transcriptional start site. At high intracellular levels of CTP, transcription starts seven bases downstream of the –10 region and the hairpin is formed. When CTP levels are low and GTP levels are high, transcription is initiated with GTP two bases downstream. This shorter transcript is not able to form the 5'-end hairpin and the gene is translated normally (57, 110). In addition to the attenuation mechanism, it has been suggested that regulation of *pyrC*, *pyrD*, *pyrE*, and *pyrF* involves a common repressor protein; this despite the fact that the genes of the pyrimidine biosynthetic pathway are not closely linked within the chromosome. The purine repressor PurR has been identified as a component of this regulatory system (Figure 6). It binds a control site similar to the pur regulon operator, repressing expression of this gene by two-fold (16, 111).

Dihydroorotate Dehydrogenase. Regulation of gene expression of *pyrD* is, as in the case of *pyrC*, associated with the action of PurR (16). The regulator binds to a site upstream of the promoter and blocks the recruitment of the transcriptional apparatus.

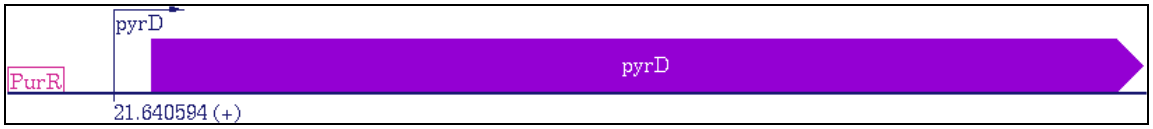

Figure 7. Schematic organization of *pyrD* (47).

This site is located near to the promoters of *pyrD*, as well as *pyrC*, *carAB* and *prsA*, which encodes phosphoribosyl pyrophosphate synthase (EC 2.7.6.1) (9, 111). As mentioned above this site has a sequence similar to the binding site for the purine repressor (Figure 7). Regulation of expression of *pyr* genes is in support of the idea that the coordination of pyrimidine and purine nucleotides synthesis must be appropriately equalized. Other examples of this coordinated regulation are found in the allosteric activation of CPSase by ATP and the GTP-mediated attenuation of *pyrC* and *pyrE*.

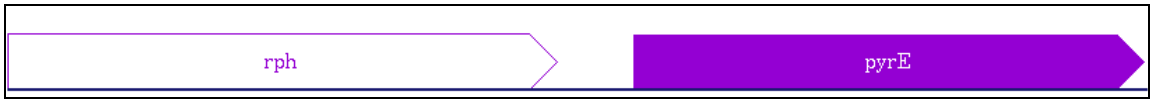

Figure 8. Schematic organization of *pyrE* (47).

Orotate Phosphoribosyl Transferase. Regulation of transcription of the gene encoding OPRTase, *pyrE*, includes an attenuation mechanism in the intercistronic *rph-pyrE* region (Figure 8). The attenuation is modulated by the intracellular levels of UTP and GTP, in the presence of the NusA regulatory protein. *pyrE* is transcribed together with the gene *rph*, which is part of the same operon. Two promoters, P1 and P2 have been located upstream of this operon and appear to initiate transcription at constitutive levels. *rph* encodes Rnase PH, an exonuclease involved in processing of tRNA 3'-ends. When the

UTP pools are low, the dicistronic *rph-pyrE* mRNA is formed and quickly processed into the monocistronic subunits. At high UTP intracellular levels, an attenuator forms at the intercistronic region and transcription is terminated before reaching the *pyrE* open reading frame (3, 4, 7, 73).

Figure 9. Schematic organization of *pyrF* (47).

Orotidine Monophosphate Decarboxylase. The *pyrF* gene, which encodes ODCase, is part of an operon in the chromosome of *Escherichia coli* that includes a downstream *orfF* gene of unknown function (Figure 9). The translational start site of *orfF* and the *pyrF* stop codon overlap, which suggests translational coupling in their expression. Transcriptional control of *pyrF*, as in the other *pyr* genes, is coordinately controlled by intracellular levels of pyrimidine nucleotides. However, analysis of the nucleotide sequence suggests that there is no attenuation mechanism involved (40, 98).

The Network of Biochemical Signaling

Carbamoyl Phosphate Synthase. CPSase (EC 6.3.5.5) synthesizes a common substrate for the arginine and pyrimidine biosynthetic pathways, carbamoyl phosphate (CP). CPSase is a dimeric enzyme composed of two non-identical subunits of 42 and 120 KDa; the small subunit catalyzes the amidotransferase reaction, while the large subunit

catalyzes the phosphorylation reactions (Figure 10). The production of CP begins with hydrolysis of glutamine to produce ammonia and the phosphorylation of bicarbonate with ATP to produce carboxy phosphate. The ammonia is channeled through the interior of the enzyme to a second active site, where it reacts with the carboxy phosphate to

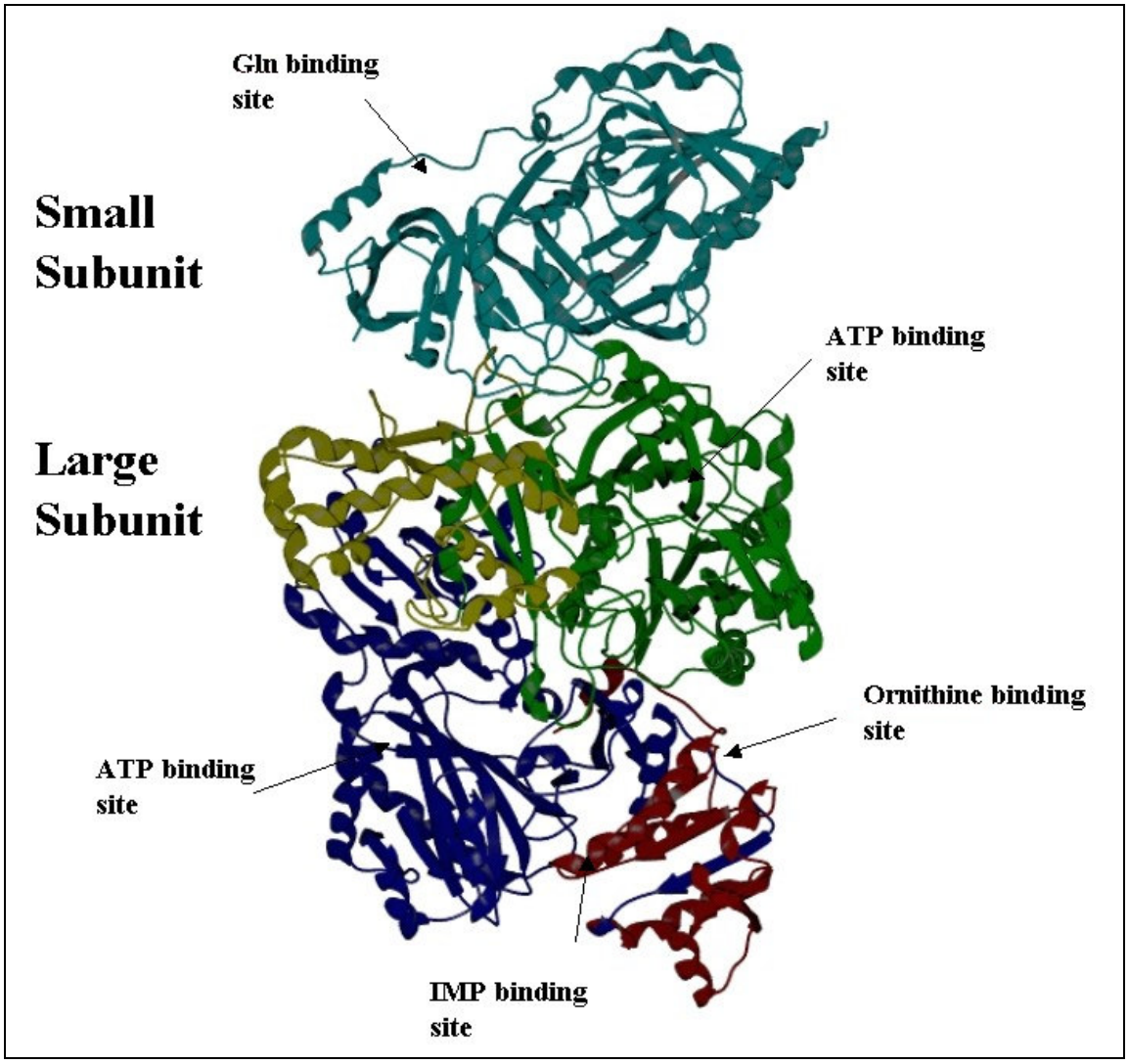

Figure 10. Structure diagram of CPSase (35).

produce the unstable intermediate carbamate. This intermediate is then channeled to the third active site, where it is phosphorylated by the second ATP molecule. The final product is thus formed and released from the enzyme at the opposite end where glutamine entered (77, 96). The small subunit contains the binding site for glutamine, and the large subunit those for bicarbonate and ATP. This subunit is also subjected to allosteric regulation by ornithine and UMP, which act as activator and feedback-inhibitor, respectively. The enzyme is also subject to cumulative repression by arginine and pyrimidine compounds (70, 97).

The combined allosteric and genetic effects provide a complex, but efficient mechanism of controlling the supply of CP for the arginine and pyrimidine pathways. Although the components of these mechanisms of control have been characterized, the details of their interaction remain unclear. Expression of the operon and activity of the enzyme, increase as does the cellular need for pyrimidine nucleotides. UMP inhibition of the enzyme provides a fast cellular response, whereas reiterative transcription and P1-mediated inhibition of expression provide a more resource-efficient, although slower, control.

Aspartate Transcarbamoylase. ATCase (EC 2.1.3.2) is a ubiquitous enzyme of pyrimidine biosynthesis that catalyzes the first step unique to the pyrimidine biosynthetic pathway in *Escherichia coli*. In different organisms, the enzyme exists in different states of oligomerization or as part as multifunctional complexes. The *Escherichia coli* enzyme is structurally complex and relatively large: it contains six catalytic chains, organized in

two trimers, that are associated with six regulatory chains, which are organized as three dimers, $2(c_3):3(r_2)$. Each catalytic chain has a molecular weight of 33,000 KDa, whereas each regulatory chain has a molecular weight of 17,000 KDa.

ATCase exerts significant control over the rate of pyrimidine biosynthesis. This is achieved by modification of the enzymatic activity in response to substrate concentration (homotropic cooperativity) and to the nucleotide end products of both the purine and pyrimidine pathways (heterotropic regulation) (25). In the oligomeric holoenzyme, catalysis proceeds by a preferred order mechanism with carbamoyl phosphate binding before aspartate and N-carbamoyl-L-aspartate leaving before inorganic phosphate. Homotropic cooperativity is induced by aspartate in the presence of a saturating

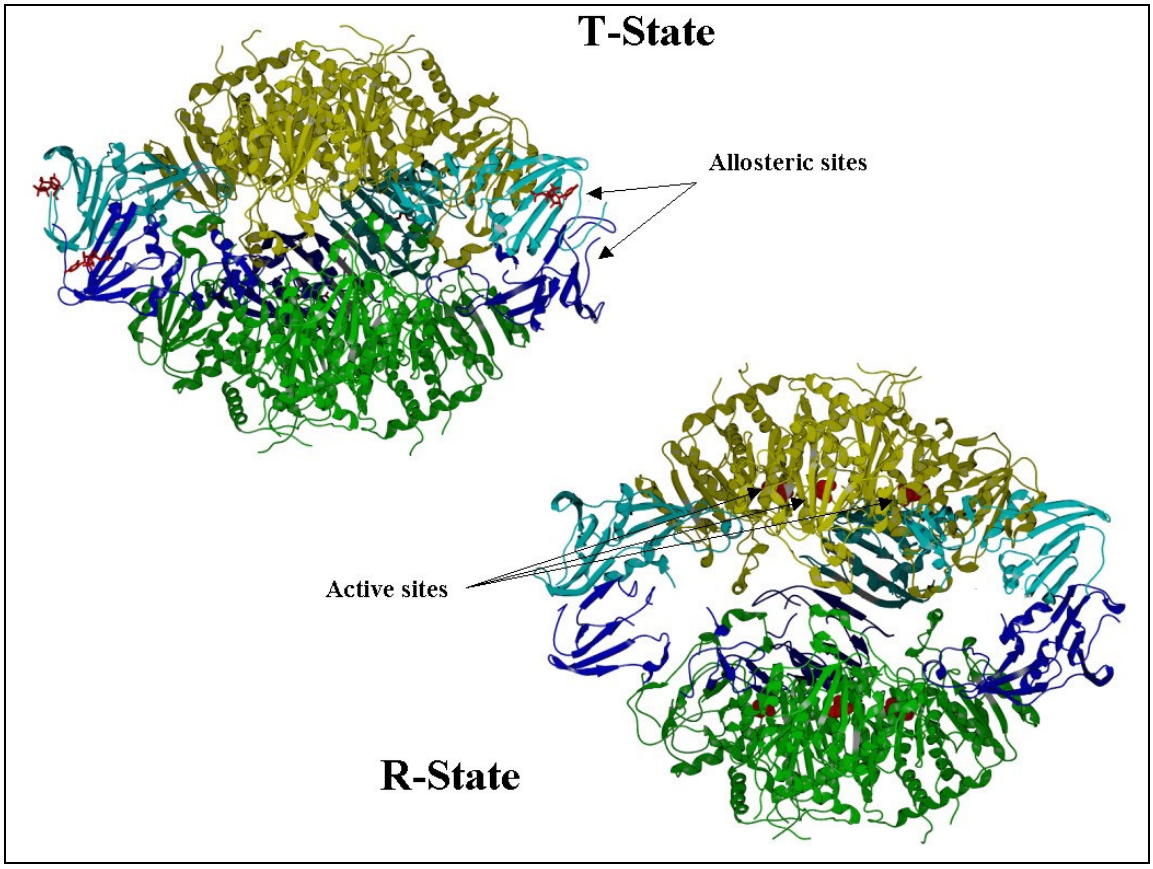

Figure 11. Structure diagram of ATCase (52, 63).

concentration of carbamoyl phosphate and involves a structural transition of the enzyme that is consistent with a two-state, concerted model. As aspartate is bound, the enzyme shifts from the T state (tense), characterized by low catalytic activity and low affinity for substrates, to the R state (relaxed) with high activity and high affinity for substrates (Figure 11). This positive cooperativity is evidenced experimentally when plotting the kinetics on a sigmoidal substrate saturation curve. Heterotropic activation is effected by the purine ATP, while the pyrimidine end products CTP and UTP feedback inhibit the enzyme. The two pyrimidine nucleotides synergistically inhibit ATCase: CTP inhibits

the enzyme's catalytic activity by, approximately, 60% and UTP has minimal effect, whereas acting in combination CTP and UTP inhibit the activity of ATCase by over 95% (Figure 12) (108). CTP, ATP and UTP compete, with different affinities, for binding to a common allosteric site on the regulatory subunits. CTP has the highest binding affinity with a pattern that is consistent with two classes of three sites each whose dissociation constants differ by a factor of 20 ($K_{d\text{-}CTP}$: 5-20 μM). The binding of ATP follows a pattern similar to that of CTP with two classes of affinity sites, except that ATP binding is one order of magnitude weaker than that of CTP ($K_{d\text{-}ATP}$: 60-100 μM). The binding of UTP appears to be limited to three sites ($K_{d\text{-}UTP}$: 800 μM), although there may be a second class of sites that is too weak to be measured. CTP binding to three sites appears to enhance the binding of UTP to the remaining three sites by almost 100-fold, resulting in a predicted K_d for UTP in the presence of CTP of 10 μM (23). These biochemical binding characteristics are explained by the physiological requirements of the pathway: while the intracellular concentration of CTP (500 μM) and UTP (900 μM) are 3 to 6-fold lower than that of ATP (3-5 mM), their stronger binding can effectively displace ATP at the allosteric sites of the enzyme.

Comparison of the crystallographic structures of the enzyme has revealed that each of the catalytic chains is composed of two independently folded structural domains: the carbamoyl phosphate (CP) domain and the aspartate (Asp) domain. The active sites are

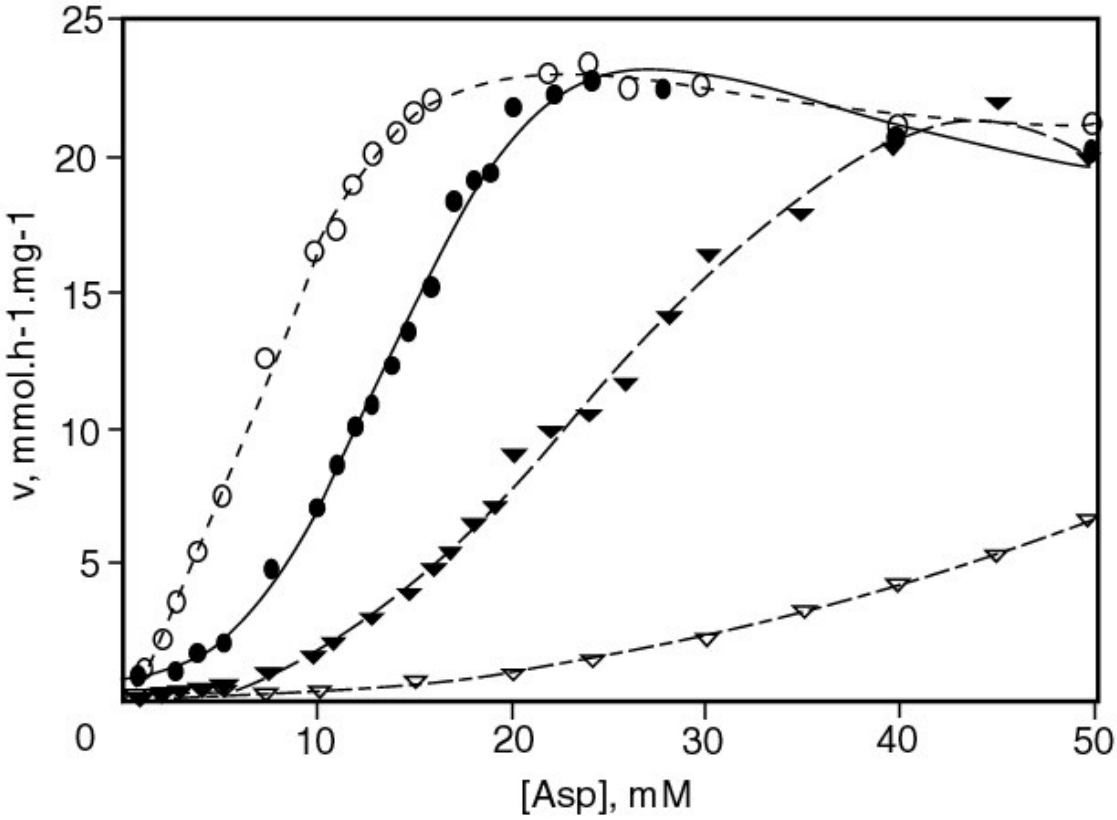

Figure 12. Aspartate saturation curve and allosteric effects of ATCase. No allosteric effectors (black circles), ATP activation (white circles), CTP inhibition (black triangles), and CTP+UTP inhibition (white triangles) (101).

located at the interface between the CP and Asp domains of one catalytic chain and the CP domain of an adjacent catalytic chain. Likewise, the regulatory chains are composed of two structural domains: the zinc-binding (Zn) domain and the allosteric (Allo) domain. Differences between the two states of the enzyme have been identified by comparison of the inhibitor-ligated (CTP) T-state structure and a substrate analogue-ligated (N-(phosphonacetyl)-L-aspartate; PALA) R-state structure (45, 50). The T→R

quaternary transition involves substantial conformational rearrangements as the catalytic trimers separate by 11Å and mutually reorient 10^{o} around the 3-fold axis, while each regulatory dimer rotates 15^{o} around the 2-fold axis. During substrate binding, the two domains of each catalytic chain (Asp and CP) undergo domain closure, while the two domains of the regulatory chain (Allo and Zn) undergo domain separation. Site-directed mutagenesis studies have shown that closure of the CP and Asp domains is important for the formation of the high affinity, high activity R-state, required to attain the proper active site conformation needed for catalysis, and for homotropic cooperativity (42).

Numerous mutational studies, along with the many structural and biochemical analyses, have contributed to our understanding of ATCase by identifying key residues within active site and allosteric sites, as well as important interactions for the stabilization of the T and R states. To clarify the allosteric mechanism, several mutants have been designed to isolate the homotropic from the heterotropic effect, ATP activation from inhibition, and CTP inhibition from the CTP+UTP synergism. Even though there is not yet a complete description of the allosteric mechanism, there is strong evidence that binding of just one ligand to an active site, is sufficient to induce the concerted structural transition from the T to the R state (60).

Dihydroorotase. L-5,6-dihydroorotate amidohydrolase (EC 3.5.2.3) is the enzyme that completes the cyclization of the pyrimidine precursors in the biosynthetic pathway. As mentioned, it is also part of the triad of enzymes that forms the CAD complex in

eukaryotes. In *E. coli*, DHOase catalyzes the dehydration of carbamoyl aspartate to form dihydroorotate.

DHOase is a homodimer with a molecular weight of 38,500 Da. It is an unusual enzyme, in that it catalyzes the synthesis of an amide bond without needing a coupled reaction to drive it. Entropy drives the reaction to the formation of dihydroorotate rather than to the less thermodynamically favorable intermolecular amide bond formation (86, 105). There are no effectors that inhibit the activity of the enzyme, although it has been reported to be sensitive to oxidative modification and trace metal ions. The structural integrity of the active site appears to be stabilized by a single Zn(II) ion. There are two other Zn(II) ions weakly bound to each monomer that are not essential for activity (11, 106).

Dihydroorotate Dehydrogenase. DHOase (EC 1.3.3.1) catalyzes the fourth and only redox sequential reaction in the de novo biosynthesis of pyrimidines, the oxidation of dihydroorotate to orotate. This enzyme is membrane bound and linked with the electron transport system in *Escherichia coli*. It has a molecular mass of 37KDa and contains an FMN (flavin mononucleotide). The overall reaction can be divided mechanistically in two partial reactions. The first reaction involves the transfer of a hydride ion to the FMN group. This is followed by the reoxidation of FMN through electron transfer from FMN to the external electron acceptor. Ubiquinone is believed to be the oxidizing substrate in vivo (43, 69). The recently solved crystal structure of this enzyme reveals that it is a monomer, but in solution can be associated through its N-terminus to behave as a dimer.

DHOdeHase folds into an α/β-barrel with the active site situated on top of the barrel. No inhibitors have been identified to bind the enzyme. The amino terminus of this molecule is responsible for binding to the membrane and channeling of electrons (58, 67).

Orotate Phosphoribosyl Transferase. OPRTase (EC 2.4.2.10) is a protein with a molecular weight of 23 KDa that is responsible for the synthesis of orotidine-5'-monophosphate (OMP), the precursor of UMP in the cell. The enzyme uses the orotate, formed in the previous reaction, and α-D-5-phosphoribosyl-1-pyrophosphate (PRPP), in the presence of divalent cations, to yield OMP and pyrophosphate (PPi). This is the fifth step in pyrimidine biosynthesis. The active form of the enzyme appears to be a homodimer with catalytically important residues available to the neighboring subunit. The reaction mechanism appears to involve a two-step process for the release of PRPP with the participation of a flexible loop at the interface of one of the subunits. The substrates bind to two different sites each per dimer with different affinities. Binding of orotate increases the binding affinity of PRPP to its site by four-fold. After binding, the flexible loop descends to shield the active site. This is followed by a very fast catalytic reaction and a much slower release of the product, that also involves the movement of the solvent-exposed loop (32, 87, 88, 102, 103).

Orotidine Monophosphate Decarboxylase. ODCase (EC 4.1.1.23) catalyzes the last reaction of the de novo pathway of biosynthesis of pyrimidines, the decarboxylation of OMP to UMP and CO_2. ODCase has a molecular weight of 27 KDa and is perhaps the

most proficient enzyme known, enhancing the rate of OMP decarboxylation by a factor of 10^{17} (the uncatalyzed reaction half-time is, approximately, 78 million years). This feat is accomplished without metal ions or cofactors and an estimated dissociation constant of less than 5 x 10^{-24} M (75). The active enzyme is a homodimer with an α/β–barrel structure. The reaction follows a mechanism in which binding of the substrate to the active site is secured by a loop that closes in, similar than OPRTase. This is followed by sequential proton transfer and decarboxylation steps that are facilitated by several charged residues in the active site (30, 31).

To summarize, there are two distinguishable, although interrelated, levels of regulation of pyrimidine biosynthesis. At the gene level, transcription is coordinately controlled by the intracellular levels of pyrimidine nucleotides, uridine for *pyrBI*, *pyrE* and *pyrF* and cytidine for *pyrC* and *pyrD*, and purine nucleotides in the cases of *pyrC* and *pyrE*. The mechanisms of control are related to promoter-induction and attenuation. At the enzymatic level, two enzymes CPSase and, the first committed step enzyme, ATCase respond to intracellular levels of allosteric effectors, again both purine and pyrimidine nucleotides. The subtleties in the coordination of these mechanisms ensure the efficient balance in the production of those molecules that are used mostly as the precursors of nucleic acids.

LIQUID CULTIVATION OF CELLS IN A CONTINUOUS FLOW SYSTEM

Description of the characteristics of liquid cultivation of cells must begin with making mention of the fact that liquid bacterial cultures are highly heterogeneous and any measurement simply serves to monitor average values in the population. Indeed, although individual cells may be genetically identical to one another, there exist variation in the physiological state, age, size and metabolic characteristics. Realization of this limitation is important for the design of a culture system that minimizes heterogeneity; a goal that can be successfully achieved with the careful optimization of continuous flow growth conditions.

Continuous cultivation of cells in a chemostat aims at obtaining a steady state that is achieved by a constant supply of fresh medium, which is added at the same rate as used media and cells are harvested (Figure 13). The term steady state in this case refers to a constant biomass and nutrient concentration inside the culture vessel. Steady state thus

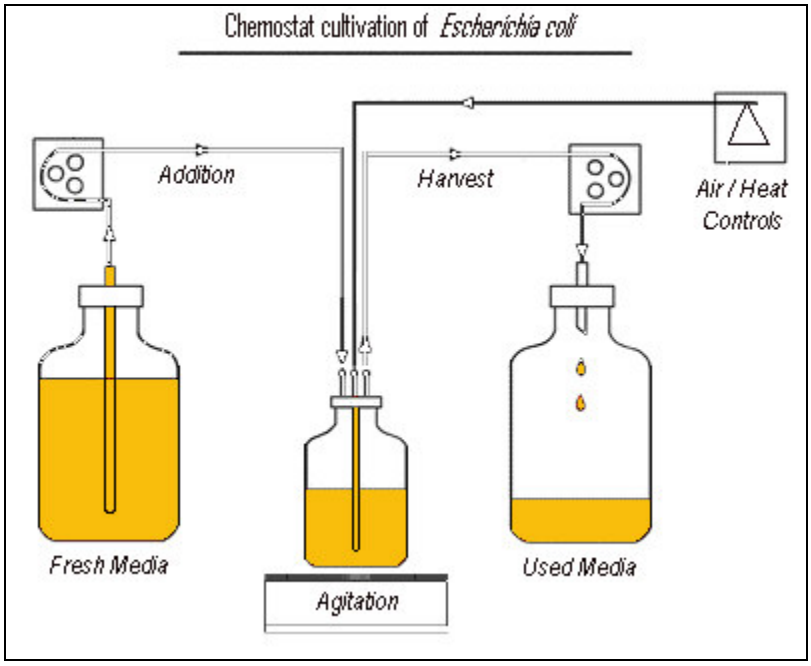

Figure 13. Chemostat cultivation of *Escherichia coli*.

allows continuous exponential growth in which a well-mixed sample taken will be representative of the population. Under steady state growth conditions this population can be defined as:

Cells added to the system	-	Cells removed from the system	+	Cells formed through growth	-	Cells consumed through death	=	Cells accumulated within the system

This can be expressed mathematically as:

Equation 1

$$\frac{FX_0}{V} - \frac{FX}{V} + \mu X - \alpha X = \frac{dX}{dt}$$

where F is the flow-rate of medium, V is the culture volume inside the vessel, X_0 and X represent the biomass in the feed and fermentor respectively, μ is the growth rate and α the death rate.

Under steady state conditions, the rate of change in biomass $dX/dt = 0$, $\alpha << \mu$, therefore the death rate can be ignored. Also $X_0=0$ in a sterile medium feed, so the equation can be rearranged to define the growth rate in terms of the dilution rate, D:

Equation 2

$$\mu = \frac{F}{V} = D$$

Steady State Growth and Perturbation

The ultimate function of a bacterial cell is the formation of new cells. This statement could very well summarize most of what is known about the life cycle of a prokaryotic organism. Irrespective of its fundamental importance in studying and understanding physiology and metabolism, less effort has been put into the objective characterization of the life cycle of a bacterium than its manipulation for research or commercial purposes. Most of the book chapters and journal articles dedicated to describing bacterial growth do so by relating the physical characteristics observed under specific culture conditions. However, it cannot be said that the description of bacterial growth as the series of phases defined for a batch culture are representative of the physiological stages of the life cycle

of the organism. In fact, microorganisms in nature grow under mixtures of nutrients and other environmental variables and are constantly adapting their physiological and metabolic apparatuses. There are several research groups that have focused their effort on uncovering the mechanisms and signal transduction governing cell cycle in bacteria; most of these groups are analyzing the segregation of the bacterial chromosome and are fueled by the availability of extensive genomic data (94).

Cellular growth in bacteria is defined by the accumulation of cell mass and it proceeds in an uninterrupted fashion, from one cell division to the next, at the same rate throughout the cell cycle. Two events mark the cell cycle, DNA replication and the septation process. DNA replication appears to proceed at a rate not directly proportional to growth and it cannot be assigned to a discrete stage in the cell cycle (as is the case in eukaryotes) (66); strikingly, recent reports suggest the existence of an apparatus of chromosome localization similar to that responsible for mitosis (72). Concomitant with the process of chromosome replication and segregation is that of septation. Cell division in *E. coli* requires the invagination of the cell envelope in a process that involves the formation of a ring across the mid-cell region by a group of proteins, some of which have been identified, although the nature of the signals that trigger this mechanism are not clear. The timing of the synthetic activities of the cell leading to cell division are dependent on the rate of growth of the cell, while the final objective of the metabolic response remains that of providing the resources (energetic and structural) to ensure

replication of the genetic material and cell elongation; the processes that lead to cell division.

The metabolic burden of a cell engaged in replication and division can vary with the nutritional and environmental conditions. Under conditions of nutritional deprivation, cells will see this burden increase in the form of a greater energy demand. This energetic demand can be momentarily satisfied at the expense of the adenylate energy charge (AEC) of the cell (defined by the ratio of intracellular concentrations of ATP, ADP and AMP) (66). However this ratio will need to recover promptly or else drive the cell to a state of senscence. How promptly the energy charge ratio can recover will depend on the rate or growth of the cell. The energy demand from a nutritional shift can also be satisfied by increased NADH oxidation in the respiratory chain. NADH is mostly produced by the tricarboxylic acid (TCA) cycle. The cell can respond to higher energy demand by induction of the regulon controlled by global transcription factors, notably cAMP-CRP, which control key enzymes in the TCA cycle. An interesting study on this metabolic adaptation of *E. coli* to environmental perturbation has been recently published (33, 107). An additional signaling mechanism, that of the ppGpp alarmone, together with ATP and GTP, may contribute to regulation of the ribosome concentration to meet biosynthetic demands (41).

Accordingly, during steady state growth the metabolic response can be evaluated according to two types of limitations, biomass accumulation or energy source demand.

In a glucose-limited chemostat, at low dilution rates (<0.3 h^{-1}), the glucose is mostly utilized as a cell-mass precursor; at higher dilution rates (>0.3 h^{-1}), nutrient utilization shifts to satisfy the energy limitation with the consequent decrease in the rate of production of ATP (therefore smaller AEC ratio). This shift also appears to increase flux through the pentose phosphate pathway and reduced TCA cycle flux and NADH turnover (44). Limitations in the respiratory NADH turnover and associated generation of ATP through oxidative phosphorylation can cause reorganization of the catabolic flux distribution to meet anabolic demands (27).

Continuous cultivation of cells in a chemostat does not describe, however, the dynamic response to famine and feast the cells endure in natural conditions. Although single-substrate limited growth is also not the natural state of most cells, experiments done in glucose-limited chemostats represent an approximation to the cellular response to nutrient availability.

MATHEMATICAL MODELING OF METABOLISM

Modeling Enzyme Kinetics

Progress of a reaction showing typical Michaelis-Menten kinetics can be simulated solving the relevant differential equation (Equation 3)

Equation 3

$$\frac{d[A]}{dt} = -\frac{V_{\max}[A]_0}{K_m + [A]_0}$$

To simulate the decrease in substrate concentration in this type of reaction, one needs to formulate the appropriate equation, describe the relevant steady state kinetic parameters (V_{max} and K_M) and initial substrate concentration and solve. Figure 14 depicts the time-dependence of substrate consumption and product formation of one such reaction. Metabolic pathways typically comprise more complicated enzymatic behaviors and numerical analysis and simulation are far more challenging.

For these studies, the powerful differential equation solver of *Mathematica* (Wolfram Research Inc.) NDSolve was chosen to find the solutions of the equations (113). Even though it is relatively straightforward to formulate sets of simultaneous first-order ordinary non-linear differential equations, the large number of parameters that need to be assigned makes it time-consuming and error-prone to manually perform the numerical calculations. NDSolve is the program *Mathematica* uses to numerically solve arrays of simultaneous differential equations. The power of NDSolve comes from its use of diverse multi-step integration methods, that is, NDSolve finds successive points on a curve with iterations of evaluation of the slope for every solution (64).

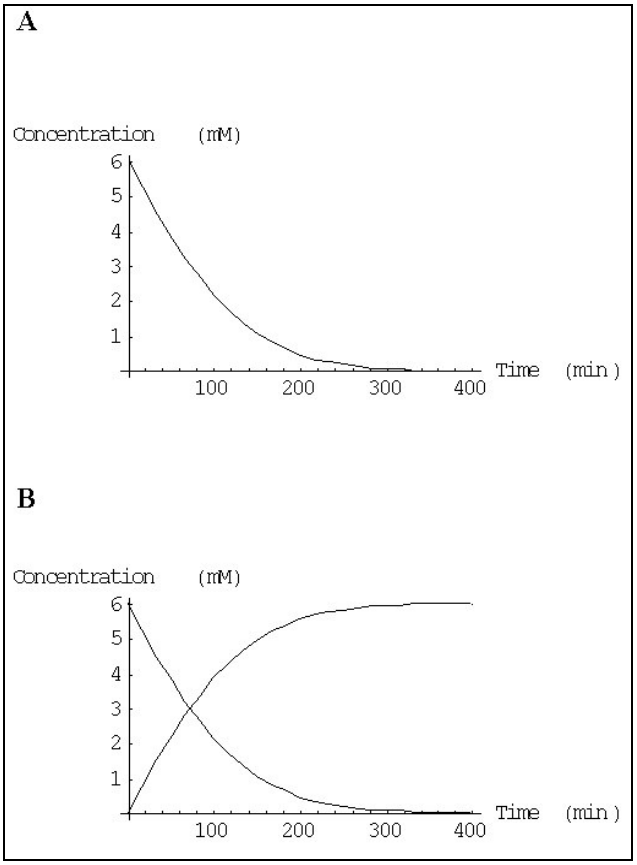

Figure 14. Time-dependent simulation of a typical enzyme-catalyzed reaction. For this simulation it was assumed Michaelis-Menten kinetics of an enzyme with *Vmax* = 80 µmol/L, K_M = 4 mM and an initial substrate concentration of 6 mM. Decrease in substrate concentration alone (A) or compared to product formation (B).

Parameter Estimation

Parameters for the development of a model can be taken from experimental observations data or the available literature produced by other research laboratories. However, for most modeling efforts there are additional kinetic constants and intracellular concentrations that have to be estimated. Often kinetic constants are determined under different experimental conditions and it is best to estimate them. For example, in the

present studies the V_{max} parameter for a number of reactions was estimated from reliable turnover numbers, taking the limit of the rate equation of the reaction of interest when the substrate (or substrates) concentration tends to infinity, assuming the concentration of product to be zero. The K_M value can then be calculated taking the limit of the rate equation as well for the value of the substrate that is half the V_{max}, assuming a product concentration to be zero.

It is necessary to emphasize that modeling cellular systems is an extremely complex task. Often it is found that real metabolic networks have a large number of parameters relative to the available experimental data. An attempt to precisely estimate all the parameters in a metabolic pathway, would involve tracing every independent variable over a large number of individual perturbation experiments. It is obvious that we do not currently possess the techniques to achieve this for most metabolic networks. Therefore, other values need to be estimated by adjusting them to maximize the correlation between the mathematical simulation and the experimental data.

Several of the parameters used in the model presented here were chosen from values that maximized the probability of the data; this is formally called maximum likelihood estimation. In these studies the FindMinimum program of Mathematica™ was used to find local minima of functions defining the sums of squares of nucleotide concentrations. FindMinimum uses several methods of optimization such as Newton, Quasi-Newton, Levenberg-Marquadt, Gradient and Conjugate Gradient (6, 15, 114). In general, the

method of least squares was used to find the vector values (φ) that led to the best simulation of the available experimental data (*d*), that is, $\max_{\varphi} p(\varphi|d)$, where *p* is the probability. For instance, if we have a data set *d* of *n* reaction rates v_i, that are associated with a defined substrate concentration a_i, then we can use $v_i = v(a_i, \varphi)$ to describe our data. If we assume that each estimate has an a normal, or Gaussian, error distribution and variance σ^2_i, then the maximum probability of reaching a reaction rate v_i with our estimated parameter is

Equation 4

$$x^2 = \sum_{i=1}^{N} \frac{(v_i - v(a_{i,\varphi}))^2}{\sigma^2{}_i}$$

The modeling presented in these studies is composed of arrays of simultaneous nonlinear differential equations and, therefore, parameter estimation is very difficult. The relatively large number of parameters makes the optimization process very slow and labor intensive.

Modeling of de novo Pyrimidine Biosynthesis

Modeling of biological systems becomes necessary when looking toward a comprehensive image of cellular physiology. If one wants to manipulate the cellular environment without conducting the research to unintended results, it is necessary to establish quantitative logical relationships that describe the control of cellular

metabolism. Fortunately, the tools that have now become widely used to organize the available biological knowledge also allow us to approach this goal. In silico models of carbohydrate and amino acids metabolism have been the focus of several research groups over the past decade and a concerted effort has been initiated to extend this research to a full mathematical description of the *E. coli* bacterium (34).

Synthesis of nucleotides constitutes an elemental component of the central metabolic processes of living organisms and, as such, pyrimidine de novo biosynthesis presents an invaluable opportunity to understanding metabolic control. As noted earlier, there exist vast amounts of information related to the control of expression of the *pyr* operons, as well as for the structure and biochemical regulation of the two allosteric enzymes involved in this pathway. It is clear that a mathematical model of the metabolic flux through a biosynthetic pathway must be integrated with the experimental data. This type of modeling faces several challenges: the growth conditions have to be stabilized and made reproducible; control from allosteric and genetic components have to be quantified; and intermediate metabolites and end-products must be measured. In addition, the dynamic behavior must be defined and validated to allow for the monitoring of the mass transfer. This is the approach used to build the mathematical model of de novo pyrimidine biosynthesis presented in this dissertation.

To solve the experimental challenges, chemostats were used for the growth of *E. coli* in culture, readily allowing the manipulation of the activity of the de novo pathway. The

chemostat constitutes a reliable culture system, allowing for the evaluation of the pathway's dynamics by enabling flux measurements at the required time intervals. Validation of the dynamic behavior then came from quantification of enzymes, metabolites and products. Each of these variables was monitored and analyzed relative to the rates of each of the reactions over several generations and upon perturbations of the pathway's equilibrium. In particular, the effort was concentrated on the regulation of the two rate-controlling enzymes of this pathway: CPSase and ATCase.

After sufficient quantitative data was obtained, it was possible to begin integrating all the information into a coherent mathematical model. For the de novo pyrimidine pathway, a series of ordinary differential equations were selected to describe the kinetic behavior of the enzymes. In the case of the first two allosterically controlled enzymes that initiate de novo pyrimidine biosynthesis, additional parameters had to be included to simulate the changes in activity induced by the allosteric effectors and substrate cooperativity. In *E. coli*, the individual kinetics of the enzymatic activities has been thoroughly studied, so the challenge resided in trying to numerically reflect the multiple and, in most cases, not fully understood interactions between the different enzymes, their dynamic substrate concentrations, cofactors and effectors. The process of building a mathematical model of the allosteric control of de novo pyrimidine biosynthesis in the model organism *Escherichia coli* has been described elsewhere (82), and is explained in chapter II. This construction was based on an extensive body of research performed in Dr. James R. Wild's laboratory as well as that published by others. The model was

developed to study the effects of repression/derepression of pyrimidine biosynthesis as controlled by exogenously supplied uracil. As opposed to standard kinetic models, this treatment considers temporal variations in nutrient uptake and in concentration of allosteric effectors. The addition of uracil as an environmental variable and parameterization of the model yielded an optimal kinetic response. Even though the model initially proposed is sufficient to approximate the allosteric responses in the de novo pyrimidine pathway, much of the control relies on the transcriptional control of the *pyr* regulon. A second-generation model was formulated that included this genetic information as well as data on metabolic dynamics following perturbation at different growth rates. The expanded version of the model was then capable of accurately simulating the contributions of both types of metabolic regulation. The model thus formulated demonstrated the significant contribution of allosteric control to the rapid physiological response as well as the more gradual contribution of transcriptional control to the adaptation of the cell to external stimuli and environmental changes. Comparison of the output of these simulations with the values obtained experimentally helped establish the validity of the model. The results show consistency between the two approaches, making the predictive value of the model highly promising.

CHAPTER II

MODELING THE DYNAMICS OF ALLOSTERIC REGULATION *

OVERVIEW

With the emergence of multifaceted bioinformatics-derived data, it is becoming possible to merge biochemical and physiological information to develop a new level of understanding of the metabolic complexity of the cell. The biosynthetic pathway of de novo pyrimidine nucleotide metabolism is an essential capability of all free-living cells, and it occupies a pivotal position relative to metabolic processes that are involved in the macromolecular synthesis of DNA, RNA and proteins, as well as energy production and cell division. This regulatory network in all enteric bacteria involves genetic, allosteric, and physiological control systems that need to be integrated into a coordinated set of metabolic checks and balances. Allosterically regulated pathways constitute an exciting and challenging biosynthetic system to be approached from a mathematical perspective. However, to date, a mathematical model quantifying the contribution of allostery in controlling the dynamics of metabolic pathways has not been proposed. In this study, a

* Reprinted from Journal of Theoretical Biology, 234, Mauricio Rodríguez, Theresa A. Good, Melinda E. Wales, Jean P. Hua, James R. Wild, Modeling allosteric regulation of de novo pyrimidine biosynthesis in *Escherichia coli*, 299-310, Copyright (2005), with permission from Elsevier.

direct, rigorous mathematical model of the de novo biosynthesis of pyrimidine nucleotides is presented. We corroborate the simulations with experimental data available in the literature and validate it with derepression experiments done in our laboratory. The model is able to faithfully represent the dynamic changes in the intracellular nucleotide pools that occur during metabolic transitions of the de novo pyrimidine biosynthetic pathway and represents a step forward in understanding the role of allosteric regulation in metabolic control.

INTRODUCTION

The bacterium *Escherichia coli* is the most thoroughly studied prokaryotic microorganism from a biochemical and genetic point of view, due primarily to its relative ease of manipulation in the laboratory and its extensively documented genetic and physiological organization. The amount of information and experimental data available on this enteric bacterium has made it the choice of a recently created alliance for cellular simulation, the International *E. coli* Alliance (34). The ultimate objective of this project is to create a virtual simulation of its cellular and molecular functions. This simulation will be comprehensive and capable of defining accurate responses to external manipulation in a way that reflects the in vivo metabolic functions and behavior of the living cell.

The functionally integrated, virtual *E. coli* is being constructed by combining currently available data with new directed research that is designed to augment accurate model building. Compilation and integration of several decades of molecular data is a monumental task in which this information has to be merged with that of genomics, transcriptomics and proteomics through step-wise mathematical simulations. The importance of simulating systemic metabolomics at the cellular level cannot be overstated. Understanding the interactions of all the cellular components will facilitate and guide future work, bringing a new level of understanding to how molecular life functions are integrated at the cellular level.

From the early work analyzing sensitivity coefficients within a pathway (90) to the more recent efforts to deal with the data pouring in from the *E. coli* genome sequencing project (1, 78, 79, 92), a growing need to integrate diverse experimental observations has resulted in the application of modeling as a powerful tool in the study of metabolic processes. Research has focused on cellular mechanisms of control such as the study of DNA replication (29), regulation of transcription (10, 20) and chemotaxis (95). Specific approaches have been applied to some metabolic pathways, as is the case of a model of attenuation in the tryptophan biosynthetic pathway (49) and the *lac* operon (99). While many of the metabolic modeling efforts with *E. coli* have been focused on improving conditions for a desired commercial application (2, 51, 53), more basic research has been performed on the metabolic pathways of different organisms (24, 76, 89). These and

other works have contributed greatly towards a general understanding of the regulatory mechanisms of cellular networks and its applications. However, to our knowledge, there is no body of literature specifically dedicated to analyzing *E. coli* metabolism from a pure description of the mechanisms controlling networks in a wild-type environment.

It is important to understand the detailed contribution and coordination of the diverse mechanisms controlling metabolic pathways. De novo nucleotide metabolism synthesizes purines and pyrimidines, the building blocks of nucleic acid polymers, which constitute a fundamental component of the central metabolic processes of all living organisms. In *E. coli*, de novo pyrimidine synthesis begins with the condensation of ammonia or glutamine with bicarbonate and ends in the formation of UMP, UTP, CTP, dCTP and dTTP. Aspartate transcarbamoylase (ATCase, EC 2.1.3.2) and carbamoyl phosphate synthetase (CPSase, EC 6.3.5.5) are considered the key allosterically regulated enzymes controlling metabolic flux through the pathway. CPSase is feedback-inhibited by UMP and activated by ornithine, and ATCase, in turn, is inhibited by UTP and CTP and activated by the purine nucleotide ATP (101). The CPSase product, carbamoyl phosphate (CP), is shared by both the arginine and the pyrimidine biosynthetic pathways, establishing ATCase as the first step unique to pyrimidine de novo biosynthesis and its primary regulatory control.

To undertake the integration of a mathematical model of the de novo pyrimidine biosynthetic pathway, a system of coupled ordinary differential equations was formulated to describe the kinetic behavior of each of the enzymic reactions in the pathway. In the case of the allosterically controlled enzymes that initiate de novo pyrimidine biosynthesis, kinetic parameters were included to simulate the changes in activity induced by the allosteric effectors. In addition, the differential equations describing the biosynthesis of the first two enzymes in the pathway need to contain expressions for the decrease in enzyme synthesis in the presence of elevated pyrimidine nucleotide concentrations. As appropriate, the kinetic parameters for the model and the form of kinetic expressions for individual enzymes in the pathway were optimized from an extensive body of research in our laboratory and that published by others. In this chapter, an initial mathematical model of the regulation of de novo pyrimidine biosynthesis in *E. coli* is described. Underlying is the significant contribution that allosteric control puts into the rapid physiological adaptation of the cell to external stimuli and environmental changes.

Enzyme Kinetics

As more genomes are sequenced, it becomes apparent that living systems are characterized not only by the complement of genes they carry but also by the mechanisms of control conducted at the molecular level. The most important intracellular molecules that are regulated include enzymes, intracellular substrate pools,

allosteric ligand effectors, cofactors and, ultimately, the metabolic products. The ability of molecular systems to regulate the complex interactions among these molecules constitutes the basis of cellular homeostasis. The kinetics of the reactions catalyzed by enzymes becomes the standard by which cellular metabolic systems have to reach and maintain metabolic steady states.

Several parameters need to be considered when analyzing enzyme kinetics: (1) the rate or maximum velocity of the reaction ($v_{\max}$) an enzyme can reach when it is saturated with substrate; (2) the Michaelis constant (K_M) or its equivalent ($S_{0.5}$) that equals the substrate concentration at which the rate of the reaction is half the $v_{\max}$; and (3) the turnover number (k_{cat}) or number of substrate molecules converted to products per second.

There are a variety of kinetic mechanisms, both homotropic and heterotropic, by which enzyme activities can be regulated. Substrates can affect the rate of a reaction by cooperative interaction at the active site of an enzyme (homotropic effects), as can reaction products and other small molecules when present in adequate concentrations. In contrast, heterotropic effectors can change the kinetics by interaction at allosteric sites distinct from the active site. Under physiological conditions, substrate concentrations near their K_M facilitate the rapid adjustments of reaction rates. In some cases, there are mechanisms of homotropic cooperativity in which the affinity of interdependent catalytic sites is altered after a substrate molecule binds. Allosteric effectors, on the other

hand, are present in a wide range of concentrations in the cell and they are readily available to bind to allosteric sites, causing structural rearrangements of the enzymes that may be transmitted as altered conformations of the active sites (80). Intracellular concentrations of allosteric effectors provide an important form of metabolic regulation by providing a system that allows for rapid adjustments in biochemical flux by affecting the activity of one or more enzymes in the pathway.

The rates of individual enzymic reactions have been studied since the 19th century. Initial studies of Adrian Brown, Emil Fischer and others, were followed by the mathematical formulations proposed by Leonor Michaelis and Maud Menten in 1913 (19). The progress of a reaction showing typical hyperbolic first-order substrate saturation kinetics can be simulated by the following differential equation (Equation 5):

Equation 5

$$\frac{d[A]}{dt} = \frac{v_{\max} \times [A]_0}{K_M + [A]_0},$$

where $[A]$ is the substrate concentration, v_{max} and K_M correspond to the limiting rate of the reaction and substrate concentration at half the limiting rate, respectively.

Even though it is relatively straightforward to formulate sets of simultaneous first-order nonlinear differential equations, the large number of parameters that need to be assigned

makes it time-consuming and error-prone to manually perform the calculations. In the studies discussed here, the powerful differential equation solver of Mathematica™ (Wolfram Research Inc.) NDSolve was used. Using NDSolve to simultaneously solve arrays of differential equations through multi-step integration methods, allows for successive points on a curve to be found with iterations of slope evaluation (64).

To simulate the decrease in substrate concentration, an equation describing the relevant steady-state kinetic parameters (v_{max}, K_M) and initial substrate concentration has been formulated. The Michaelis–Menten equation is traditionally used to show the time-dependence of substrate consumption and product formation of one such reaction. The numerical analysis and simulation of metabolic pathways comprising more complicated enzymic behavior is far more challenging.

Previous Studies

A previous study emphasized the role of ATCase in the pyrimidine pathway (36). This genetic and physiological analysis included a deconstruction of the reaction to determine the value of allosteric regulation in controlling intracellular concentrations of NTPs. An interesting experiment was included in the study that assigned the value of allosteric regulation in terms of the evolutionary adaptive advantage. This experiment was done by shifting a mixed culture of cells, with and without allosterically-controlled ATCase,

through cycles of repression/derepression with uracil. The study concluded that allosteric regulation provides an advantage, as the cells harboring ATCase with the allosteric regulation accumulated over those cells with an unregulated version of the enzyme. The study also concluded that the allosteric regulation contributed to the control of NTP pools by buffering the effects of nutritional perturbation. When the cells were expressing plasmids harboring ATCase either with or without allosteric control, the pyrimidine nucleotide pools decreased rapidly followed by a gradual recovery of normal levels. In the case of the allosterically-controlled ATCase, the pyrimidine nucleotides did not drop as low and had a more gradual rate of recovery that in cells expressing ATCase without allosteric control. Allosteric control, therefore, appears to contribute significantly to preserving the cell from reckless disruptions from metabolic homeostasis. These findings encouraged the research presented here.

MATERIALS AND METHODS

Model Development

Mathematically describing each individual enzyme is the necessary first step in the simulation of the flux through a metabolic pathway. The model described here has been developed to study the dynamic transitional effects of repression/derepression of pyrimidine biosynthesis. The de novo biosynthetic pathway, shown in Figure 15, encompasses a series of nine reactions that lead to the production of UTP and CTP.

CPSase (EC 6.3.5.5), ATCase (EC 2.1.3.2), dihydroorotase (DHOase, EC 3.5.2.3), dihydroorotate dehydrogenase (DHOdeHase, EC 1.3.3.1), orotate phosphoribosyl

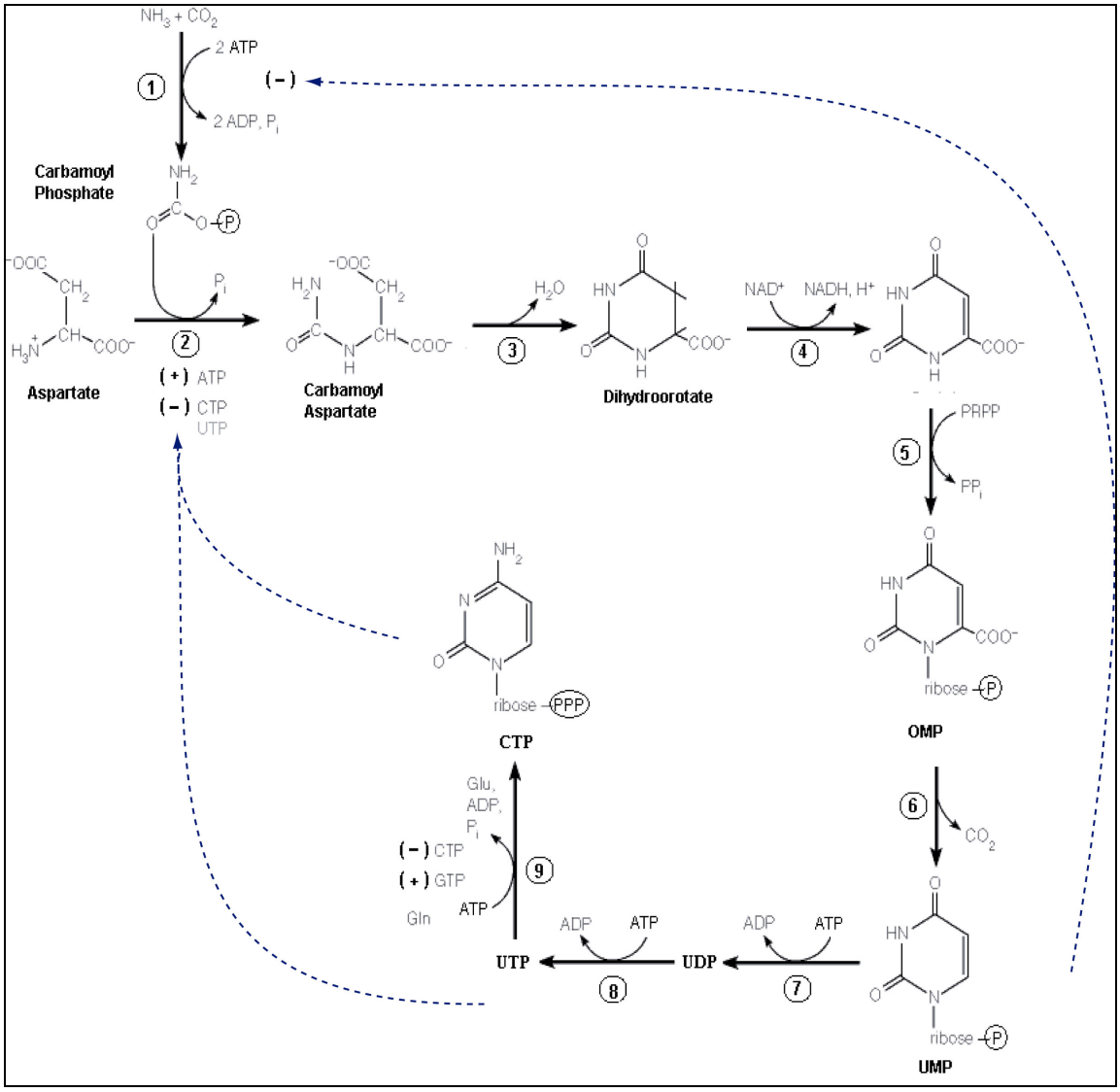

Figure 15. Schematic representation of de novo biosynthesis in *E. coli*. The reactions catalyzed by the pyr enzymes bring about the formation of UMP from aspartate, ammonia/glutamine, bicarbonate ATP and PRPP. Further reactions convert UMP to UTP and CTP. 1, carbamoyl phosphate synthase; 2, aspartate transcarbamoylase; 3, dihydroorotase; 4, dihydroorotate dehydrogenase; 5, orotate phosphoribosyl transferase; 6, orotidine-5′-phosphate decarboxylase; 7, uridylate kinase; 8, nucleoside diphosphate kinase; and 9, CTP synthase. The dashed arrow lines denote specific allosteric effects.

transferase (OPRTase, EC 4.1.1.23), and orotidine-5′-phosphate decarboxylase (ODCase, EC 2.4.2.10), catalyze the formation of UMP. UMP is phosphorylated to UDP by uridylate kinase (UMP kinase, EC 2.7.4.-) and UDP is subsequently transformed into UTP and CTP, through the action of nucleoside-5′-diphosphate kinase (NDKinase, EC 2.7.4.6) and CTP synthase (EC 6.3.4.2).

The definition of the mathematical functions, or rate equations, of the biochemical steps of this pathway must take into consideration the presence or absence of allosteric effects. In the first biochemical step (r_1), the reaction rate for the formation of CP, which is catalyzed by CPSase (E_1), is described by Equation 6. In this equation and all those following, the term v_{maxi} refers to the apparent maximal velocity of the reaction *i.* Eqn. 6 includes terms for the binding of the substrates bicarbonate (K_{bc}, K_{ibc}) and glutamine (K_q) and for the allosteric inhibitory effect exerted by UMP intracellular concentration (K_{iump}) (84):

Equation 6

$$r_1 = \frac{v_{\max 1} E_1 \times bc \times glu}{\left(1 + \frac{ump}{K_{iump}}\right)\left(K_{ibc} \times K_q + K_q \times bc + K_{bc} \times glu + bc \times glu\right)}$$

CP condenses with aspartate in a reaction (r_2) to yield carbamoyl aspartate (CA), as described by

Equation 7

$$r_2 = \frac{v_{\max 2} E_2 + 2cp \times \frac{asp^{nH2}}{K_{i2}^{nH2}}}{\left(\frac{1}{1+\frac{atp}{K_{atp}}}\right)\left(1+\frac{ctp}{K_{ctp}}+\frac{ctp \times utp}{K_{utp}}\right)+\left(\frac{K_{m2}^{nH1}}{cp} \times asp^{nH1} + cp \times \frac{asp^{nH2}}{K_{i2}^{nH2}}\right)}$$

This reaction is catalyzed by ATCase (E_2) and the mathematical expression includes a Hill coefficient (nH_1) that describes the cooperativity between the substrates and a second Hill coefficient (nH_2) for cooperativity under substrate inhibition (55). Additionally, a term for the allosteric effects is included. The rate of formation of CA is favorably affected by ATP, whereas CTP and UTP synergistically inhibit the enzyme.

The rate of change in concentration of CP is then given by the rate of its formation in reaction (1) minus the rate of its depletion in reaction (2), as seen in Equation 8. An analogous expression can be developed for the rate of change of concentration of CA, seen in Equation 9

Equation 8

$$\frac{d[cp]}{dt} = r_1 - r_2$$

Equation 9

$$\frac{d[ca]}{dt} = r_2 - r_3$$

where r_3 is the rate of formation of dihydroorotate from CA

Equation 10

$$r_3 = \frac{v_{\max 3} \times ca}{K_{m3} + ca}$$

Analogous to r_3, the expressions for the remaining steps in the pathway are much simpler, as they do not include cooperativity or heterotropic interactions. Rather, as seen below, they follow simple Michaelis–Menten kinetics

Equation 11

$$\frac{d[dho]}{dt} = \frac{v_{\max 3} \times ca}{K_{m3} + ca} - \frac{v_{\max 4} \times dho}{K_{m4} + dho}$$

where *dho* represents the dihydroorotate formed in the reaction catalyzed by DHOase serving as substrate for the following reaction, catalyzed by DHOdeHase

Equation 12

$$\frac{d[oro]}{dt} = \frac{v_{\max 4} \times dho}{K_{m4} + dho} - \frac{v_{\max 5} \times oro \times prpp}{K_{m5} + oro \times prpp}$$

where *oro* and *prpp* are the substrates of the reaction catalyzed by OPRTase

Equation 13

$$\frac{d[omp]}{dt} = \frac{v_{\max 5} \times oro \times prpp}{K_{m5} + oro \times prpp} - \frac{v_{\max 6} \times omp}{K_{m6} + omp}$$

where *omp* is orotate-5′-phosphate

Equation 14

$$\frac{d[ump]}{dt} = \frac{v_{\max 6} \times omp}{K_{m6} + omp} - \frac{v_{\max 7} \times ump}{K_{m7} + ump} + \frac{v_{\max 9} \times ura \times prpp}{K_{m9} + ura \times prpp}$$

where *ump* is the product yielded by the decarboxylation of *omp* by ODCase; and *ura* represents the external uracil incorporated into the cell from the culture media

Equation 15

$$\frac{d[utp]}{dt} = \frac{v_{\max 7} \times ump}{K_{m7} + ump} - \frac{v_{\max 8} \times utp}{K_{m8} + utp} - \frac{g_{pyr} \times ctp}{K_{Mp} + ctp}$$

Equation 16

$$\frac{d[ctp]}{dt} = \frac{v_{\max 8} \times utp}{K_{m8} + utp} - \frac{g_{pyr} \times ctp}{K_{Mp} + ctp}$$

where g_{pyr} and K_{Mp} are the pyrimidine utilization rate and constant of pyrimidine utilization, respectively. These two terms are based on the assumption that the UTP and CTP produced are part of an intracellular pool that is constantly used to supply metabolic demands. The products *utp* and *ctp* are formed by the action of the enzymes NDKinase and CTP synthase, respectively.

Equation 17

$$\frac{d[ura]}{dt} = -\frac{v_{\max 9} \times ura \times prpp}{K_{m9} + ura \times prpp}$$

In Equation 14, there is a term for the synthesis of *ump* from uracil, when uracil is supplied in the external medium. Since experimental evidence indicates that an *E. coli* culture, upon changing the media from excess to absence of uracil, undergoes a metabolic adjustment that is reflected in the intracellular pools of NTPs, a simple expression for the degradation of the uracil was also included in Equation 17.

In Equations 15 and 16, there are terms for the consumption of UTP and CTP, respectively, as the nucleotides are incorporated into RNA. For both UTP and CTP, it was assumed that the rate of NTPs incorporation into RNA was proportional to the

growth rate of the organism as we assumed growth was limited by some other, external component. In future formulations of the model, the effects that the growth rate has on different NTP pools and the ability of the organism to adapt to different environments will be incorporated.

Since regulation of the pathway depends not only on biochemical regulation, but also on rates of synthesis and degradation of the CPSase and ATCase, expressions for the UTP- and CTP-dependent enzyme synthesis and enzyme degradation were included

Equation 18

$$\frac{d[E_1]}{dt} = \frac{K_{e1}}{(K_{e1} + ump)} - k_{\deg 1} \times E_1$$

Equation 19

$$\frac{d[E_2]}{dt} = \frac{K_{e1} \times 60}{(K_{e2} + ctp + ura)} - k_{\deg 2} \times E_2$$

where K_{e1} and K_{e2} are synthesis coefficients, and k_{deg1} is a degradation coefficient. These terms account for a simplification of additional genetic parameters involved in enzyme synthesis that are not included in this model. Importantly, however, the concentrations of the feedback regulatory molecules are also present in each of the expressions.

A total of 11 reaction rates and equilibrium expressions were formulated as differential expressions and integrated using the NDSolve algorithm (Mathematica™). Initial conditions were estimated, as described above, for steady state conditions with a doubling time of 42 min.

Parameter Estimation

Modeling cellular systems is a complex task and, often, metabolic networks have a large number of parameters in relation to the available experimental data. An attempt to precisely estimate all the parameters in a metabolic pathway involves tracing every independent variable over a large number of individual perturbation experiments. It is obvious that the techniques to achieve this for most metabolic networks are not currently available and, therefore, several parameters had to be computationally estimated. Kinetic parameters and relative enzyme and metabolite concentrations are listed in Table 2. Kinetic constants such as $v_{\max}$ and K_M were estimated from experimental data using standard techniques (6). In brief, an algorithm was developed which minimized the sum of the squares of the residuals between the output of the model (nucleotide concentration) and experimental data at discrete time points. The model consisted of the set of differential equations that describe the dynamics of pyrimidine biosynthesis.

Model input parameters were the set of unknown kinetic constants. The local optimization was performed in Mathematica™ via a built-in function (FindMinimum)

Table 2. List of parameters used in the model. Summary of the parameters used to define the rate equations modeling the allosteric response on pyrimidine de novo biosynthesis in *E. coli*

Parameter	Definition	Value	Reference
Vmax1	v_{max} for carbamoyl phosphate synthetase	0.38 mmol L^{-1}	Calculated from Robin et al. (1989)
Bc	Intracellular concentration of bicarbonate	8 mM	Estimated
Glu	Intracellular concentration of glutamine	4 mM	Calculated from Neidhardt (1987)
Asp	Intracellular concentration of aspartate	4 mM	Calculated from Neidhardt (1987)
Prpp	Intracellular concentration of phosphoribosyl pyrophosphate	0.18 mM	Estimated
Kibc	Bicarbonate inhibition constant	0.75 mol L^{-1}	Estimated
Kiump	UMP inhibition constant	0.98 mol L^{-1}	Estimated
Kbc	K_M for bicarbonate	36 mM	Calculated from Robin et al. (1989)
Kq	K_M for glutamine	22 mM	Calculated from Robin et al. (1989)
Vmax2	v_{max} for aspartate	24 mmol L^{-1}	Calculated from LiCata et al. (1997)
K_M2	K_M for aspartate	19.8 mM	from LiCata et al. (1997)
Katp	ATP binding constant	4.8 mM	Estimated
Kctp	CTP binding constant	4.1 mM	Estmated
Kutp	UTP binding constant	4.9 mM	Estimated
NH1	Hill coefficient	2.3	from LiCata et al. (1997)
Vmax3	v_{max} for dihydroorotase	24.7 mmol L^{-1}	Calculated from Jensen et al. (1984)
K_M3	K_M for dihydroorotase	0.7 mM	Estimated
Vmax4	v_{max} for dihydroorotate dehydrogenase	6.4 mM L^{-1}	Calculated from Jensen et al. (1984)
K_M4	K_M for dihydroorotate dehydrogenase	0.24 mM	Estimated
Vmax5	v_{max} for orotate phosphoribosyl transferase	0.6 mmol L^{-1}	Calculated from Jensen et al. (1984)
K_M5	K_M for orotate phosphoribosyl transferase	9.9 mM	Estimated
Vmax6	v_{max} for OMP decarboxylase	0.8 mmol L^{-1}	Estimated
K_M6	K_M for OMP decarboxylase	32 mM	Estimated
Vmax7	v_{max} for UMP kinase	1.18 mmol L^{-1}	Estimated
K_M7	K_M for UMP kinase	19.8 mM	Estimated
Vmax8	v_{max} for nucleoside diphosphate kinase	0.28 mmol L^{-1}	Estimated
K_M8	K_M for nucleoside diphosphate kinase	8.4 mM	Estimated
Vmax9	v_{max} for uracil phosphoribosyl transferase	2.8 mmol L^{-1}	Estimated
K_M9	K_M for uracil phosphoribosyl transferase	0.08 mM	Estimated
Ki2	Substrate inhibition coefficient for ATCase	2	Estimated
Kdeg1	Degradation coefficient for CPSase	0.12	Estimated
Kdeg2	Degradation coefficient for ATCase	0.072	Estimated
NH2	Second Hill coefficient	2	from LiCata et al. (1997)
grate	Growth rate	42 min^{-1}	Measured
K_Mg	Coefficient for growth rate	396	Estimated
gpyr	Pyrimidine utilization rate	0.4 min^{-1}	Estimated
K_Mp	Constant for pyrimidine utilization	5.8	Estimated
Ke1	Synthesis rate coefficient for CPSase	36	Estimated
Ke2	Synthesis rate coefficient for ATCase	120	Estimated

which employed the following methods: Conjugate Gradient, Gradient, Levenberg-Marquardt, Newton and Quasi-Newton. As the solution was a local optimum, the parameter estimates obtained were dependent upon judicious choice of the initial conditions.

Model Testing and Validation

Whenever possible, individual estimates from the model were compared to available experimental data to validate the mechanistic steps in the model, forms of the mathematical expressions, and estimates of model constants. Several examples of model verification are described. Each of the rate equations was validated by comparison with experimentally obtained kinetic information for each of the enzymes. In this manner, an internal quality control of the model was established and stringent parameterization procedure was followed in the optimization of those kinetic parameters that had to be estimated. The process of optimization is a lengthy and intensive one, as integration of multiple biochemical activities in a series of reactions is considerably less trivial than deriving descriptions of single mechanisms. Added to this complexity was the multiple and overlapping interaction of the mechanisms of regulation. Multiple iteration cycles had to be computationally executed to optimize the parameters described in the model.

RESULTS AND DISCUSSION

Case 1: CPSase

A step-wise validation of the model resulted in confidence that each of the differential equations was appropriately formulated. Validation was obtained by comparing the simulated results with available experimental data. Rate 1, shown in Equation 6, represents the rate of CP synthesis by CPSase in the absence of other enzymes in the pathway. The form of the equation mimics that of Michaelis–Menten but with an inhibition term included to account for the experimentally observed effects of UMP on CPSase activity. Simulation of the inhibitory effect of UMP on CPSase activity was achieved via this mathematical formulation as shown in Figure 16. In the simulation, the reaction reaches saturation at approximately the same glutamine concentration as has been determined experimentally. In addition, the extent of the inhibitory effect is reproduced precisely as previously reported (81).

Case 2: ATCase

ATCase presents a more complex system given the multiple homotropic and heterotropic effects to which it is subjected. Previous studies have agreed on the cooperative behavior

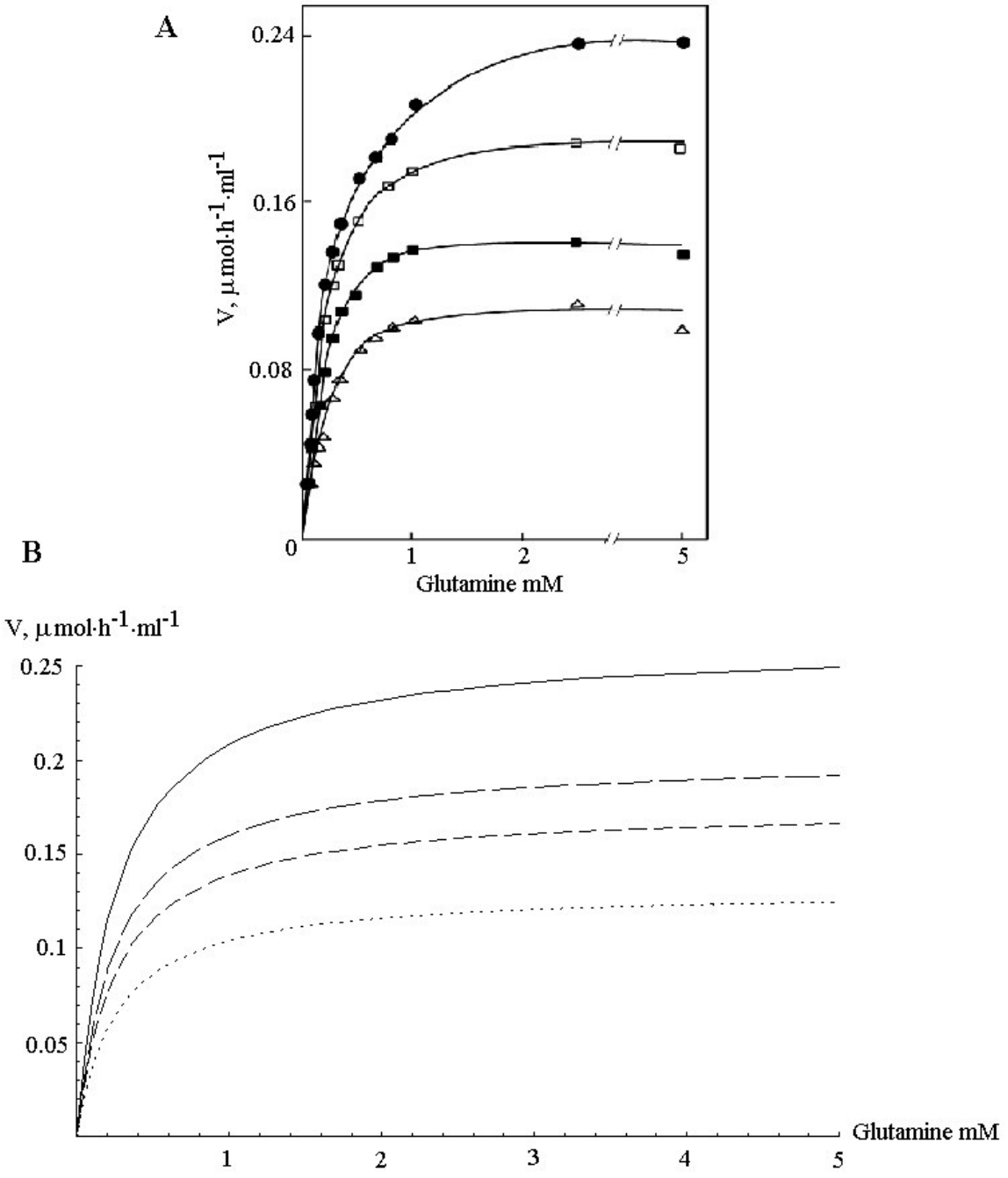

Figure 16. Simulation of CPSase inhibition by UMP vs. experimental data. (A) Data published by (81). No uracil added (●), 15 μg ml^{-1} (□), 25 μg ml^{-1} (■) and 50 μg ml^{-1} (△) of uracil. (B) Simulation of the rate of formation of CP as a function of the concentration of glutamine, both, in the presence of 50 μg ml^{-1} of UMP (····) and its absence (—).

of substrate binding and the extent of allosteric effects induced by ATP, CTP, and UTP acting synergistically with CTP. The mathematical description of the enzymic reaction, rate 2, given in Equation 7 accurately mimics all of these effects, as shown in Figure 17.

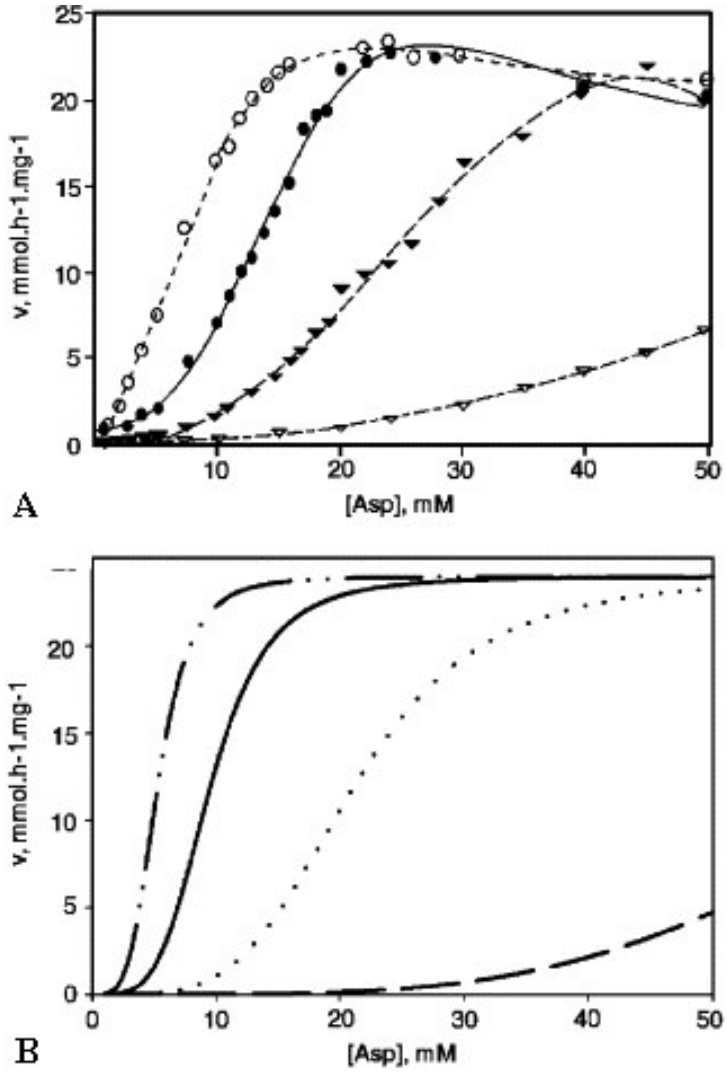

Figure 17. Simulation of ATCase kinetic and allosteric behavior, compared to experimental data. (A) Saturation curves for ATCase unregulated (●) and its response to allosteric effectors: ATP (○), CTP (▼) and CTP+UTP (▽), as previously published (101). (B) Mathematical simulation of the allosteric effects in ATCase: kinetic sigmoidal behavior in the absence of allosteric effectors (—); activation kinetics in the presence of ATP (· – ·); inhibitory effect by CTP (····); or UTP+CTP (– –).

Case 3: Correlation Between CPSase and ATCase Enzyme Levels and Nucleotide Pools

It has been established that the level of the intracellular pools of CTP and UTP correlate with the levels of expression of the *pyr* genes (40); thus, the proposed model should accurately couple CTP and UTP levels with synthesis and degradation rates of the relevant enzymes. As seen in Equations 18 and 19, while the enzyme synthesis rate, the first term in each expression, is reduced in the presence of UMP and CTP, degradation of enzymes remains constant. Figure 18 illustrates the changes in the UMP, CTP and UTP levels in the cell and the accompanying dynamic response of enzymes 1 and 2 (CPSase and ATCase, respectively). These simulations, however, do not include experimental data describing the transcriptional derepression of the *pyr* genes and represent hypothetical descriptions of this type of response. Notably, the simulation of nutritional derepression using the mathematical model coincides qualitatively with the expected onset of enzymatic reactivation.

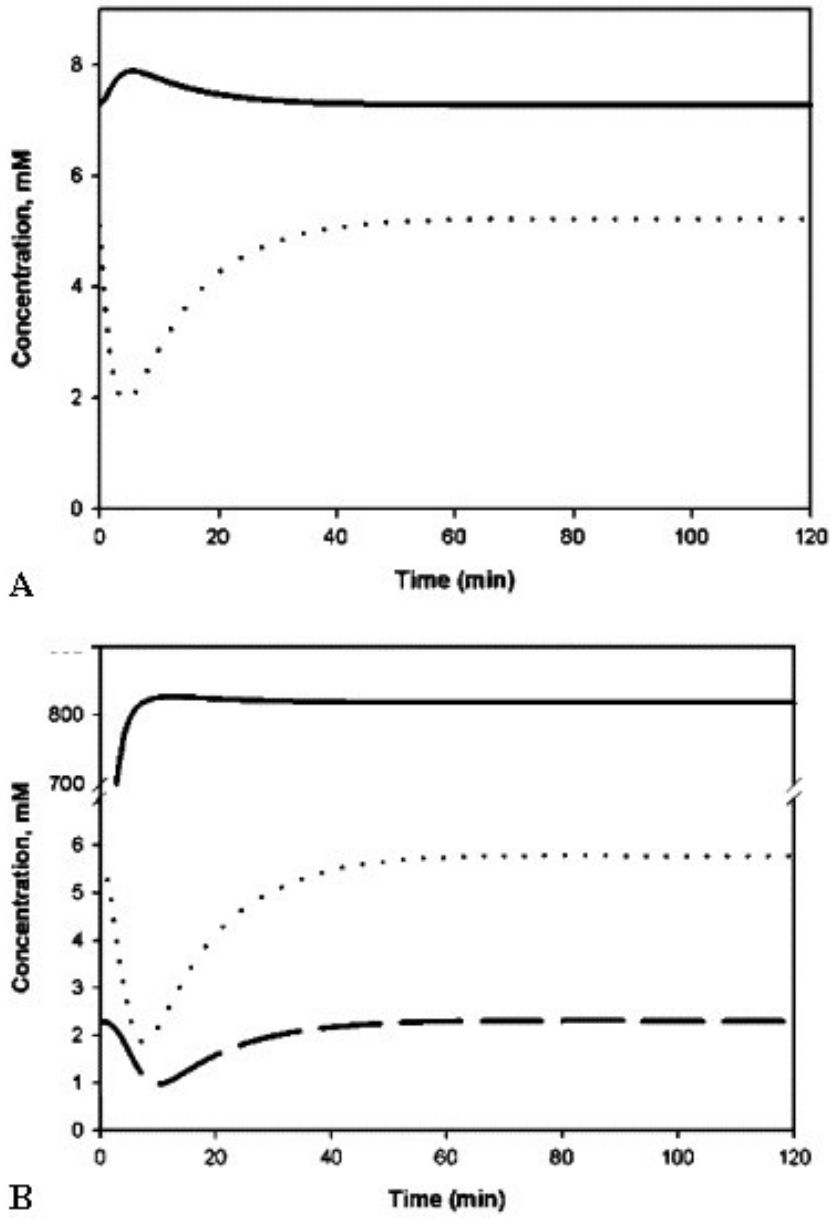

Figure 18. Nucleotide levels change in the cell and the accompanying dynamic response of enzymes 1 and 2 (CPSase and ATCase, respectively). (A) UMP levels in response to derepression (····) and the corresponding response in CPSase levels (—). (B) UTP (····) and CTP (– –) levels and the corresponding overexpression response of ATCase (—) in response to derepression.

Case 4: Responses of CTP and UTP Pools to Nutritional Perturbation

Typically, the transition following nutritional perturbation of the pyrimidine pathway enzymes causes a change in the size of the NTP pools. After the perturbation, CTP and UTP pools drop rapidly due to depletion. CTP levels drop to 66% and 46% of their initial level for the allosterically regulated vs. the unregulated enzyme, respectively. UTP drops to 51% and 30%. As the pyrimidine pathway derepresses, the intracellular concentrations of UTP and CTP recover to their normal levels. Figure 19 shows the dynamic response of the model to an initial high level of uracil that is rapidly consumed. Experimentally, this was achieved by taking repressed cells to a derepressed state by removing the uracil from the medium. Our model satisfactorily simulates the derepression behavior observed under these conditions. In addition, by simply removing the allosteric effect terms in rate 2, a parallel model was created that mimics the behavior of the cell without allosteric control of the second enzyme in the pathway (just catalytic subunits). Comparison of model predictions with and without allosteric terms in the equations qualitatively captures the experimentally observed differences in dynamic response of nucleotide pools in wild-type cells and those with their allosteric subunits deleted. As seen in Figure 19, response of cells deficient in allosteric control is more dramatic compared to those with allosteric control. The complexity of the interrelation of all the equations makes this a finely tuned and sensitive model. Subtle changes in the kinetic parameters are continually being tested and used to predict outcomes of changes in experimental conditions.

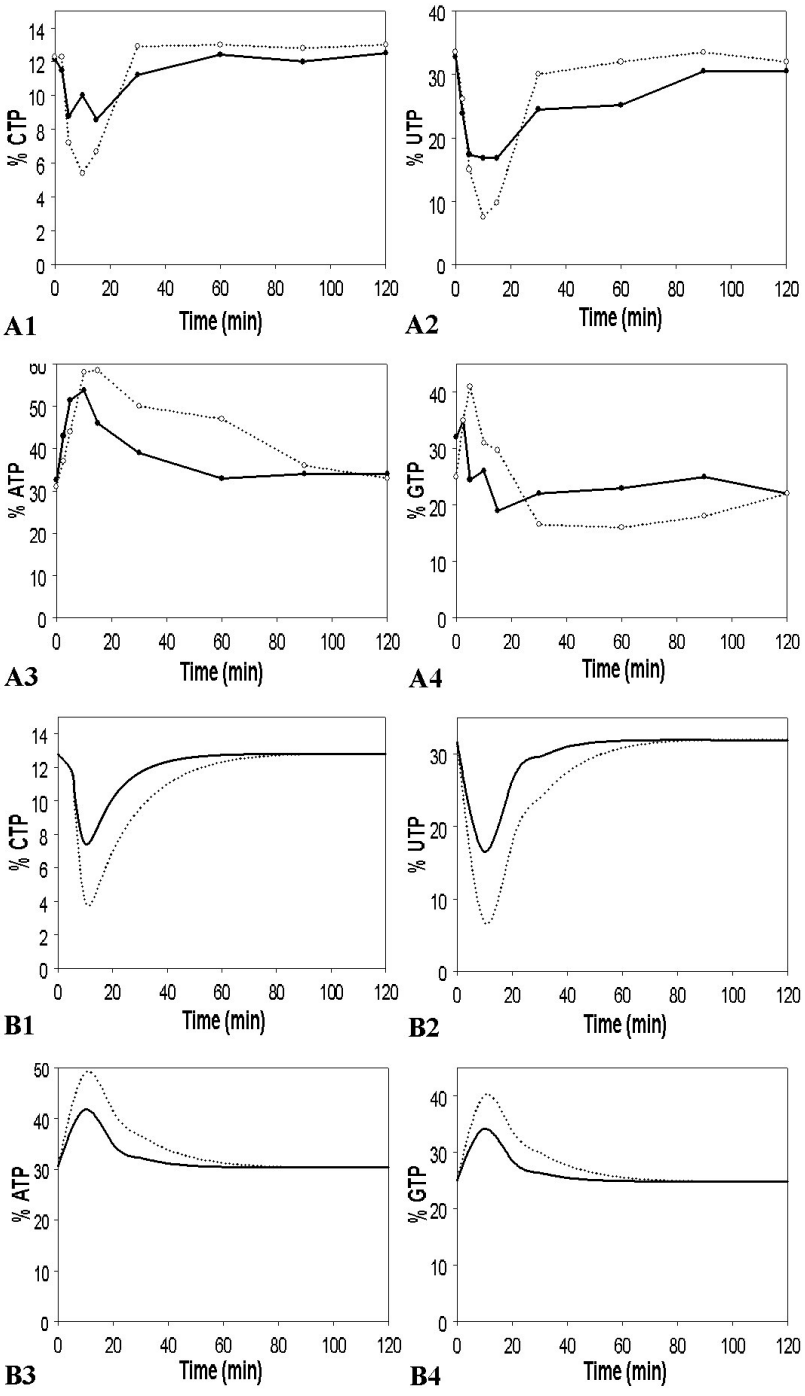

Figure 19. Simulation of NTP pools responses after pyrimidine pathway derepression. (A1–4) The experimental results reflect a sharp drop in the levels of CTP and UTP rapidly after derepression. (B1–4) The corresponding simulation shows remarkable similarity. Holoenzyme (—); catalytic subunit (····).

Several models have been published describing different metabolic pathways in *E. coli*, beginning with models 15 years ago describing the whole cell, but omitting control of metabolic pathways (90). Currently, there are several models that describe specific pathways in *E. coli* such as the tryptophan biosynthetic pathway (49), replication (29), and chemotaxis (95), all of which use computational tools in an attempt to understand mechanisms of cell regulation and control.

This study presents a computational simulation that includes allosteric regulation of the de novo pathway of pyrimidine biosynthesis. As opposed to standard kinetic models, this treatment considers temporal variations in the nutrient uptake and in concentration of allosteric effectors. This type of dynamic modeling allows the physiological adaptation of the cell, as evidenced in response of the nucleotide pools, to be evaluated. Not only is allosteric control of de novo pyrimidine biosynthesis simulated, but also the model formulation potentially allows for the prediction of differences in adaptation when the cells are grown under different environments.

The equations used to simulate the overall pathway response were tested individually and validated relative to existing literature data. In the case of the first reaction, which is catalyzed by CPSase, the model accounts for the allosteric inhibition effected by UMP binding. In this simulation, saturation is achieved with comparable glutamine

concentrations as has been observed experimentally (81). The addition of uracil as an environmental variable and parameterization of the model yielded an optimal kinetic response.

A similar approach was utilized to evaluate the behavior of the model with respect to ATCase activity. The kinetic optimization in this case was more demanding, since the second enzyme of the pathway is subject to the action of multiple homotropic and heterotropic controls. The critical step was to optimize the parameters and equations such that the regulatory lag caused by substrate cooperativity is seen as a sigmoidal path in a saturation curve. Multiple iteration steps had to be taken before each of the allosteric effects was simulated in agreement with the experimental observations from our laboratory. Successful simulation of the physiological response, including allosteric effects of the first two reactions, allowed us to simplify the addition of the remaining kinetic expressions and focus on the NTP levels as the objective of the refinement process.

The expression levels of the first two enzymes in the pathway were found to respond to the derepression simulation by a transient overexpression of CPSase, and an increase in steady-state levels in the case of ATCase. The timing and extent of these events correlated directly with the shift in the nucleotide pools. It is interesting to hypothesize

about the roles of these two enzymes in the regulation of the flux through the metabolic pathway. CPSase levels respond to the concentration of its regulator UMP. ATCase levels rapidly build to increase the decaying levels of UMP and, ultimately, results in pyrimidine nucleotide homeostasis. CP, the product of the reaction catalyzed by CPSase, is a highly unstable metabolite that, in addition, has to be partitioned between the pyrimidine and arginine biosynthetic pathways. While other organisms have multienzyme complexes that effectively channel this substrate through several catalytic sites (18, 59, 109), this is not the case with *E. coli*. Studies performed with *Pyrococcus abyssi* provide an example of CPSase and ATCase that associate to form a transient complex or pseudo-compartment, thus facilitating transfer of the unstable CP produced from one catalytic site to the other (74). However, while there is evidence of substrate channeling in *E. coli* during protein synthesis, purine biosynthesis, carbohydrate phosphorylation through the phosphotransferase system and aspartic acid metabolism (38, 39, 83, 85), to our knowledge there are no reports of channeling involving pyrimidine metabolism. More recently, the process of metabolic channeling has been investigated in other biological systems using mathematical modeling (61), thus opening the door to the directed study of these and other metabolic control processes through computer simulations.

In the case of pyrimidine biosynthesis, integration of individual kinetics into the complete pathway required the development of a way to quantify the result of

parameterization at each step of the metabolic pathway. Repression/derepression experiments have substantiated the role of the allosteric regulation in NTP pools consumption and production in *E. coli,* acting in concert with the important contribution of genetic control. The rapid drop in the observed CTP and UTP levels upon starvation for pyrimidines indicates the initial depletion of their intracellular concentrations, which was followed by a recovery as de novo biosynthesis of pyrimidines replenished the pools. The most sensitive component of this approach was the estimation of local minima used for the parametric calculations. Using a few selected parameters at a time, the sums of the squares of the residuals of the experimental data and the nucleotide fractions at specific times were calculated. Following this concept, the minimal set of parameters that were capable of capturing the allosteric response to uracil-induced repression/derepression was identified.

The initial drop in nucleotide pools corresponded to the depletion of pools as pyrimidine nucleotide synthesis shifted to the de novo pathway. Initially, the concentrations of CTP and UTP synthesized from uracil were sufficient to keep ATCase repressed. Immediately after uracil depletion, the NTP levels dropped. Allosteric inhibition and genetic repression were relieved and the activation of the enzyme was evidenced by the de novo synthesis of nucleotides as their pools stabilized at the normal physiological levels. Our model faithfully captured this behavior. In fact, the simulations showed the difference in the extent of the NTP levels between the holoenzyme and catalytic subunits

that was observed experimentally. This demonstrated that the experimental results obtained for changes in CTP and UTP pool levels could be emulated by including allosteric parameters for CPSase and ATCase.

Even though the model presented is sufficient to approximate the allosteric responses in the de novo pyrimidine pathway, one would imagine that much of the control in vivo relies on the transcription of the *pyr* regulon. This first generation model includes a very simple mathematical description of the modulation of enzyme synthesis in response to pyrimidines. For a more detailed description of transcriptional control, additional parameters have to be defined and experimental data obtained that serve to validate those formulations. The results of this work are described in the following chapters.

CHAPTER III

DYNAMICS OF THE REGULATION OF METABOLIC FLUX IN RESPONSE TO PERTURBATIONS AT DIFFERENT GROWTH RATES

OVERVIEW

Induction of pyrimidine repression/derepression provides a valuable opportunity for quantifying the dynamics of the metabolic response of the cell. Monitoring the intracellular accumulation of nucleotide triphosphates (NTPs) in the cell becomes, in this case, an indicator of the metabolic response. An efficient and highly reproducible method of extraction and separation allows reliable quantification of the NTPs. Two types of physiological conditions were chosen to induce perturbation, middle exponential and steady state cultures. Results obtained highlight the importance of the rapid adaptive response provided by allosteric regulation at different growth rates. The two physiological states analyzed permit a simulation of natural conditions of feast and famine to be explored, as well as to draw hypotheses regarding the interplay of genetic versus metabolic mechanisms of homeostatic control.

INTRODUCTION

Pyrimidine Biosynthesis Repression/Derepression

When *Escherichia coli* is grown under conditions of minimal supplied nutrients, most biosynthetic pathways are activated, including that of de novo pyrimidine biosynthesis. Growth under such derepressing conditions will continue at steady state as long as the nutrient source and environmental conditions remain constant. In the case of pyrimidine biosynthesis, the addition of uracil to the media results in repression of the de novo pyrimidine pathway and the nucleotide interconversion and/or the salvage pathways maintain production of pyrimidine nucleotides. Under these conditions, de novo biosynthesis has been estimated to account for less than 20% of pyrimidine nucleotide production (17). It has been established that the level of the intracellular pools of CTP and UTP correlate with the levels of expression of the de novo pathway genes (40, 112). As uracil is depleted, UTP and CTP levels from salvage reutilization of this precursor will drop. This decrease will cause the reactivation of the de novo pathway genes and the concentration of enzymes involved in de novo biosynthesis returns to higher levels to restore pyrimidine nucleotide concentrations.

Using this experimental approach in combination with mathematical modeling of the pathway has demonstrated the physiological role that allosteric regulation of ATCase plays in controlling flux through the de novo pathway (82). Analysis of metabolic flux

from cells grown in batch cultures is limited by the lack of standardization, resulting in sampling variable physiological states. Following the dynamics of transition after nutritional perturbation using chemostat-grown cultures provided the additional information needed. Cells grown under controlled conditions in a chemostat, allow the system to provide a population of cells to be tested with similar average physiological states. Additionally, use of chemostat cultures allows for the possibility of subjecting cellular cultures to nutritional perturbation at different, and controlled, growth rates. Use of this approach, with iterations of rounds of experimental and mathematical analysis, provided evidence that suggests distinct roles for allosteric and transcriptional controls in regulating the dynamics of metabolic flux.

MATERIALS AND METHODS

Growth Conditions

Escherichia coli E63 (5) cultures were maintained in minimal TF (65) medium agar plates, supplemented with 0.2% glucose, 2 μg/ml thiamine and 1% casamino acids. Fresh plates (less than 1 week old) were grown prior to experiments. Startup inoculums were prepared with the same medium from a single colony in a 5 ml roller tube and incubated overnight at 37°C. One milliliter of the inoculum was used to start 100 ml culture flasks or 5 ml for the chemostat experiments. Care was taken to prepare the inoculums in the same medium (with or without uracil) contained in the flask or

chemostat, which were in turn pre-equilibrated at 37°C to avoid unnecessary disruption of cell growth.

Batch Cultures

Shaker flasks were used to grow *E. coli* cells in 150 ml of TF medium. In addition to supplementing the media with glucose, thiamine and amino acids, 50 μg ml^{-1} uracil was added when appropriate to induce repression of the de novo pathway. The flasks were inoculated as described above and the cells grown to middle exponential phase (defined at 100 Klett units) at 37°C with 200-rpm agitation. At that point samples for further analysis were taken as described below.

Continuous Cultures

Similarly, *E. coli* cells were grown in 1 L TF supplemented medium using chemostats. Medium with uracil was pre-warmed at 37°C before inoculating with 5 ml of the starter culture. Cells were allowed to grow until steady state was reached based on spectrophotometric measurements of the cell density, which typically was obtained within five residence times. Cells were allowed to continue for at least three more residence times before the culture was processed for further analysis of nutritional perturbation.

Nutritional Perturbation

Derepression experiments were conducted with *E. coli* cells grown in supplemented TF media in the presence of uracil until they reached middle exponential growth phase (batch growth, $\sim 8\times10^{7}$ cells ml^{-1}), or cell concentration steady state level (chemostat growth, $\sim 2\times10^{9}$ cells ml^{-1}), as determined spectrophotometrically at 420 nm. The nutritional perturbation was implemented by the rapid harvesting (< 5 min) of culture by centrifugation at 4,500-rpm and immediate resuspension in media without uracil.

Nucleotide Pools Extraction

Nucleotide pools were extracted at the defined time intervals by sample precipitation with 6% trichloro-acetic acid and nucleoside triphosphates (NTPs) were separated and quantified using HPLC within 48 h after extraction (100). Batch or chemostat cultures were sampled at specific times, with the initial (pre-centrifugation) sample taken immediately before initiating the nutritional perturbation. Additional samples were taken immediately after resuspension of the cells in minimal media without uracil (time 0) and then, as appropriate, at 2.5, 5, 10, 15, 25, 30, 50, 60, 90, 100, 120, 150, 180, 300, 600, 900, 1200, 1500 and 1800 minutes. Shorter time interval samples (up to 600 minutes) were taken for batch cultures and higher growth rate (1 h^{-1}) continuous cultures. Continuous cultures at intermediate (0.5 h^{-1}) or lower growth rates (0.2 h^{-1}) were sampled at longer time intervals (up to 1800 minutes). Samples were processed promptly

at the specified times as follows: 5 ml of cells suspension were pipetted onto a cellulose membrane of 0.45 µm pore size and the liquid quickly removed by filtration using a vacuum manifold. The filter was immediately submerged into pre-chilled 500 µl 6%TCA and vortexed for 1 minute at maximum speed. The sample was then incubated on ice for 30 minutes. This suspension was subsequently transferred into microfuge tubes containing 500 µl of 0.7 M Tri-N-Octylamine/Freon (1,1,2-tricholo-trifluoroethane) solution, freshly prepared and pre-chilled before the extraction. The tubes were again vortexed for 1 min at maximum speed and incubated for another 30 minutes on ice. After incubation, the tubes were centrifuged for 30 seconds at 13,000 rpm and the aqueous (upper) phase transferred to a pre-chilled clean microfuge tube. The centrifugation and transfer steps were repeated to ensure that the sample was clean from debris or any other residue. After the extraction, the samples were stored immediately at –70°C and separated on the HPLC within 48 hours.

Chromatographic Separation of Nucleotides

Nucleotide extraction samples were separated and analyzed by anion exchange HPLC through a Partisil-10 SAX column from Whatman. The stationary phase consists of quaternary nitrogen groups on an organic chain that is Si-O-Si bonded to 10 µm silica gel particles media. Sample volume was 100 µl. A 15 min isocratic separation with 25mM ammonium phosphate buffer, pH 3.3, at a flow rate of 1.3 ml/min, followed by a linear gradient from 0 to 100% 750mM ammonium phosphate buffer in 20 min, pH 3.8,

at a flow rate of 2 ml/min. Data was collected throughout the 45 minute run on a Beckman HPLC, using the System Gold Nouveau software and a diode array detector monitoring 254 and 280 nm.

RESULTS AND DISCUSSION

Optimization of Chromatographic Quantification of Pyrimidine Nucleotides

The chromatographic separation was optimized to separate and quantify all four nucleotide triphosphates (UTP, CTP, ATP, GTP) as well as the monophosphate UMP. Figure 20 shows the retention times of the NTPs and UMP based on this separation protocol.

An important observation was that the chromatographic spectra of separation of nucleotides showed less variation in experiments conducted using chemostat cultures, as opposed to those from batch cultures. The quantification had to be accomplished within 48 hours post-extraction to avoid misleading results from nucleotide dephosphorylation.

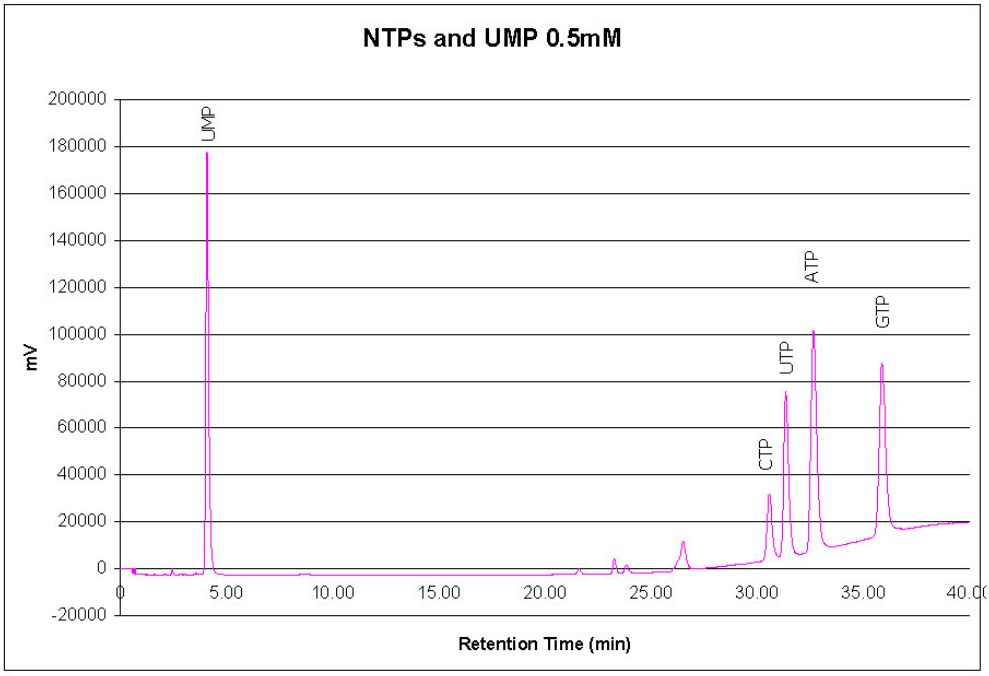

Figure 20. Chromatographic spectrum of de novo pyrimidine nucleotides.

Analysis of Nutritional Perturbation Using Batch Cultures

As previously described, the cells responded to the nutritional perturbation by the readjustment of the intracellular levels of NTPs. It was noted that variability could be observed from one experiment to another based on the efficiency of the extraction, particularly from batch cultures, although the dynamics of the levels of NTPs was consistent. To standardize the presentation of the data, variations in levels of NTPs are

presented as values relative to the total pool, as opposed to the absolute values. The horizontal dotted line represents, in each case, the steady state levels prior to nutritional perturbation.

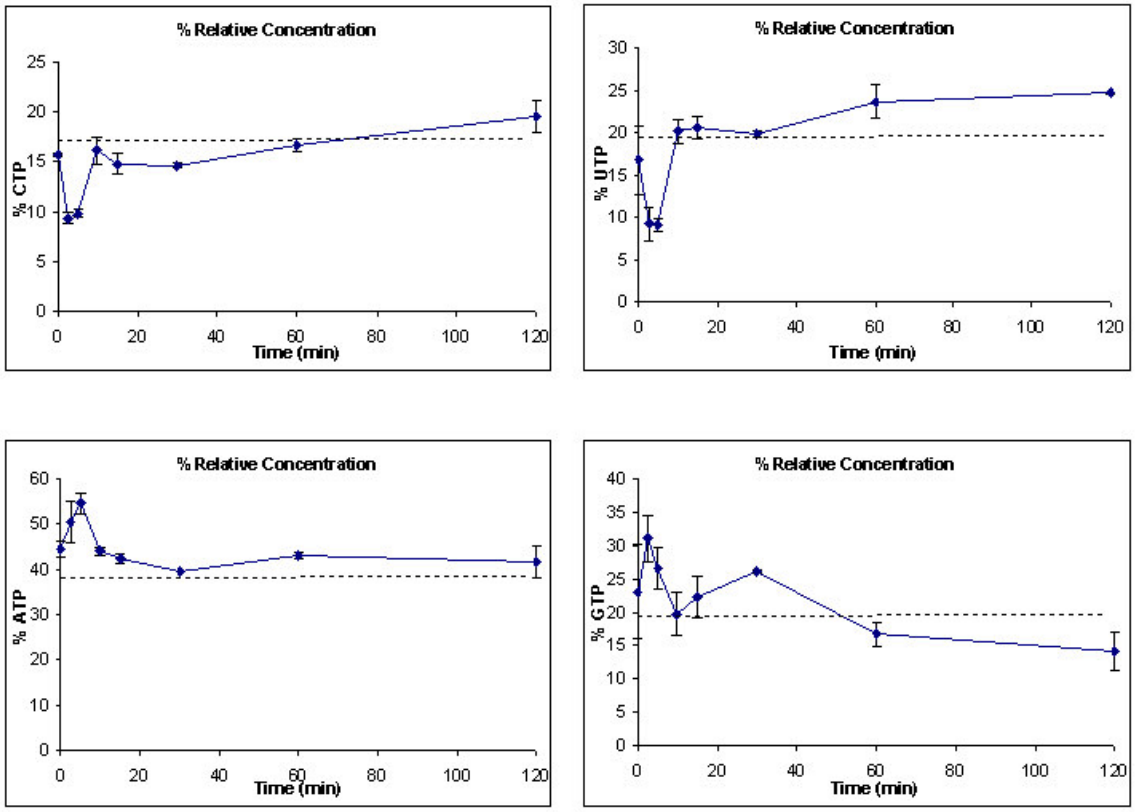

Figure 21. Dynamics of intracellular NTPs following derepression in batch cultures.

Following the nutritional perturbation, relative levels of UTP and CTP decreased, dropping to 54 and 60% their initial values, respectively. The relative change in the purine pool concentration was reflected as an increase in the ATP and GTP concentrations of 23 and 35%, respectively. Remarkably, the response reached its peak level within 5 minutes following derepression and the cells were able to replenish their

nucleotide pools within 15 minutes to bring the concentrations back to their initial levels (Figure 21).

Standardization of Derepression Experiments Under Steady State Conditions

To extend these studies to homeostatic conditions, chemostats were used to grow cells to steady state to ensure that the average cell population was in the same physiological state at each perturbation experiment (~$2x10^9$ cells/ml). Chemostats achieve steady state by supplying a constant flow of nutrients to the culture and controlling other sources of environmental variation. Table 3 summarizes the growth parameters established for the steady state experiments.

Table 3. Chemostat cultivation parameters

Parameter	Equation	Value
Volume (V)		1.0 liter
Flow Rate (F)	D = F/V	200 ml/h
Dilution Rate (D)		0.2 h-1
Growth Rate (μ)	μ = Ln2/td	0.2 h-1
Doubling Time (td)		208 min
Aeration		1 psi
Agitation		300 rpm
Temperature		37°C

Analysis of Nutritional Perturbation Using Steady State Cultures

As seen in Figure 22, the dynamics of derepression demonstrated an initial increase in the intracellular concentrations of pyrimidine trinucleotides, followed by a relatively rapid recovery to initial levels. The time responses differ from those seen in Figure 21. Two possible explanations for these differences are growth rate, as these experiments were conducted at a growth rate five times slower than that obtained in shaker flasks, or because of differences in the physiological states of the cells between the two culture

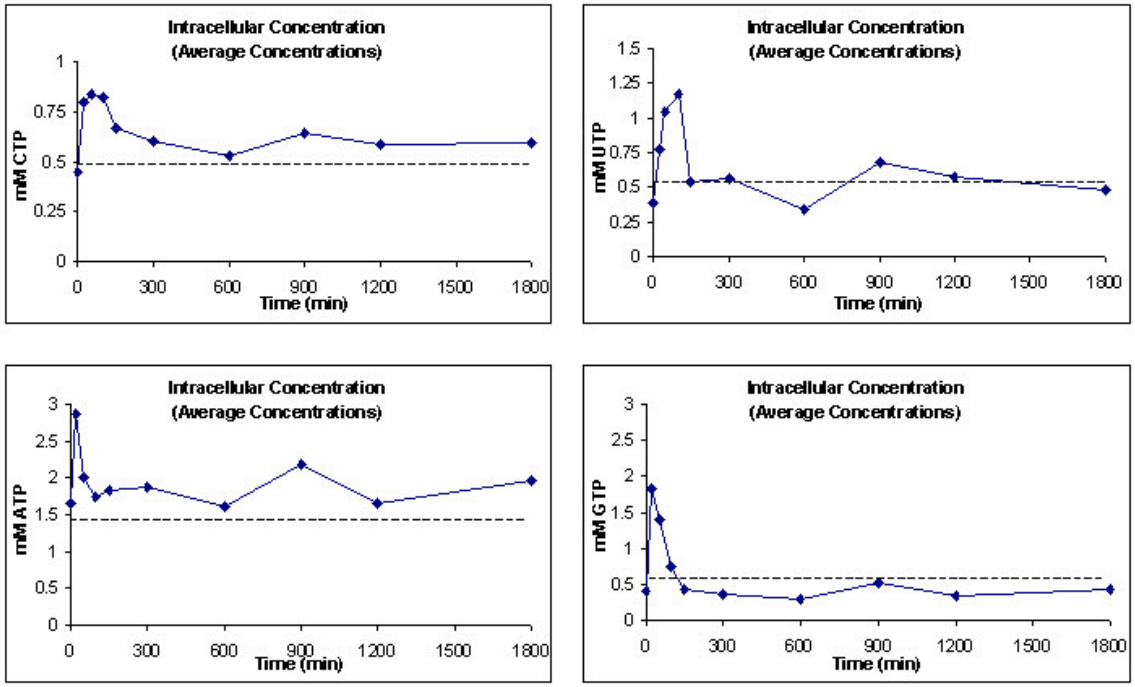

Figure 22. Dynamics of pyrimidine perturbation from steady state.

Table 4. Dynamics of intracellular NTPs

Nucleotide	Initial Concentration (mM)	Final Concentration (mM)	Min Concentration (mM)	Max Concentration (mM)	Time Max (min)	Fold Increase
CTP	0.45	0.6	0.45	0.84	50	1.8
UTP	0.38	0.48	0.38	1.18	100	3.5
ATP	1.67	1.96	1.61	2.87	25	1.8
GTP	0.4	0.44	0.29	1.82	25	6.2

systems. UTP and CTP showed an average 1.8 and 3.5-fold increase, respectively, relative to the initial concentrations. Purine intracellular pools also increased, showing a 1.8 and 6.2-fold gain for ATP and GTP, respectively (Table 4).

In order to compare these results with the batch culture response, analysis of concentration change relative to that of the total NTP pool is provided in Figure 23. Both

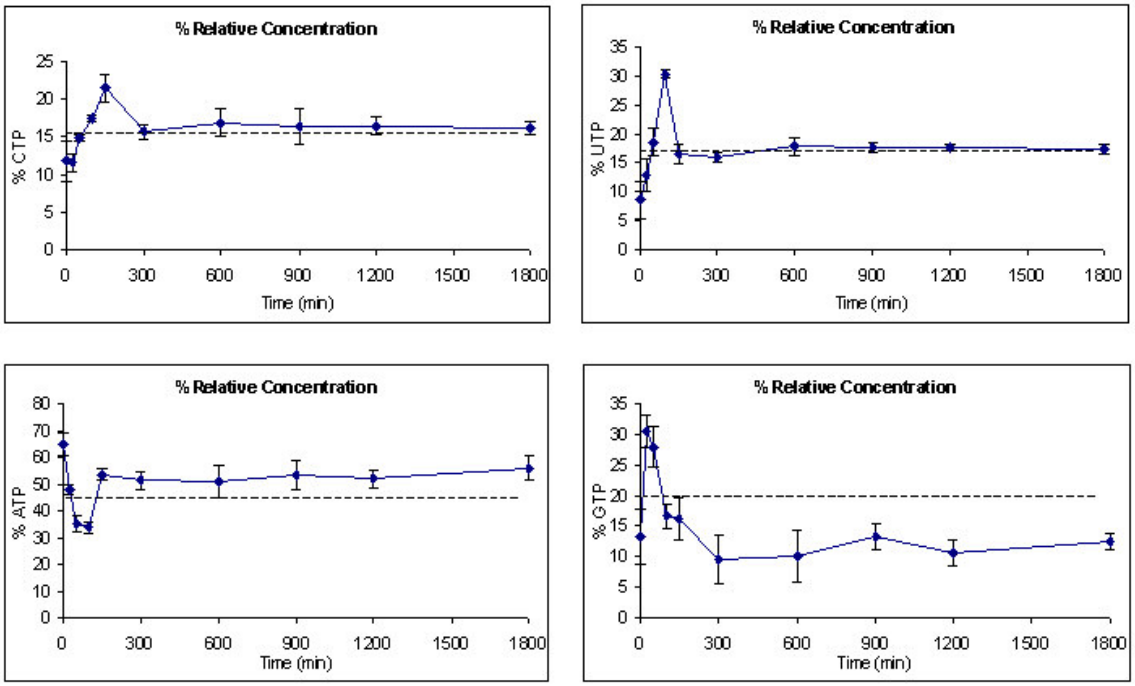

Figure 23. Relative dynamics of intracellular NTPs.

Table 5. Dynamics of relative intracellular NTPs

Nucleotide	Relative Pre-harvest (%)	Relative Initial Concentration (%)	Relative Final Concentration (%)	Relative Min Concentration (%)	Relative Max Concentration (%)	Time Max (min)
CTP	11.75	16.18	11.56	21.48	150	1.86
UTP	8.57	17.31	8.57	30.37	100	3.54
ATP	64.76	55.96	33.66	64.76	0	-1.92
GTP	13.35	12.5	9.51	30.52	25	3.21

pyrimidine NTP pools increase relative to the total pool, as does GTP. ATP relative change, however, is negative compared to the total change in the pools. Important values of this transition are summarized in numerical form in Table 5.

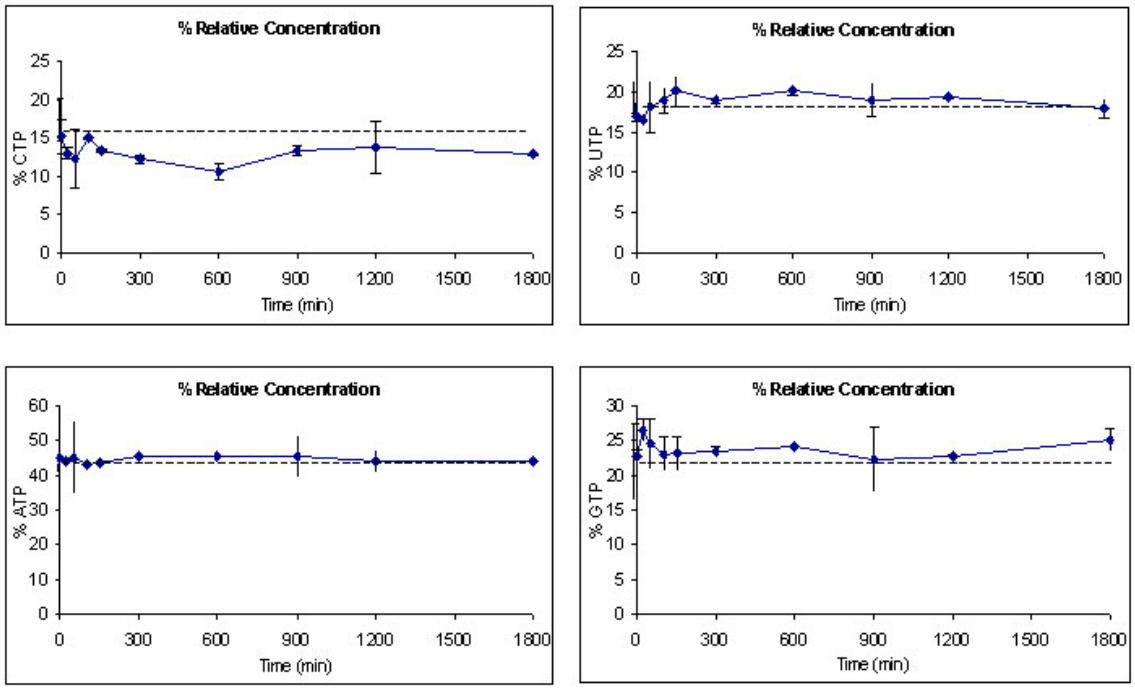

Figure 24. Control derepression experiments.

Table 6. NTP levels during control experiments

Nucleotide	Relative Pre-harvest (%)	Relative Initial Concentration (%)	Relative Final Concentration (%)	Relative Min Concentration (%)	Relative Max Concentration (%)	Time Max (min)
CTP	16.59	15.18	12.82	10.58	15.18	0
UTP	18.5	16.89	17.93	16.55	20.10	600
ATP	39.74	45.09	44.14	43.02	45.37	300
GTP	25.18	22.83	25.10	22.31	26.46	25

Control experiments were carried out to determine the effect, if any, of culture manipulation during the derepression experiments over the pathway's flux. Figure 24 and Table 6 show the average response of experiments in which cells were manipulated in the same way as the previous experiments, but without inducing the nutritional perturbation. As evidenced by the results of the control experiments, physical manipulation of the cell cultures has a negligible effect on the levels of NTP pools.

UMP Quantification

In addition to quantifying formation of nucleotide triphosphates, the extraction and separation protocols were optimized to allow characterization of UMP levels. UMP is an intermediate product in the de novo pathway of pyrimidine biosynthesis that has also an important role in regulation. UMP is responsible for the feedback-inhibition of CPSase, the first enzyme of the pathway.

As observed in Figure 25, UMP levels show a considerable increase in response to uracil depletion. From its initial concentration, intracellular UMP increased 1.7-fold within 150

minutes post-derepression. Steady state levels were reached again around 600 minutes after uracil removal.

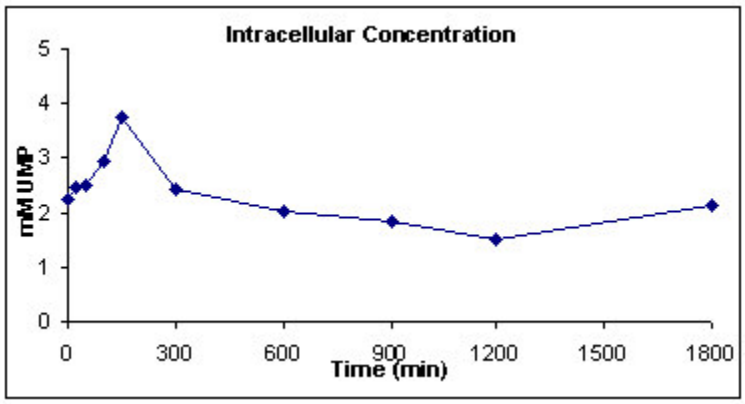

Figure 25. UMP quantification.

Nucleotide Dynamics in Relation to Steady State Growth Rate

At first sight, comparison of the results obtained using batch versus chemostat culture experiments features some striking differences. During batch cultivation, following nutritional perturbation, UTP and CTP levels responded with an initial decrease in their levels followed by a relatively fast recovery and progressive stabilization of normal levels (Figure 21). Chemostat cultures, however, exhibited the opposite response, with an increase in the intracellular levels of UTP and CTP that was followed by recovery and stabilization of steady state levels (Figure 22). Two hypotheses are proposed to explain this observation; first, that the difference in the direction of the response was a

consequence of the difference in the cell doubling time between the two experiments (40 min versus 208 min, batch versus chemostat culture, respectively). The second hypothesis was that the different response was associated with the different physiological states of the two experiments (middle-exponential versus steady state growth). To test these hypotheses, chemostat experiments were conducted to examine the dynamics of the metabolic response to perturbation at different doubling times: 208 min, 104 min and 42 min. This last rate corresponds to that observed in shaker flask

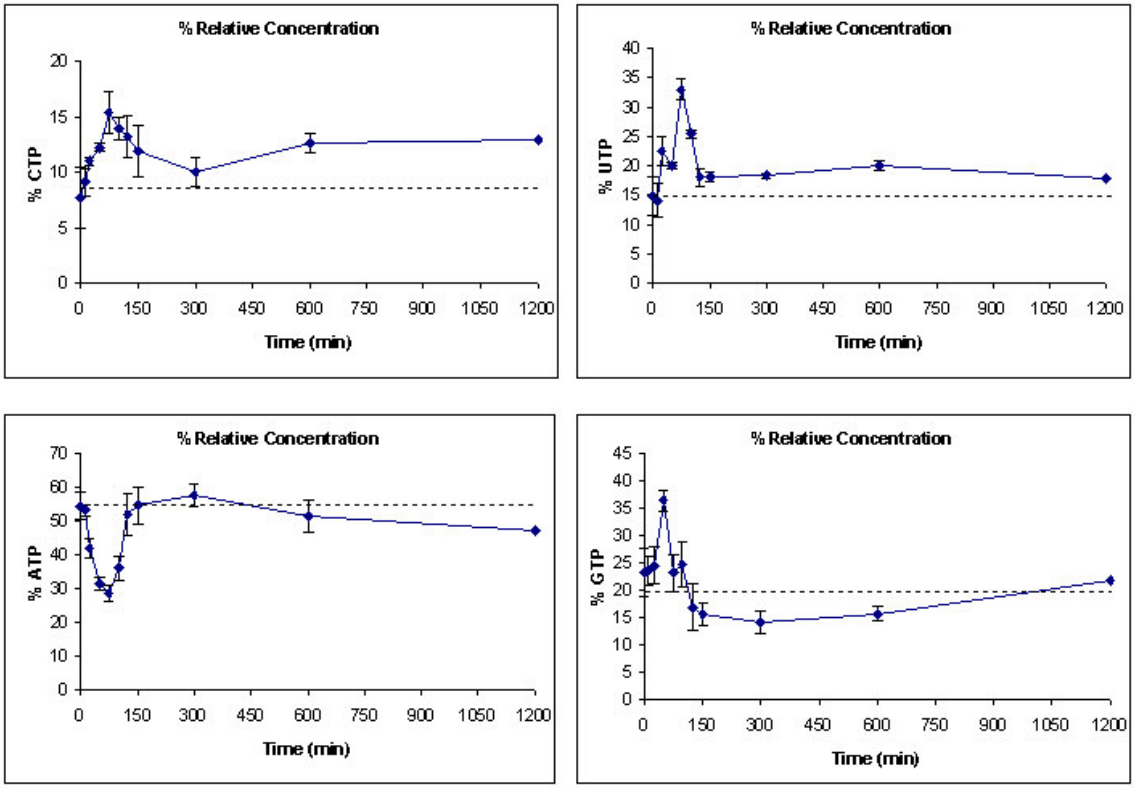

Figure 26. Dynamics of NTP response at intermediate growth rate.

experiments. When reducing the doubling time by half (104 min), the response corresponded directly to that seen at slower doubling time, as UTP and CTP levels increased in response to nutritional perturbation. The dynamics was the same, with the NTP levels reaching its maximum change 75 min after the perturbation (Figure 26). This corresponded to half the response time seen at 208 min. When the doubling time was reduced to 42 min the response was the opposite, with UTP and CTP levels decreasing after the nutritional perturbation. As seen in Figure 27, the dynamics of the intracellular

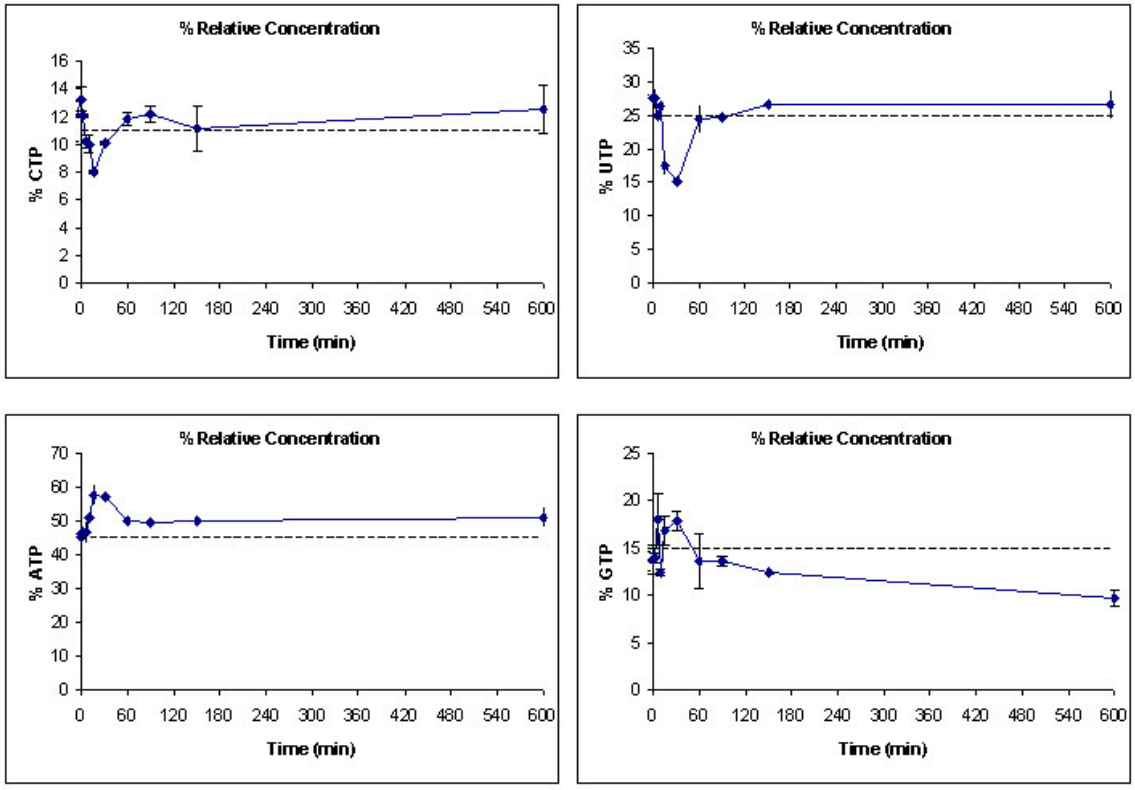

Figure 27. Dynamics of NTP response at high growth rate.

NTP pools very closely resembles that observed with middle exponential cultures. A plausible explanation for this observation relates to the possibility that the cells may be in a different physiological state when growing at different rates (48). Differences in the physiological state of the cells at different growth rates are related to specific energetic and metabolic demands. The energetic requirement of the cell during nutritional readjustment may imply a shift of the adenylate energy charge as an exacting biosynthetic function is reactivated. Looking at an approximate calculation of the adenylate energy charge (AEC) from chemostat experiments at different growth rates provided interesting observations. Figure 28 and Table 7 show the results of an approximate AEC estimation using the intracellular concentration values for ADP and ATP (AMP had to be excluded from this calculation, since the chromatographic separation had not been optimized to resolve this nucleotide). It is apparent from the data obtained that there is no net change in the AEC during the dynamics of readjustment following nutritional perturbation. Changes in ATP levels corresponded directly with those of ADP. It is interesting to note, however, that there was a readjustment in the adenylate nucleotide levels at slower doubling time that coincided with that of pyrimidine nucleotides. At faster doubling times, the levels of ADP and ATP remained near their steady state values. Noticeably, the steady state concentration of ATP is higher and the AEC slightly lower at faster doubling times. It is possible that the higher concentration is due to a higher energetic demand in rapidly growing cells, as all biosynthetic pathways are highly active. Slowly growing cells have, presumably, fewer

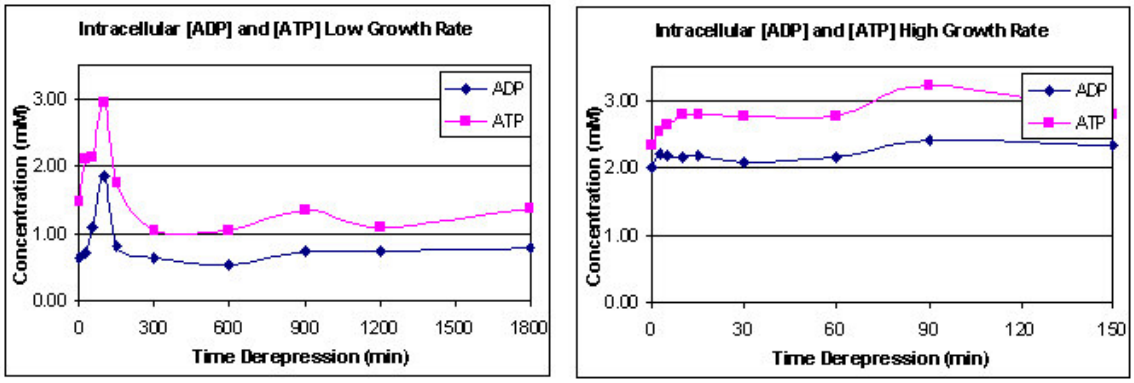

Figure 28. Intracellular levels of ADP and ATP after nutritional perturbation.

Table 7. Approximate AEC values after nutritional perturbation

Low Growth Rate		High Growth Rate	
Time (min)	**Approximate AEC**	**Time (min)**	**Approximate AEC**
0	0.85	0	0.77
25	0.87	2.5	0.77
50	0.83	5	0.77
100	0.81	10	0.78
150	0.84	15	0.78
300	0.81	30	0.78
600	0.83	60	0.78
900	0.82	90	0.79
1200	0.80	150	0.77
1800	0.82		

biosynthetic processes highly active at the same time, therefore imposing less energetic demands. If this is the case, then it is likely that the activation of the pyrimidine de novo biosynthetic pathway does not have a net effect large enough to cause a noticeable decrease in the levels of ATP.

In summary, the levels of pyrimidine NTPs are partially depleted at high growth rates as the cells build up enzyme levels to cope with the ongoing DNA replication and increased transcriptional needs. It is possible that under such conditions, higher growth rates, the allosteric response is essential in controlling the depletion before it reaches critical levels. Eventually derepressed levels are recovered as a consequence of the transcriptional reactivation of the biosynthetic pathway genes. Conversely, at lower rates of growth, pyrimidine NTPs accumulate initially, presumably as a consequence of reactivation of the de novo pathway genes. It then follows that slower doubling cells rely more on transcriptional control, as cell division is not imminent, eventually reaching normal levels once the system fully adapts to the new nutritional conditions. If this is the case, analysis of enzymatic activity should reflect the transcriptional reactivation of the genes that encode enzymes involved in de novo biosynthesis of pyrimidine triphosphonucleotides.

CHAPTER IV

INSIGHT INTO THE INTERACTIONS BETWEEN THE BIOCHEMICAL AND GENETIC MECHANISMS THAT COOPERATE TO ACHIEVE METABOLIC CONTROL

OVERVIEW

An analysis of the interactions between biochemical and genetic mechanisms of metabolic control requires an evaluation of specific enzymatic activity. Quantification of intracellular levels of enzymes was achieved by the analysis of multiple samples extracted over a period of time selected to reflect dynamics. Cell-free extracts were analyzed for all of the enzymatic steps participating in de novo pyrimidine biosynthesis. Results show a distributed and highly coordinated control along the pathway. The initial enzymes, carbamoylphosphate synthetase and aspartate transcarbamoylase, demonstrated a greater range of response corresponding to the degree of complexity and evolutionary association found at these steps. The remaining enzymes in the pathway, dihydroorotase, dihydroorotate dehydrogenase, orotate phosphoribosyl transferase and orotidine monophosphate decarboxylase, showed a more moderate response to nutritional perturbation.

INTRODUCTION

Interaction of the Genetic and Biochemical Networks

Most cells change their enzymatic activity and composition in any adaptive response to specific environmental challenges. In practical terms this means that enzymatic reactions do not occur in the cell at the same extent of activity all the time. Two seemingly independent, although highly interconnected, modes of control, therefore, regulates enzymatic reactions. Cells can, for example, shut down biosynthetic pathways when the end products are no longer needed or can be promptly obtained from the environment. In this case the amount of enzymes that carry out the biochemical reactions decrease as a consequence of genetic control of their rates of synthesis. A more rapid-response mechanism is charged with fine-tuning the activity of enzymes, once they have been synthesized. This is achieved mainly by allosteric inhibition of regulatory enzymes. The coordination of the two mechanisms of control is what ultimately contributes to the determination of flux through the pathway.

Analysis of enzymatic activity from cell-free extracts, taken at discrete time intervals after nutritional perturbation, is used in this study to quantify metabolic regulation. This dynamic analysis leads to an appreciation of how the production and utilization of metabolites are kept in balance. More importantly, it leads to separation in the analysis of transcriptional versus allosteric control of metabolism at steady state. This analysis

was accomplished through the formulation of a second generation mathematical model, constructed from that described earlier (82), that includes the same equations and parameters plus several additional ones that complement their description of metabolic control. Addition of the new parameters was based on the experimental data obtained from the quantification of nucleotide pools and enzymatic activities described here. These data provided information regarding the relative responses and contributions at each step along the pathway. This new model has been validated and its robustness offers an indication of its applicability for the design of new hypotheses that speed up research directed towards a complete understanding of control of cellular metabolic biosynthesis.

MATERIALS AND METHODS

Preparation of Cell-free Extracts

An initial inoculum of *Escherichia coli* E63 was started in a 5 ml roller tube of supplemented TF medium with uracil. This was used to inoculate a 2-liter chemostat with the same culture medium and allowed to grow for 8 generations to reach steady state. Before inducing nutritional perturbation of the steady state culture, a 25 ml sample was taken and the cells immediately pelleted by centrifugation to be used as a control. Nutritional perturbation was induced by rapid (<5 min) collection of the cells by centrifugation and prompt transfer to supplemented TF medium without uracil.

Additional 25 ml samples were taken immediately after resuspension of the cells (time 0) and after 2.5, 5, 10, 15, 25, 50, 100, 150, 300, 600, 900, 1200 and 1800 minutes. All samples were immediately pelleted by centrifugation and kept frozen at –20°C.

Cell pellets were resuspended in 1 ml of 1M Tris-HCl, pH 8.3, and sonicated at 20 KHz for 4 cycles of alternating 1 min burst with 1 min on ice. The samples were centrifuged for 15 minutes at 13500 rpm, the supernatant was removed into clean 1.5 ml tubes and stored at –20°C.

CPSase Activity Assays

Activity of carbamoyl phosphate synthase was determined using the sensitive radiochemical assay described by Ingraham and Abdelal (37), with some modifications. The assay traps the labile carbamoyl phosphate produced by CPSase using hydroxylamine to produce hydroxyurea. The reaction mix included, for a final reaction volume of 1 ml, each of the following: 0.1 M Tris-HCl buffer, pH 8.3, 0.2 M KCl, 2 mM ATP, 0.1 M $MgCl_2$ and 100 mM L-glutamine. Cell-free extracts for this assay were prepared using the BugBuster Protein Extraction Reagent (Novagen^{TM}) as follows: frozen cell pellets were resuspended in 2 ml of BugBuster reagent supplemented with 1mg/ml lysozyme and 2 units of benzonase, incubated at room temperature for 20 minutes and pelleted by centrifugation. Assay tubes were prepared containing 500 µl of

cell-free extract plus 420 µl of reaction mix. The assay tubes were preincubated at 37°C for 5 minutes and the reaction started with 80 µl of radiolabeled bicarbonate (127 mM $NaHCO_3$:127 µM $NaH^{14}CO_3$) and mixed well. Each reaction was evaluated after 5, 10 and 15 minutes by removing 250 µl and mixing with 25 µl of 1.3M hydroxylamine/HCl. The assay time points were then incubated for 10 minutes at 95°C, allowed to cool down and mixed with 75 µl of 40% trichloroacetic acid. Dry ice was added to the tubes to drive off unreacted bicarbonate as gaseous CO_2 overnight. Radioactive content was quantified by mixing reactions with 1 ml of Ultima Gold scintillation cocktail (Packard™) and counting in a Liquid Scintillation Counter Model LS 7000 (Beckman™).

ATCase Activity Assays

The assay used was based on the conditions described by Shepherdson (93) and Gerhart (25) with some modifications. A carbamoyl aspartic acid standard curve was prepared by making serial dilutions of a 1mM CAA stock solution. The final concentrations of these were 0, 0.1, 0.2, 0.3, 0.4, 0.5, 0.6 mM. A pre-mixed solution was prepared, containing 1.5 ml of 1 M Tris-HCl, pH 8.3, 3 ml of 0.2 M K-Asp and 19.5 ml of deionized water and kept on ice. Dilutions of the cell-free extracts (1:20) were prepared with 1 M Tris-HCl, pH 8.3 and kept on ice. Carbamoyl phosphate (0.024 g) was weighted out and kept on ice, dissolved in 3 ml of deionized water immediately before use. A stop mix

consisting of 33.3 ml of antipyrine/H_2SO_4 solution (0.5 g / 100 ml of 50% acid), 16.7 ml of monoxime/acetic acid (0.4 g / 50 ml of 5% CH_3COOH) and 25 ml of deionized water was also prepared. 1.5 ml of this mix was dispensed in each of 30 test tubes, covered with aluminum foil and kept on ice; the remaining was kept in a beaker, on ice, also covered to shield from light. The premixed reaction solution (1.6 ml) was dispensed into 10 tubes containing the cell-free extracts. These 10 tubes, as well as those for the CAA standard curve were placed in a water bath at 28°C. The CP was suspended, and used to start the assay by dispensing 200 µl into the 10 reaction tubes (with 10 sec intervals) and vortexing. At 10, 20 and 30 min after initiating the reaction, 500 µl were transferred to the tubes with stop mix and vortexed. The remaining stop mix dispensed (1.5 ml) into each CAA dilution. All reactions were incubated in the light at 60°C for 110 minutes. At that time the samples were placed on ice and their light absorbance at a 466 nm wavelength promptly determined.

DHOase Activity Assays

This assay was adapted from that used by Kelln (43, 46) and followed a procedure similar to the activity assay for ATCase. A standard curve of varying concentrations of carbamoyl aspartic acid was prepared from a 1 mM stock solution. A 1:20 dilution of the cell-free extracts in 1 M Tris-HCl, pH 8.3 was used as before and the reaction initiated with 20 mM L-Dihydroorotate. The reactions were allowed to proceed at 28°C for 10, 20 and 30 minutes. At the specified times, the reactions were stopped with a mixture of

antipyrine/sulfuric acid and monoxime/acetic acid. The stopped reactions, together with the CAA and DHO controls were incubated for approximately two hours at 60°C to develop color. As with the ATCase assay, the absorbance at 466 nm was determined and used to calculate specific activities of each sample.

DHOdeHase Activity Assay

Activity of dihydroorotate dehydrogenase was quantified following a procedure adapted from Karibian (43). For each experiment, an appropriate cell-free extract dilution was preincubated with 1 M Tris pH 8.8, 100 mM $MgCl_2$ and deionized water. Dihydroorotate was used as the substrate from a 20 mM stock solution. The final volume of the reaction was kept to 100 µl. The reaction was followed by quantifying the absorbance change in a Ultrospec 2000 spectrophotometer (Amersham ^{TM}) at 290 nm. An increase in the absorbance of the reaction, in a 1 cm length path, of 1.93 units was correlated with a change in the substrate concentration of 1 mM. The analysis of the data collected was performed as described later in this chapter.

OPRTase Activity Assay

This assay was adapted from that used by Schwartz and Neuhard (91), which uses the production of OMP as the measured variable. The conditions of the assay, very similar to those used in the DHOdeHase assay, include 100 mM Tris pH 8.8, 6 mM MgCl2 and

water, mixed with an appropriate dilution of the cell-free extract. Two substrates are needed for this reaction, orotate, at a final concentration of 0.25 mM and 5-phosphoribosyl-1-pyrophosphate, at a final concentration of 0.6 mM. A decrease in the absorption of the reaction of 3.67 was equated to an increase in the concentration of product, OMP, of 1 mM. The wavelength for detection was 295 nm.

ODCase Activity Assay

This assay (22) followed the decrease in concentration of OMP at a 290 nm wavelength over 20 minutes. The assay conditions were the same as those used for OPRTase with the exception of the substrate, which was 0.4 mM OMP. The millimolar extinction coefficient of OMP is 1.38.

CTP Synthase Activity Assay

The assay for CTP synthase was adapted from that used in the studies of Zalkin (115). It followed the synthesis of CTP, which has an extinction coefficient of 1520 $M^{-1}cm^{-1}$, at 291 nm. The conditions used were as follows: 20 mM Tris pH 8.3, 0.5 mM ATP, 10 mM $MgCl_2$, 0.5 mM UTP, 2 mM glutamine and 0.1 mM GTP in deionized water, mixed with the appropriate dilution of cell-free extract. The reaction was started by addition of UTP and followed at 38°C during 5 minutes.

Analytical Procedures

Measurements of optical density (OD) at the appropriate wavelengths were performed to monitor color development in the reactions. Samples were used for absorbance quantification on Ultrospec 2000 and Ultrospec 3300 Pro spectrophotometers (Amersham/Pharmacia Biotech). Absorbance readings were recorded for all sets of samples and calibration curves.

Protein concentration was determined using the absorbance readings of 1:20 dilutions of the cell-free extracts at 260 and 280 nm wavelengths. The spectrophotometer was zeroed with a buffer blank. The following equation was used to estimate the protein concentration:

$$[\text{Protein}]\ (\text{mg/ml}) = 1.55 \times A_{280} - 0.76 \times A_{260}$$

Determination of protein concentration by ultraviolet absorption (260 to 280 nm) depends on the presence of aromatic amino acids in proteins. Tyrosine and tryptophan absorb at approximately 280 nm, whereas the 260 nm reading was used to correct for nucleic acid content. The main advantages of this method of determining protein concentration are that the sample is not destroyed and that it is very rapid.

Calculation of specific activity was done using the following equation:

Equation 20

$$SpecificActivy = \frac{\Delta A_{\lambda} / t}{\varepsilon * [P] / V}$$

where ΔA_{λ} is the rate of change in absorbance and t the time units, ε is the extinction coefficient of the substrate consumed or product formed during the reaction and $[P]$ is the concentration of protein in the cell-free extract and V the volume of the reaction.

RESULTS AND DISCUSSION

Dynamics of Enzymatic Activity in Response to Metabolic Perturbation

The regulation of the enzymatic activity along the pathway of de novo biosynthesis of pyrimidines is coordinated between the allosteric and transcriptional control mechanisms. Although some of the enzymes respond to allosteric effectors, thus providing an immediate and fine-tuning responsive mechanism, all are coordinately regulated at the gene expression level. These experiments allowed for a clear insight into the interplay of both mechanisms of regulation. Following the flux of metabolites at different growth rates during derepression allowed a dissection of the allosteric response

and measurement of specific activities of the enzymes complemented the analysis by providing information regarding transcriptional activation. Analysis of enzymatic levels of activity provided a quantifiable method of observing the contribution of gene expression in restoring metabolic steady state. As expected, all the enzymes exhibited responsiveness to the nutritional perturbation, with steady state derepressed levels of expression higher than repressed levels. The extent and dynamics of these responses are described in the following pages.

CPSase Response. The first enzyme of the pathway is a critical regulatory point controlling flux through the pathway. In *E. coli*, the activity of CPSase is shared between the pyrimidine and arginine biosynthetic pathways. This requires that the product of this first reaction, CP, be partitioned in order to satisfy competing demands. The hierarchy of this decision-making process is still unclear; however, CPSase responds to pyrimidine de novo activation by increasing its activity within 100 minutes by 10.3-fold with respect to steady-state values (Figure 29). Expression of the *carAB* operon is regulated by the cumulative repression of the end products of both pathways and it is interesting to observe, from the results of pyrimidine derepression, the extent of the response induced by the reactivation of this pathway. UMP, as shown in figure 25, also follows a similar trend of accumulation and likely plays a role in controlling the activity of this enzyme as it regains steady state levels.

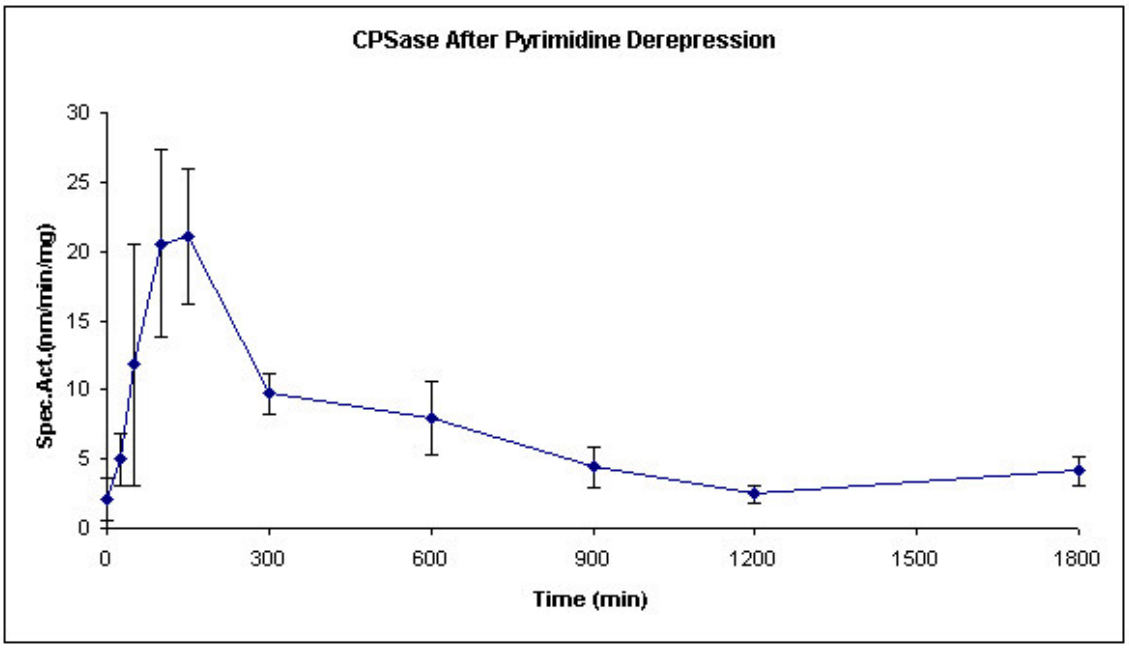

Figure 29. Dynamics of CPSase perturbation from steady state.

ATCase Response. The second step of this pathway is the first reaction devoted exclusively to the production of UTP and CTP de novo. The specific activity of ATCase is much greater than that of any other enzyme in the pathway and, therefore, a 3.8-fold increase in activity provided a considerable amplification of the metabolic flux. The levels of enzyme rose within 100 minutes after the perturbation and they gradually receded over approximately three generation times (Figure 30). Activation of the P2 promoter and transcriptional attenuation are responsible for the control of synthesis of ATCase. The response observed for derepression of ATCase follows the time scale observed for the accumulation of the end products of the pathway, UTP and CTP, responsible for these mechanisms of control (Figures 22 and 23). Present also in this enzyme is the contribution of allosteric inhibition brought about by the accumulation of

UTP and CTP, which are likely contributing to the control of activity as the enzyme accumulates in response to nutritional perturbation.

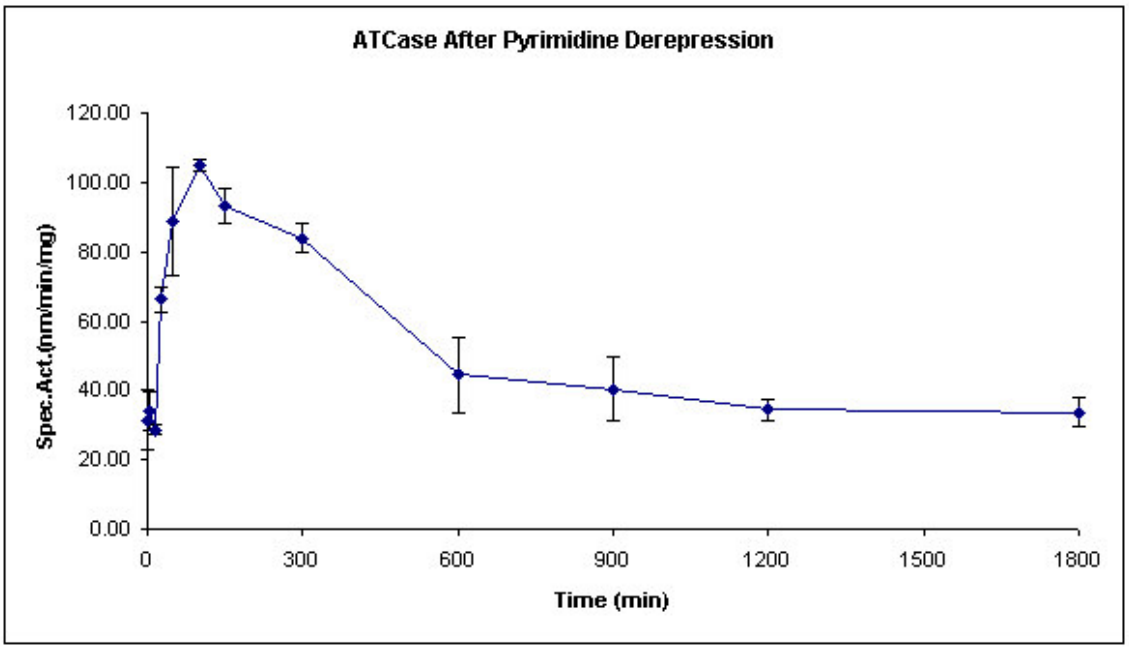

Figure 30. Dynamics of ATCase perturbation from steady state.

DHOase Response. DHOase also had a significant activity increase following derepression. As seen in Figure 31, derepression levels reached 5.6-fold activation with respect to initial values. Importantly, in higher organisms, this enzyme is present as a multi-enzyme complex together with CPSase and ATCase and therefore an important step in controlling flux through the pathway. Although lacking the allosteric-level regulation present in the first two enzymes, DHOase transcription also responds to the intracellular concentration of pyrimidine nucleotides. As in the case of ATCase, transcriptional regulation involves also an attenuation mechanism. CTP levels are

involved in this mechanism by forcing initiation of transcription from a site that results in formation of a terminator when pyrimidine trinucleotide levels are high. Although derepression of DHOase is not as high as that of CPSase, it still is relatively high when compared to the response of the enzymes downstream in the pathway.

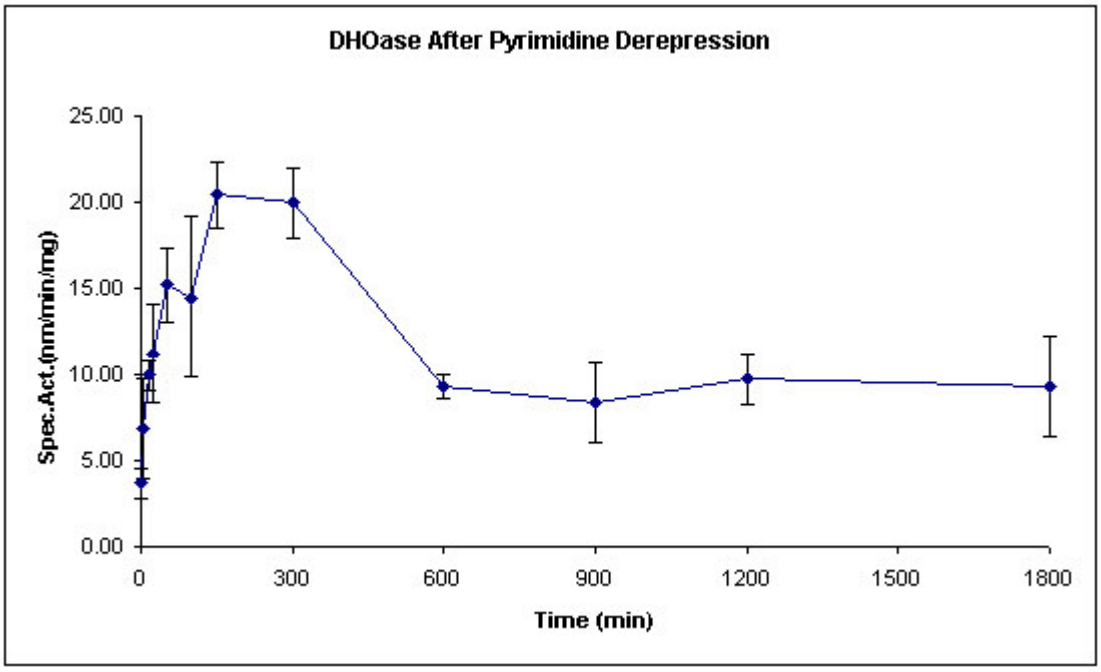

Figure 31. Dynamics of DHOase perturbation from steady state.

DHOdeHase Response. Subsequent de novo reaction steps, beginning with DHOdeHase exhibited a less dramatic response associated with the metabolic perturbation. Figure 32 shows the dynamics of this response, which reached 2.2-fold increase within 150 minutes after derepression. Regulation of *pyrD* is also responsive to

the intracellular concentration of CTP and, as is the case for *pyrC, pyrE* and *pyrF,* to the action of a common repressor (PurR). The repressor is believed to bind to sites conserved in these operons and block the recruitment of transcriptional accessory proteins. As evidenced from the observations of the dynamics in the response of this and the other enzymes in the pathway, the response to nutritional perturbation is coordinate in timing and extent.

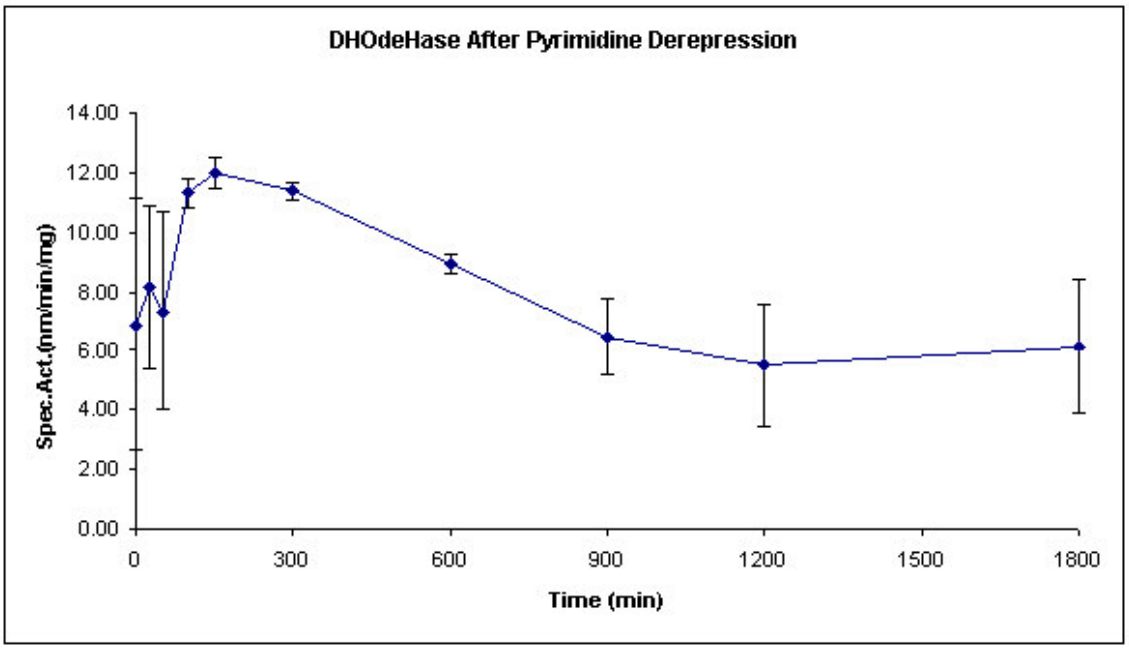

Figure 32. Dynamics of DHOdeHase perturbation from steady state.

OPRTase Response. The phosphorylation of orotate had a similar increase in transcriptional activation as that observed for DHOdeHase. A 2.3-fold increase was

observed and steady state values subsequently recovered (Figure 33). In addition to the action of PurR, *pyrE* transcription is regulated through attenuation modulated by the levels of UTP.

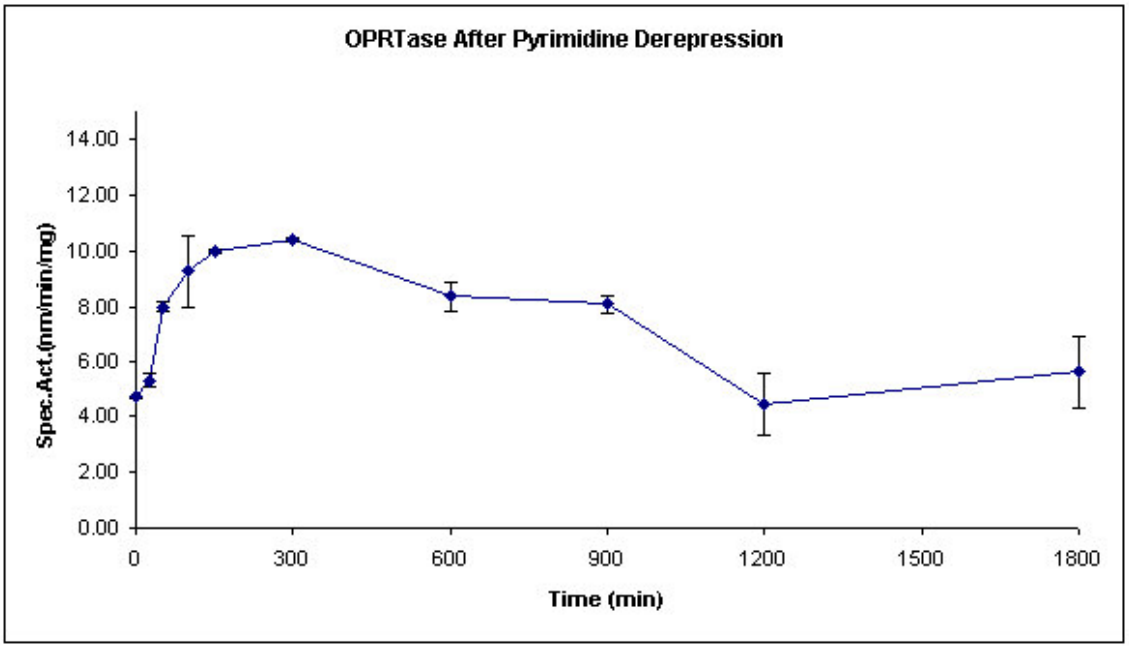

Figure 33. Dynamics of OPRTase perturbation from steady state.

ODCase Response. UMP formation can be considered a threshold step in de novo pyrimidine production in the cell. The last step in the de novo pathway is also an important step given the role of UMP as a controller for the activity of CPSase, the first step in the pathway. In addition, UMP is the step that connects nucleotide interconversion and salvage reutilization with de novo biosynthesis. Being at this junction, may help explain why the activity of ODCase, as shown in Figure 34, increased

by 1.7-fold 100 minutes following derepression; slightly less than any of the previous steps in the pathway. Although analysis of the nucleotide sequence of *pyrF* suggests that there is no attenuation mechanism involved in its expression, transcription of this gene is also coordinately controlled by the intracellular levels of pyrimidine nucleotide and responded accordingly to nutritional perturbation.

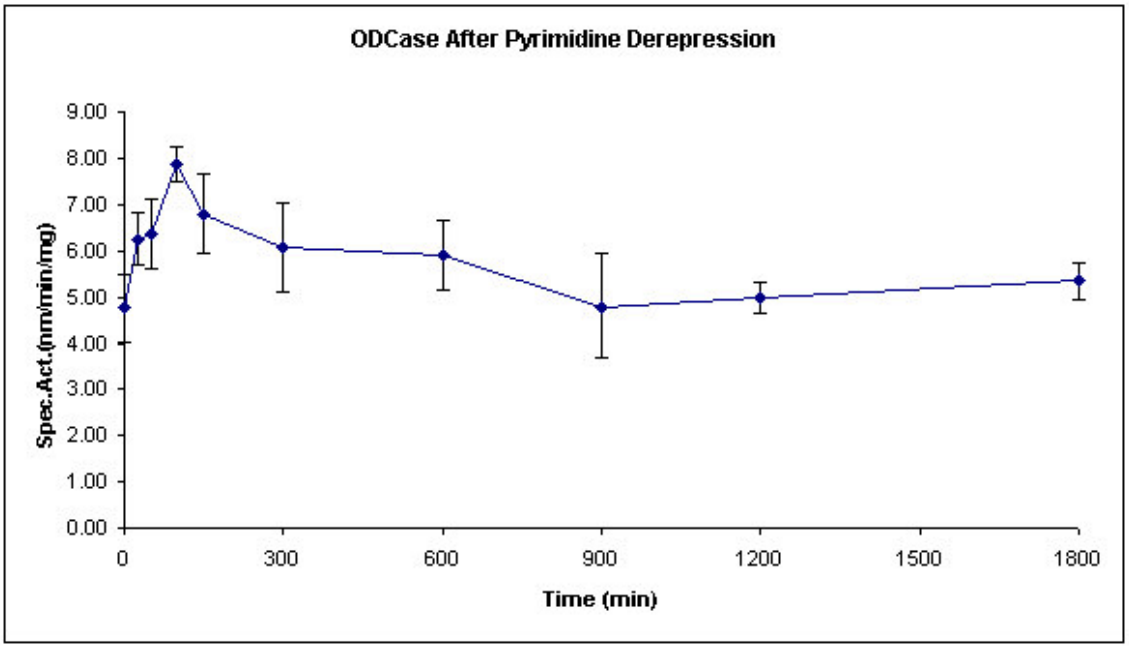

Figure 34. Dynamics of ODCase perturbation from steady state.

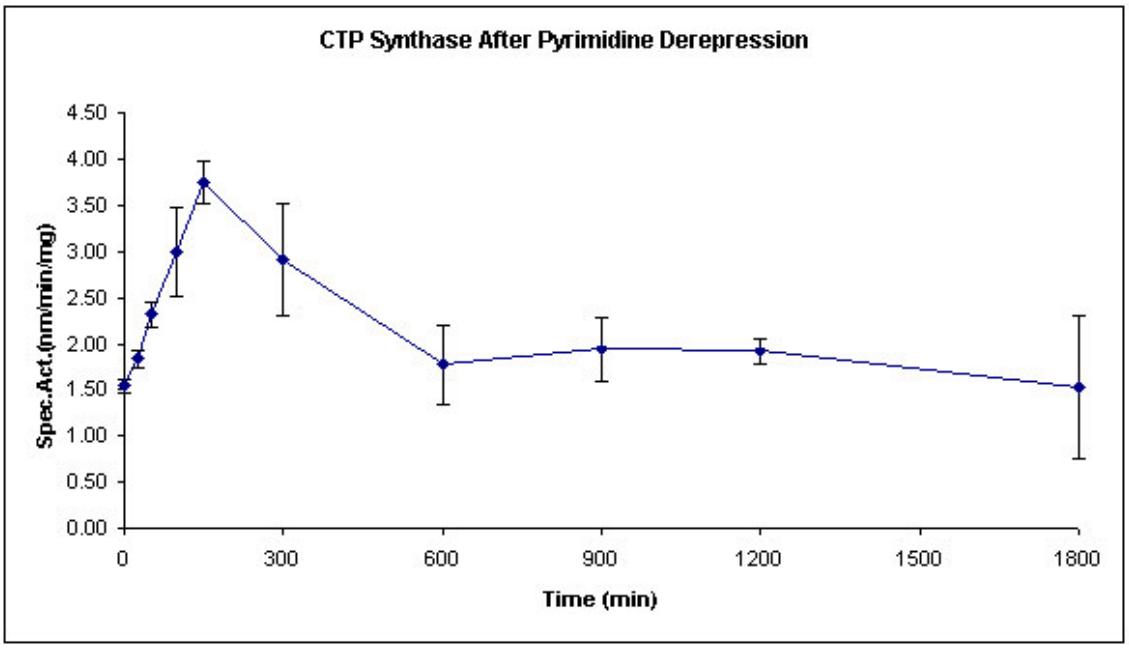

Figure 35. Dynamics of CTP synthase perturbation from steady state.

CTP Synthase Response. Synthesis of CTP was an interesting step to consider under this study given its key role in controlling the fate of the de novo products. CTP synthase is also allosterically regulated by ATP, CTP and GTP. The derepression change of CTP synthase activity was measured to be 2.4-fold within 150 minutes, as observed in Figure 35. The results obtained from the activity assays of this enzyme suggest that the response to nutritional perturbation may extend beyond the genes involved solely in de novo biosynthesis of pyrimidine nucleotides, into those involved in the accessory reactions of interconversion and salvage reutilization.

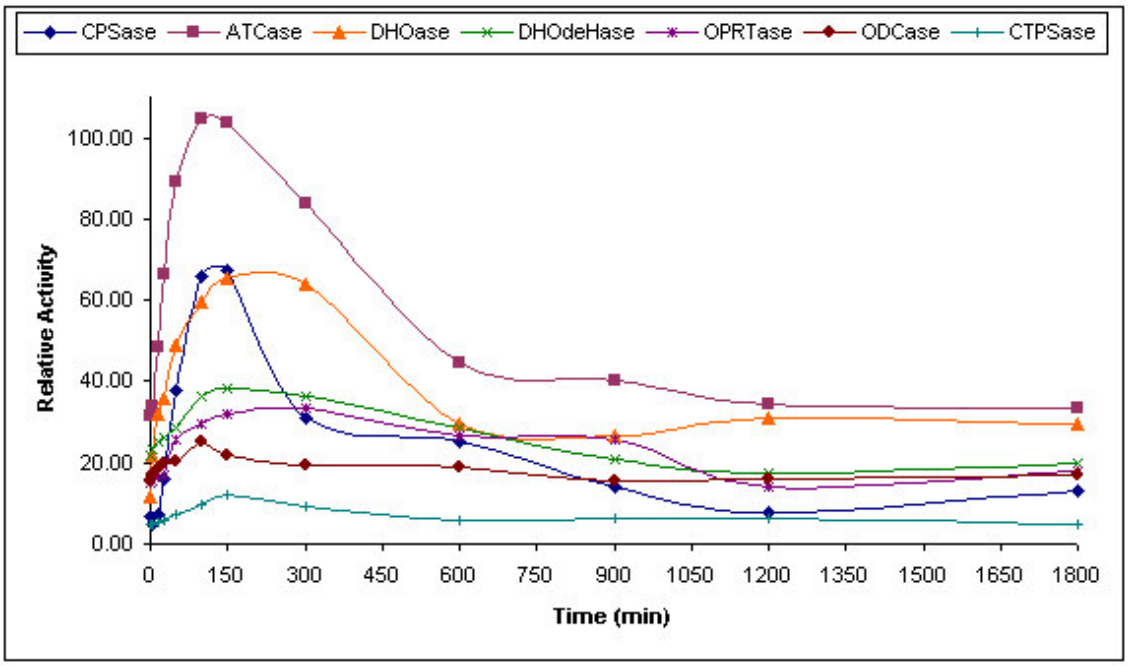

Figure 36. Comparative enzymatic response relative to ATCase.

Taken together, the results of the enzymatic assays suggest a larger role for the initial pathway steps in controlling the metabolic response than that of the latter steps. The reactions catalyzed by CPSase, ATCase and DHOase exhibited the greater change in activity. The activation seemed to be less dramatic for the remaining steps of the pathway. Interestingly, the first three steps in the pathway have evolved to become a single multi-activity enzymatic complex in higher eukaryotes. This supramolecular association may be a function of a significant role of these three enzymes in flux regulation, given their location within the pathway organization. The dynamics of enzymatic expression and activity correlated with the results obtained from NTP pools, both in extent and duration. ATCase had the largest activity level overall and a comparison of the activity of the enzymes relative to that of ATCase helps illustrate the

significance of the contribution of this enzyme in controlling metabolic readjustments (Figure 36). ATCase showed activity levels ranging from 4.5 to 20 times that of the other enzymes of the pathway (Table 8). CPSase, with derepression levels over 10-fold higher than repressed levels, showed a range of response larger than any other enzyme in the pathway. A question that arises concerns the control mechanism responsible for funneling the excess CP in the UMP versus the arginine biosynthesis direction. The answer may be in the coordinated control of all the enzymes within a pathway, as it is shown here to be the case for the *pyr* genes (Figure 37). On the other hand, it may also be the case that allosteric regulation of ATCase serves as a controller of how much CP goes to UMP formation, indirectly directing flux in both pathways. Regarding de novo pyrimidine biosynthesis, these results, together with the responses observed with NTP levels, provide the necessary information to construct a model of metabolic control that help us approach some of these questions.

Table 8. Enzymatic response to metabolic perturbation

Enzyme	Initial Conc. (mM)	Final Conc. (mM)	Minimal Conc. (mM)	Maximal Conc. (mM)	Time Min Conc. (min)	Time Max Conc. (min)	Fold increase
CPSase	2.06	4.09	2.45	21.12	0	150	10.3
ATCase	31.19	33.6	30.66	100	0, 15	150	3.8
DHOase	3.65	9.3	3.65	20.45	0	150	5.6
DHOdeHase	6.89	6.17	5.49	12	1200	150	2.2
OPRTase	4.69	5.62	4.44	10.40	0, 1200	300	2.3
ODCase	4.77	5.36	4.77	7.88	0, 1800	100	1.7
CTP Synthase	1.53	1.53	1.53	3.75	0, 1800	150	2.4

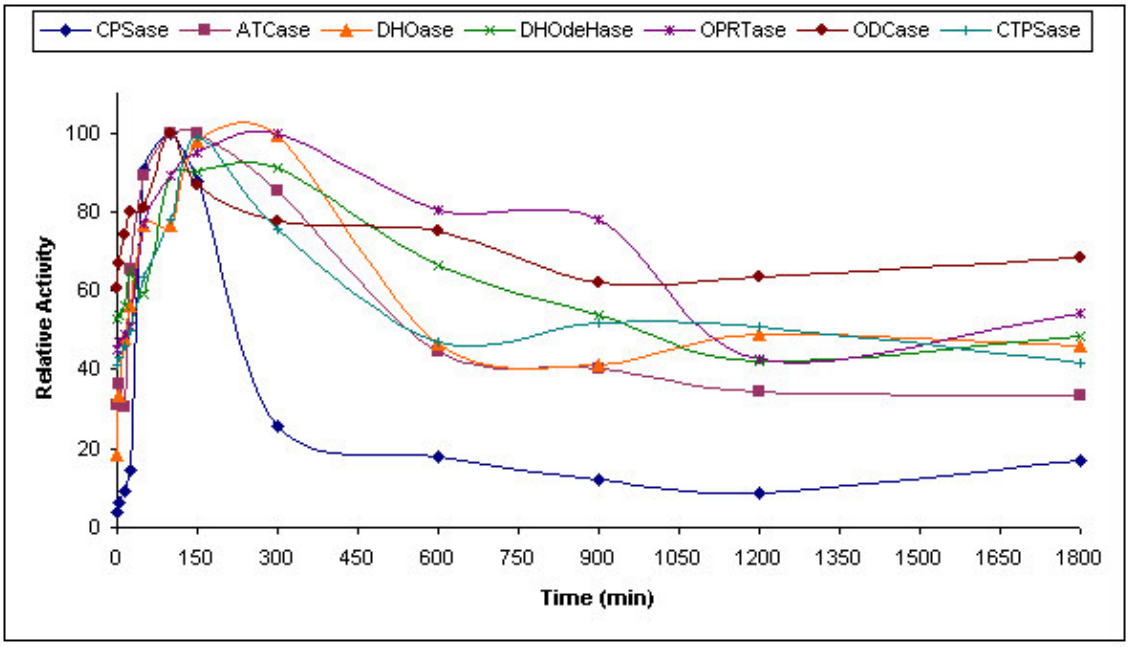

Figure 37. Profile of enzymatic activity following metabolic perturbation.

Model Flexibility to Varying Experimental Conditions

Following the studies of nutritional perturbation using batch cultures and the development of the mathematical formulation describing it, the chemostat-derived data provided important additional parameters. As a test of the robustness of the mathematical formulation of the pathway, the same model was used to determine whether it could describe the dynamic response observed at a lower growth rate in chemostat cultivation. As additional data had been obtained describing the dynamics of

enzymatic activation, several new equations were added to the initial model to include this information in the formulation of a second-generation model.

The second-generation model was formulated including the same equations and parameters defined for the initial model plus additional ones to describe the transcriptional response. Adjustment of the growth rate parameters was then sufficient to approximate the physiological response observed in the cells grown in chemostat at lower growth rate. Expressions for the pyrimidine-dependent enzyme synthesis and degradation were defined as

Equation 21

$$\frac{d[E_1]}{dt} = \frac{K_{e1}}{(K_{e1} + ump)} - k_{\deg 1} \times E_1 \times \frac{atp + atp}{gtp + utp} \times \frac{\frac{atp}{cdiv}}{\frac{greg \times ctp}{Kmg + ctp}} \times \frac{Kg}{grate}$$

Equation 22

$$\frac{d[E_2]}{dt} = \frac{K_{e2} \times 60}{(K_{e2} + ctp + ura)} - k_{\deg 2} \times E_2 \times \frac{atp + ctp}{gtp + utp} \times \frac{\frac{atp}{cdiv}}{\frac{greg \times ctp}{Kmg + ctp}} \times \frac{Kg}{grate}$$

where K_{e1} and K_{e2} are synthesis coefficients, and k_{deg1} and k_{deg2} are degradation coefficient for CPSase and ATCase, respectively, as described previously. Terms added

to these equations account for a description of additional genetic parameters involved in enzyme synthesis. Cell division, *cdiv*, is normalized to the energetic state of the cell, by describing it in association with ATP concentration. Two parameters, *greg* and *Kmg*, describe the transcriptional regulation dependence on intracellular CTP levels; whereas *grate* and *Kg* are an expression of the growth rate-dependence of the equation.

Analogous to equations 1 and 2, expressions for the transcriptional control of the remaining steps in the pathway were included

Equation 23

$$\frac{d[E_3]}{dt} = \frac{K_{e3}}{(K_{e3} + ctp + ura)} - k_{\deg 3} \times E_3 \times \frac{atp + ctp}{gtp + utp} \times \frac{\frac{atp}{cdiv}}{\frac{greg \times ctp}{Kmg + ctp}} \times \frac{Kg}{grate}$$

where E_3 represents the synthesis of DHOase while K_{e3} and k_{deg3} are the respective synthesis and degradations coefficients

Equation 24

$$\frac{d[E_4]}{dt} = \frac{K_{e4}}{(K_{e4} + ctp + ura)} - k_{\deg 4} \times E_4 \times \frac{atp + ctp}{gtp + utp} \times \frac{\frac{atp}{cdiv}}{\frac{greg \times ctp}{Kmg + ctp}} \times \frac{Kg}{grate}$$

where E_4 represents the synthesis of DHOdeHase while K_{e4} and k_{deg4} are the respective synthesis and degradations coefficients

Equation 25

$$\frac{d[E_5]}{dt} = \frac{K_{e5}}{(K_{e5} + utp + ura)} - k_{\deg 5} \times E_5 \times \frac{atp + ctp}{gtp + utp} \times \frac{\frac{atp}{cdiv}}{\frac{greg \times ctp}{Kmg + ctp}} \times \frac{Kg}{grate}$$

where E_5 represents the synthesis of OPRTase while K_{e5} and k_{deg5} are the respective synthesis and degradations coefficients

Equation 26

$$\frac{d[E_6]}{dt} = \frac{K_{e6}}{(K_{e6} + utp + ura)} - k_{\deg 6} \times E_6 \times \frac{atp + ctp}{gtp + utp} \times \frac{\frac{atp}{cdiv}}{\frac{greg \times ctp}{Kmg + ctp}} \times \frac{Kg}{grate}$$

where E_6 represents the synthesis of ODCase while K_{e6} and k_{deg6} are the respective synthesis and degradations coefficients.

Importantly, the K_{ei} values used corresponded to the derepression data obtained for each step in the pathway reported in Table 8. In addition, initial concentrations of the NTPs were adjusted proportionally using the values obtained from HPLC analyses. Table 9

summarizes the parameters added to those described for the first-generation model in the formulation of the second-generation model.

Table 9. List of parameters added in the second-generation model. Summary of the parameters used to define the equations modeling the transcriptional derepression on pyrimidine de novo biosynthesis in *E. coli*

Parameter	Definition	Value	Reference
Ke3	Synthesis rate coefficient for DHOase	5.6	This study
Ke4	Synthesis rate coefficient for DHOdeHase	2.2	This study
Ke5	Synthesis rate coefficient for OPRTase	2.3	This study
Ke6	Synthesis rate coefficient for ODCase	1.7	This study
Kdeg3	Degradation coefficient for DHOase	0.1	Estimated
Kdeg4	Degradation coefficient for DHOdeHase	0.1	Estimated
Kdeg5	Degradation coefficient for OPRTase	0.12	Estimated
Kdeg6	Degradation coefficient for ODCase	0.12	Estimated
greg	*pyr* gene regulation rate	0.4	Estimated
Kmg	*pyr* gene regulation coefficient	5.8	Estimated
gregb	*pur* gene regulation rate	0.78	Estimated
Kmgb	*pur* gene regulation coefficient	3.5	Estimated
cdiv	Cell division coefficient	2.3	Estimated
Vmax10	v_{max} for nucleoside diphosphate kinase (ATP)	2.37 mmol L^{-1}	Estimated
Km10	K_M for nucleoside diphosphate kinase (ATP)	12.3 mM	Estimated
Vmax11	v_{max} for nucleoside diphosphate kinase (GTP)	1.69 mmol L^{-1}	Estimated
Km11	K_M for nucleoside diphosphate kinase (GTP)	12.2 mM	Estimated

The second-generation model was then used in the simulation of derepression of NTP levels at lower growth rate and showed a behavior qualitatively similar to that observed experimentally (Figure 38). Quantitatively, the simulation showed also remarkable similarity to the experimental values without the need to readjust additional parameters for the rates of reactions.

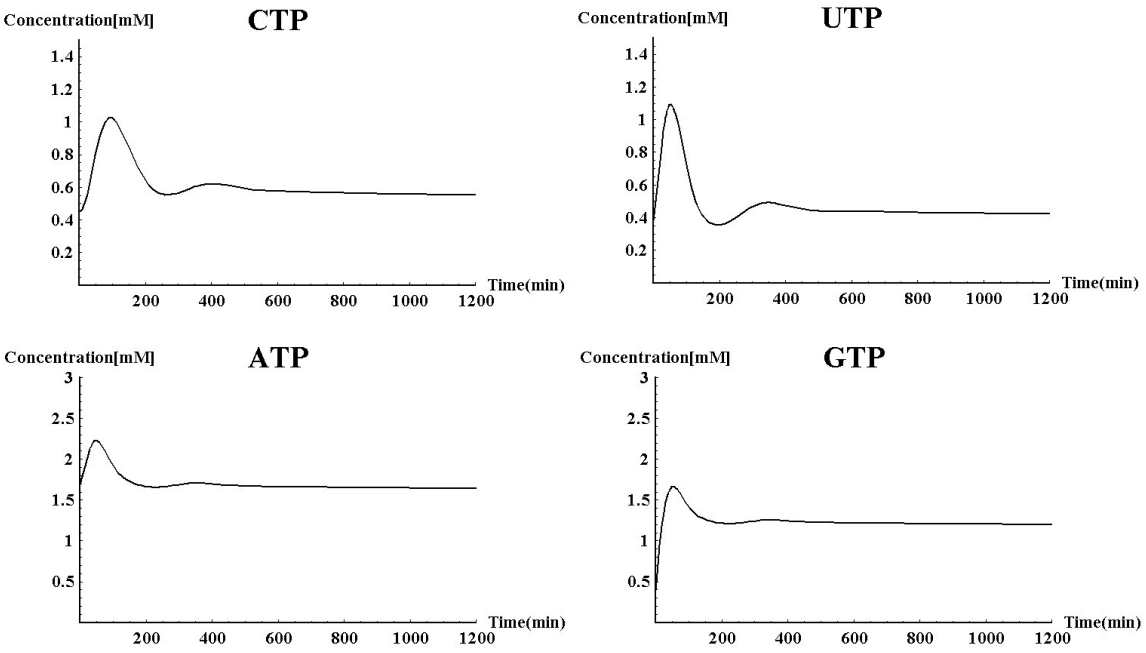

Figure 38. Simulation of NTP derepression at low growth rate.

Response of the enzymes involved in the pathway was also successfully simulated using the same model (Figure 39). The dynamics of derepression exhibited by the enzymes in the model was quantitatively similar to the experimental data (Table 10). These results provide significant support of the validity of the model, as they constitute a test of its descriptive value as well as an indication of its predictive power.

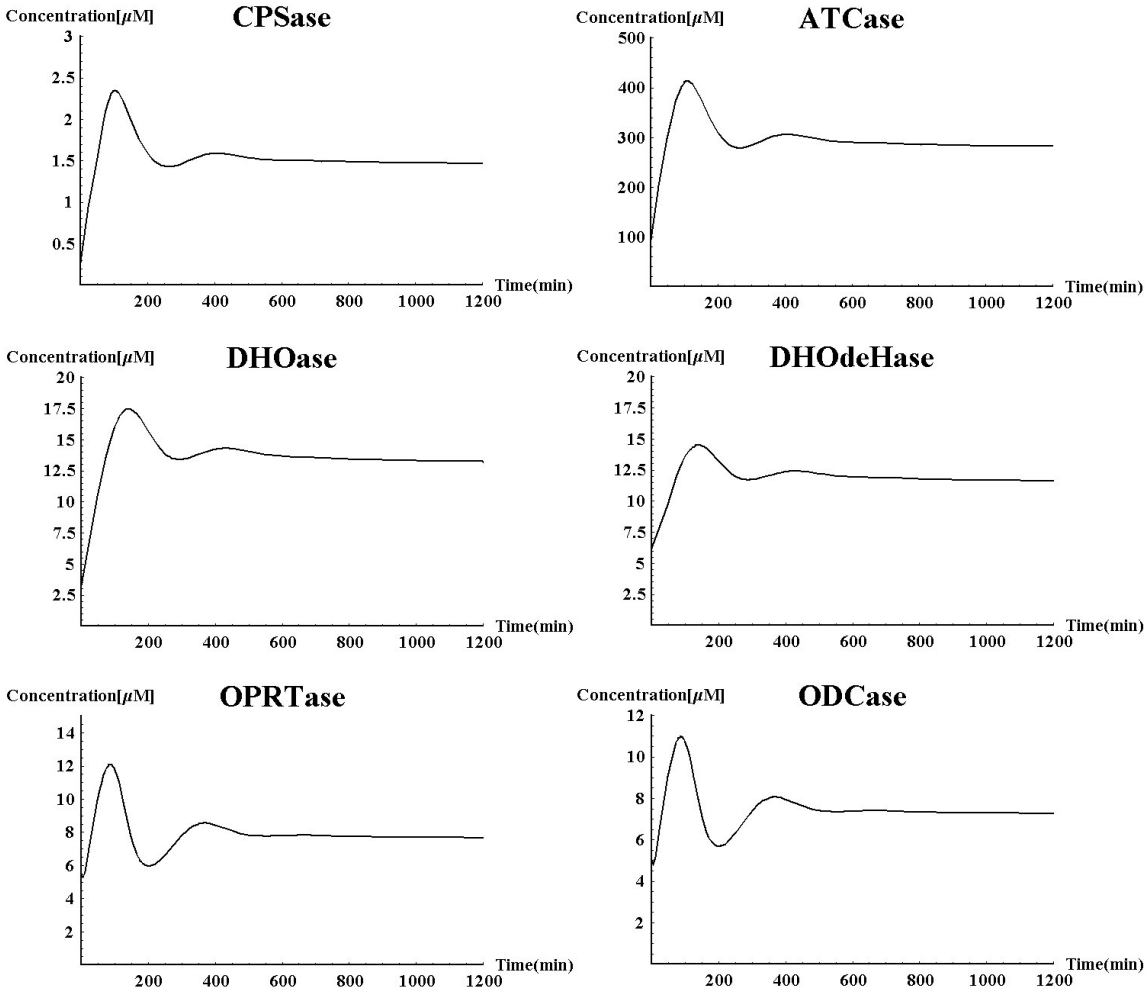

Figure 39. Simulation of enzymatic response following nutritional perturbation.

Table 10. Comparison of transcriptional derepression experimental vs. model

Enzyme	Derepression (Experimental)	Derepression (Model)
CPSase	10.3	8.4
ATCase	3.8	4.3
DHOase	5.6	5.3
DHOdeHase	2.2	2.3
OPRTase	2.3	2.1
ODCase	1.7	2.1

During the formulation of the first generation model, its inability to simulate precisely the dynamics of derepression of the UTP and CTP pools was noticed, as the measured recovery rate of the pools with allosterically regulated ATCase was slower compared to that seen for the unregulated enzyme. By including transcriptional control data into the second-generation model, which allowed the refinement of the previous simulations, the model is now capable of simulating the dynamics of both the variation (allosteric control) and speed of recovery (transcriptional derepression). Figure 40 shows the comparison of the data obtained experimentally (Figure 40A) to the simulations using the first (Figure 40B) and second-generation models (Figure 40C).

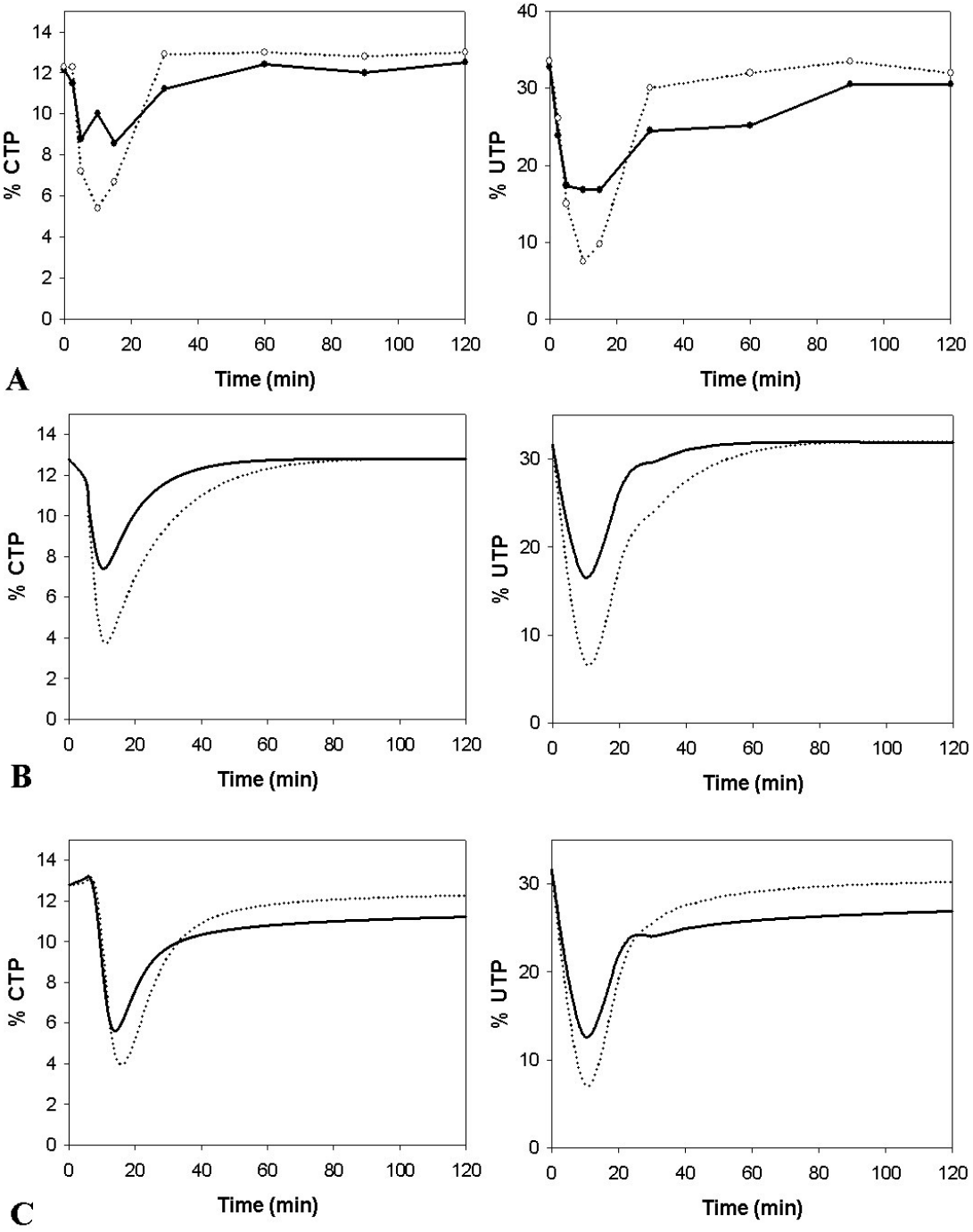

Figure 40. Simulation of allosteric only (B) or allosteric and transcriptional (C) controls following nutritional perturbation compared to experimental data (A).

One of the objectives driving the formulation of a model of metabolic control is to develop the ability to make biochemically sound predictions of important features and the role of individual components in maintaining overall biosynthetic control in the cell. The model of metabolic control presented here provides a greater understanding of the control of a biosynthetic pathway and represents a departure from reductionist investigations of isolated components that overlook the importance of the interaction and interdependence of the multiple components. As such, it is desirable to use a model like the one developed for this study in the formulation of hypotheses that can help lead the direction of future research that expands understanding of interactive regulatory networks. The model of control of de novo biosynthesis of pyrimidines presents the opportunity to look at such interactions, as it intersects with the process of arginine biosynthesis in *E. coli*. The first enzyme of this pathway, CPSase, produces an essential metabolite for the production of arginine and pyrimidines, carbamoyl phosphate (CP). A fundamental question that remains in the interaction of the two pathways that compete for the allocation of CP is what regulates the distribution of CP towards each pathway. Using the model, the dynamics at each step along the pathway can be dissected. By examining the first two reactions for the formation of CP and CA (carbamoyl aspartate), it was possible to observe their dynamics following the nutritional perturbation and transition back to steady state levels (Figure 41A). Eliminating allosteric control from ATCase in the model by removing the terms that account for this type of regulation, leaving all other parameters unchanged, provides an interesting view of its effect.

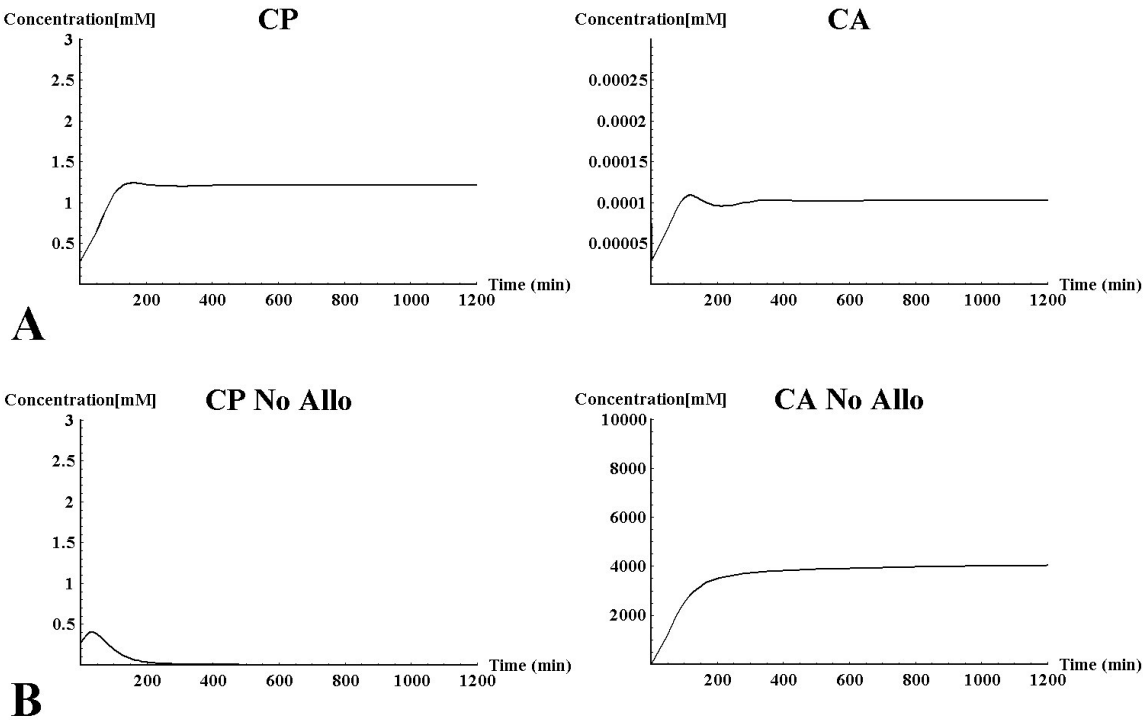

Figure 41. Theoretical prediction of the role of allosteric control in directing the allocation of resources between branching biochemical pathways. (A), Allosterically regulated ATCase. (B) Unregulated ATCase.

The levels of CA increase several thousand-fold before regaining steady state, whereas those of its precursor metabolite, CP, drop significantly before reaching steady state (Figure 41B). An interesting hypothesis from these findings relates to the role of allosteric regulation in controlling not only the fate of pyrimidine biosynthesis, but also that of allocation of an important metabolite between the competing pathways. It is likely based on what is known about both pathways that ATCase plays such a role in directing traffic at this biochemical intersection. The three steps downstream from CPSase in the direction of arginine biosynthesis lack the allosteric regulation present in

ATCase along the pyrimidine biosynthesis route. Several experiments can be designed from these observations, including the responses to nutritional perturbation from *E. coli* mutants defective in the allosteric regulation of both ATCase and CPSase.

Given the wealth in amount and quality of the biochemical experimental data used in the formulation of this model, it constitutes an important approximation to a quantitative understanding of the contribution of allosteric and transcriptional mechanisms in achieving cellular metabolic control. Scholarly utilization of this model of metabolic control will contribute to the development and testing of hypotheses concerning the mechanisms used by the cell to regulate production of metabolites that are energy intensive. Our ability to make predictions of the outcomes of manipulating related cellular processes should be greatly enhanced.

CHAPTER V

CONCLUSIONS

Evolution has selected the framework of genetic, biochemical and regulatory signals that bring about success in life; at least success at the cellular level. There coexist in any cell, distinct levels of networks interacting through nonlinear and, perhaps, even stochastic processes of thousands of molecules. Such an array of complex associations fulfills the ultimate goal of providing the cell the adaptability it needs to execute its functions in an ever-unpredictable environment. In order to be able to understand successful cellular function, one needs to recognize the communication among the different types of cellular signals. Metabolic control is such communication process, as it is defined by the regulatory properties of the cellular networks.

There are common regulatory properties that are recurrent on most metabolic processes, including those signals that act upon genes or directly on the enzymes catalyzing biochemical reactions. The most frequent mode of controlling gene networks involves coordinated regulation of transcription, whereas enzymatic regulation almost invariably follows the topology of feedback inhibition.

An ideal model for the study metabolic control is represented in *Escherichia coli* by the de novo biosynthetic pathway of pyrimidine nucleotides. The genes encoding all of the enzymes participating in this pathway have been characterized and cloned. The mechanisms and structures of the enzymes themselves have been resolved, as has been the nature of the regulatory signals controlling the allosteric steps. This pathway exhibits coordinated regulation of gene expression, transcriptional attenuation, feedback inhibition and pathway branching. Extensive amount of scientific literature has documented most of what is technically possible to know about the individual components of this pathway. Still missing is a more comprehensive view of the interplay among metabolites, enzymes, genes and signal molecules that results in sustainable production of pyrimidines.

The studies described in this dissertation provide a framework for understanding how cells coordinate central metabolic processes. Dynamic analyses of metabolic repression and derepression were used to dissect the regulatory components and to quantify their contribution in maintaining cellular homeostasis. Flux of metabolites was used to visualize and quantify the efficiency of transcriptional and allosteric regulation in restoring intracellular balance. The activities of all the enzymes involved in the pathway were measured to determine in vivo responses following metabolic perturbation. The experimental information gathered was analyzed using arrays of differential equations to yield a new way of understanding the deterministic balance provided to the cell by

metabolic control. The mathematical description was validated to establish its predictive value.

Analyses of intracellular nucleotide pools served to demonstrate the partitioning of metabolic control, evidencing how the regulation of gene expression affects the response of rapidly growing cells. Relative levels of UTP and CTP dropped within a few minutes after uracil depletion, while the transcription, translation and biosynthetic processes were activated; allosteric inhibition was promptly relieved to help maintain physiologically safe levels. A different behavior was detected when the cells were doubling more slowly. Both UTP and CTP seemed to accumulate, presumably as an effect of a temporarily increased output produced by the activation of the pathway; physiological levels were restored once the activities of transcriptional and allosteric controls regained balance.

Assays of enzymatic activity provided supporting evidence of the type of response, as fluctuation in the amount of enzymes expressed correlated with the measurement of end products. Initial overexpression of the Pyr enzymes was reflected in increased UTP and CTP levels; once the amounts of enzymes reached balanced active levels, metabolic output returned to steady state concentration.

The mathematical formulation of this processes, faithfully simulated metabolic flux as well as allosteric and transcriptional responses. We anticipate that this mathematical description will continue to improve and “evolve” as more input becomes available

through experimentation. In turn, the mathematical model will help in the selection and design of the experiments to be performed, such as an investigation into the role of allosteric regulation in controlling metabolic flux across branched pathways. Iterations of this process should help speed up data acquisition and analysis for this and, we expect, other biosynthetic pathways in *Escherichia coli* and other cellular organisms.

REFERENCES

1. **Allen, T. E., M. J. Herrgard, M. Liu, Y. Qiu, J. D. Glasner, F. R. Blattner, and B. O. Palsson**. 2003. Genome-scale analysis of the uses of the *Escherichia coli* genome: model-driven analysis of heterogeneous data sets. J.Bacteriol **185**:6392-6399.

2. **Alvarez-Vasquez, F., M. Canovas, J. L. Iborra, and N. V. Torres**. 2002. Modeling, optimization and experimental assessment of continuous L-(-)-carnitine production by *Escherichia coli* cultures. Biotechnol.Bioeng. **80**:794-805.

3. **Andersen, J. T., K. F. Jensen, and P. Poulsen**. 1991. Role of transcription pausing in the control of the *pyrE* attenuator in *Escherichia coli.* Mol.Microbiol. **5**:327-333.

4. **Andersen, J. T., P. Poulsen, and K. F. Jensen**. 1992. Attenuation in the *rph-pyrE* operon of *Escherichia coli* and processing of the dicistronic mRNA. Eur.J.Biochemistry **206**:381-390.

5. **Bachmann, B. J.** 1987. Derivations and Genotypes of some Mutant Derivatives of *Escherichia coli* K-12. *In* F. C. Neidhardt (ed.), *Escherichia coli* and *Salmonella typhimurium*. Cellular and Molecular Biology. American Society for Microbiology, Washington, DC.

6. **Beale, E. M. L.** 1988. Introduction to Optimization. Wiley, New York.

7. **Bonekamp, F., K. Clemmesen, O. Karlstrom, and K. F. Jensen**. 1984. Mechanism of UTP-modulated attenuation at the *pyrE* gene of *Escherichia coli*: an example of operon polarity control through the coupling of translation to transcription. EMBO J. **3**:2857-2861.

8. **Bouvier, J., J. C. Patte, and P. Stragier**. 1984. Multiple regulatory signals in the control region of the *Escherichia coli carAB* operon. Proc.Natl.Acad.Sci.USA **81**:4139-4143.

9. **Bower, S. G., B. Hove-Jensen, and R. L. Switzer**. 1988. Structure of the gene encoding phosphoribosylpyrophosphate synthetase (*prsA*) in *Salmonella typhimurium*. J.Bacteriol **170**:3243-3248.

10. **Bremer, H., P. Dennis, and M. Ehrenberg**. 2003. Free RNA polymerase and modeling global transcription in *Escherichia coli*. Biochimie **85**:597-609.

11. **Brown, D. C. and K. D. Collins**. 1991. Dihydroorotase from *Escherichia coli*. Substitution of Co(II) for the active site Zn(II). J.Biol.Chem. **266**:1597-1604.

12. **Charlier, D., D. Gigot, N. Huysveld, M. Roovers, A. Piérard, and N. Glansdorff**. 1995. Pyrimidine regulation of the *Escherichia coli* and *Salmonella typhimurium carAB* operons: CarP and integration host factor (IHF) modulate the methylation status of a GATC site present in the control region. J.Mol.Biol. **250**:383-391.

13. **Charlier, D., G. Hassanzadeh Gh., A. Kholti, D. Gigot, A. Piérard, and N. Glansdorff**. 1995. *carP*, involved in pyrimidine regulation of the *Escherichia coli* carbamoylphosphate synthetase operon encodes a sequence- specific DNA-binding protein identical to XerB and PepA, also required for resolution of ColEI multimers. J.Mol.Biol. **250**:392-406.

14. **Charlier, D., M. Roovers, D. Gigot, N. Huysveld, A. Pierard, and N. Glansdorff**. 1993. Integration host factor (IHF) modulates the expression of the pyrimidine-specific promoter of the *carAB* operons of *Escherichia coli* K12 and *Salmonella typhimurium* LT2. Mol.Gen.Genet. **237**:273-286.

15. **Cheney W. and D. Kincaid**. 1994. Locating Roots of Equations, p. 82-118. *In* Numerical Mathematics and Computing. Brooks/Cole Publishing Company, Pacific Grove, CA.

16. **Choi, K. Y. and H. Zalkin**. 1990. Regulation of *Escherichia coli pyrC* by the purine regulon repressor protein. J.Bacteriol. **172**:3201-3207.

17. **Christopherson, R. I. and L. R. Finch**. 1978. Response of the pyrimidine pathway of *Escherichia coli* K12 to exogenous adenine and uracil. Eur.J.Biochem. **90**:347-358.

18. **Coleman, P. F., D. P. Suttle, and G. R. Stark**. 1977. Purification from hamster cells of the multifunctional protein that initiates de novo synthesis of pyrimidine nucleotides. J.Biol.Chem. **252**:6379-6385.

19. **Cornish-Bowden, A.** 1997. New Beer in an Old Bottle: Eduard Buchner and the Growth of Biochemical Knowledge. Universitat de Valencia, Valencia, Spain.

20. **Covert, M. W. and B. O. Palsson**. 2002. Transcriptional regulation in constraints-based metabolic models of *Escherichia coli*. J.Biol.Chem. **277**:28058-28064.

21. **Donahue, J. P. and C. L. Turnbough, Jr.** 1994. Nucleotide-specific transcriptional pausing in the *pyrBI* leader region of *Escherichia coli* K-12. J.Biol.Chem. **269**:18185-18191.

22. **Donovan, W. P. and S. R. Kushner**. 1983. Purification and characterization of orotidine-5'-phosphate decarboxylase from *Escherichia coli* K-12. J.Bacteriol. **156**:620-624.

23. **England, P. and G. Hervé**. 1993. Synergistic inhibition of *Escherichia coli* aspartate transcarbamylase by CTP and UTP: binding studies using continuous-flow dialysis. Biochemistry **31**:9725-9732.

24. **Forster, J., I. Famili, P. Fu, B. O. Palsson, and J. Nielsen**. 2003. Genome-scale reconstruction of the *Saccharomyces cerevisiae* metabolic network. Genome Res. **13**:244-253.

25. **Gerhart, J. C. and A. B. Pardee**. 1962. The enzymology of control by feedback inhibition. J.Biol.Chem. **237**:891-896.

26. **Gollnick, P. and P. Babitzke**. 2002. Transcription attenuation. Biochim.Biophys.Acta **1577**:240-250.

27. **Han, K., H. C. Lim, and J. Hong**. 1992. Acetic-acid formation in *Escherichia coli* fermentation. Biotechnology and Bioengineering **39**:663-671.

28. **Han, X. and C. L. Turnbough, Jr.** 1998. Regulation of *carAB* expression in *Escherichia coli* occurs in part through UTP-sensitive reiterative transcription. J.Bacteriol. **180**:705-713.

29. **Hansen, F. G., B. B. Christensen, and T. Atlung**. 1991. The initiator titration model: computer simulation of chromosome and minichromosome control. Res.Microbiol. **142**:161-167.

30. **Harris, P., J. C. Navarro Poulsen, K. F. Jensen, and S. Larsen**. 2000. Structural basis for the catalytic mechanism of a proficient enzyme: orotidine 5'-monophosphate decarboxylase. Biochemistry **39**:4217-4224.

31. **Harris, P., J. C. Poulsen, K. F. Jensen, and S. Larsen**. 2002. Substrate binding induces domain movements in orotidine 5'-monophosphate decarboxylase. J.Mol.Biol. **318**:1019-1029.

32. **Henriksen, A., N. Aghajari, K. F. Jensen, and M. Gajhede**. 1996. A flexible loop at the dimer interface is a part of the active site of the adjacent monomer of *Escherichia coli* orotate phosphoribosyltransferase. Biochemistry **35**:3803-3809.

33. **Hoffmann, F., J. Weber, and U. Rinas**. 2002. Metabolic adaptation of *Escherichia coli* during temperature-induced recombinant protein production: 1. Readjustment of metabolic enzyme synthesis. Biotechnol.Bioeng. **80**:313-319.

34. **Holden, C.** 2002. Cell biology. Alliance launched to model *E. coli*. Science **297**:1459-1460.

35. **Holden, H. M., J. B. Thoden, and F. M. Raushel**. 1999. Carbamoyl phosphate synthetase: an amazing biochemical odyssey from substrate to product. [Review]. Cellular & Molecular Life Sciences **56**:507-522.

36. **Hua, P. J.** 1994. Physiological evaluation of the role of aspartate transcarbamoylase in the pyrimidine pathway. Doctoral Dissertation. Texas A&M University, College Station, TX.

37. **Ingraham, J. L. and A. T. Abdelal**. 1978. Carbamoyl-phosphate synthetase (glutamine): *Salmonella*. Methods Enzymol. **51:29-35**:29-35.

38. **Jakubowski, H.** 1995. Proofreading in vivo. Editing of homocysteine by aminoacyl-tRNA synthetases in *Escherichia coli*. J.Biol.Chem. **270**:17672-17673.

39. **James, C. L. and R. E. Viola**. 2002. Production and characterization of bifunctional enzymes. Substrate channeling in the aspartate pathway. Biochemistry **41**:3726-3731.

40. **Jensen, K. F., J. N. Larsen, L. Schack, and A. Sivertsen**. 1984. Studies on the structure and expression of *Escherichia coli pyrC*, *pyrD*, and *pyrF* using the cloned genes. Eur.J.Biochem. **140**:343-352.

41. **Joseleau-Petit, D., D. Vinella, and R. D'Ari**. 1999. Metabolic alarms and cell division in *Escherichia coli*. J.Bacteriol **181**:9-14.

42. **Kantrowitz, E. R. and W. N. Lipscomb**. 1990. *Escherichia coli* aspartate transcarbamoylase: the molecular basis for a concerted allosteric transition. TIBS **15**:53-59.

43. **Karibian, D.** 1978. Dihydroorotate dehydrogenase (*Escherichia coli*). Methods Enzymol. **51**:58-63.

44. **Kayser, A., J. Weber, V. Hecht, and U. Rinas**. 2005. Metabolic flux analysis of *Escherichia coli* in glucose-limited continuous culture. I. Growth-rate-dependent metabolic efficiency at steady state. Microbiology **151**:693-706.

45. **Ke, H., W. N. Lipscomb, Y. Cho, and R. B. Honzatko**. 1988. Complex of N-phosphonacetyl-L-aspartate with aspartate transcarbamoylase: X-ray refinements, analysis of conformational changes and catalytic and allosteric mechanism. J.Mol.Biol. **204**:725-747.

46. **Kelln, R. A., J. J. Kinahan, K. F. Foltermann, and G. O'Donovan**. 1975. Pyrimidine biosynthetic enzymes of *Salmonella typhimurium*, repressed specifically by growth in the presence of cytidine. J.Bacteriol. **124**:764-774.

47. **Keseler, I. M., J. Collado-Vides, S. Gama-Castro, J. Ingraham, S. Paley, I. T. Paulsen, M. Peralta-Gill, and P. D. Karp**. 2005. EcoCyc: a comprehensive database resource for *Escherichia coli*. Nucleic Acids Res. **33**:D334-D337.

48. **Koch, A. L.** 1971. The adaptive responses of *Escherichia coli* to a feast and famine existence. Adv.Microb.Physiol **6**:147-217.

49. **Koh, B. T., R. B. Tan, and M. G. Yap**. 1998. Genetically structured mathematical modeling of trp attenuator mechanism. Biotechnol.Bioeng. **58**:502-509.

50. **Kosman, R. P., J. E. Gouaux, and W. N. Lipscomb**. 1993. Crystal structure of CTP-ligated T state aspartate transcarbamoylase at 2.5 Å resolution: implications for ATCase mutants and the mechanism of negative cooperativity. Proteins **15**:147-176.

51. **Kramer, M., J. Bongaerts, R. Bovenberg, S. Kremer, U. Muller, S. Orf, M. Wubbolts, and L. Raeven**. 2003. Metabolic engineering for microbial production of shikimic acid. Metab.Eng **5**:277-283.

52. **Krause, K. L., K. W. Volz, and W. N. Lipscomb**. 1985. Structure at 2.9-Å resolution of aspartate carbamoyltransferase complexed with the bisubstrate analogue N-(phosphonacetyl)-L-aspartate. Proc.Natl.Acad.Sci.USA **82**:1643-1647.

53. **Lee, S. Y., S. H. Hong, and S. Y. Moon**. 2002. In silico metabolic pathway analysis and design: succinic acid production by metabolically engineered *Escherichia coli* as an example. Genome Inform.Ser.Workshop **13**:214-223.

54. **Lengeler, J. W., G. Drews, and H. G. Schlegel**. 1999. Biology of the Prokaryotes. Blackwell Science Ltd., Stuttgart, Germany.

55. **LiCata, V. J. and N. M. Allewell**. 1997. Is substrate inhibition a consequence of allostery in aspartate transcarbamylase?. Biophys.Chem. **64**:225-234.

56. **Liu, C., J. P. Donahue, L. S. Heath, and C. L. Turnbough, Jr.** 1993. Genetic evidence that promoter P_2 Is the physiologically significant promoter for the *pyrBI* operon of *Escherichia coli* K-12. J.Bacteriol. **175**:2363-2369.

57. **Liu, J. and C. L. Turnbough, Jr.** 1994. Identification of the Shine-Dalgarno sequence required for expression and translational control of the *pyrC* gene in *Escherichia coli* K-12. J.Bacteriol. **176**:2513-2516.

58. **Liu, S., E. A. Neidhardt, T. H. Grossman, T. Ocain, and J. Clardy**. 2000. Structures of human dihydroorotate dehydrogenase in complex with antiproliferative agents. Structure Fold.Des **8**:25-33.

59. **Lue, P. F. and J. G. Kaplan**. 1970. Metabolic compartmentation at the molecular level: the function of a multienzyme aggregate in the pyrimidine pathway of yeast. Biochim.Biophys.Acta **220**:365-372.

60. **Macol, C. P., H. Tsuruta, B. Stec, and E. R. Kantrowitz**. 2001. Direct structural evidence for a concerted allosteric transition in *Escherichia coli* aspartate transcarbamoylase. Nature Struct.Biol. **8**:423-426.

61. **Maher, A. D., P. W. Kuchel, F. Ortega, P. de Atauri, J. Centelles, and M. Cascante**. 2003. Mathematical modelling of the urea cycle. A numerical investigation into substrate channelling. Eur.J.Biochem. **270**:3953-3961.

62. **Makoff, A. J. and A. Radford**. 1978. Genetics and biochemistry of carbamoyl phosphate biosynthesis and its utilization in the pyrimidine biosynthetic pathway. Microbiological Reviews **42**:307-328.

63. **Monaco, H. L., J. L. Crawford, and W. N. Lipscomb**. 1978. Three dimensional structure of aspartate carbamoyltransferase from *Escherichia coli* and of its complex with cytidine triphosphate. Proc.Natl.Acad.Sci.USA **75**:5276-5280.

64. **Mulquiney, P. J. and P. W. Kuchel**. 2003. Modeling Metabolism with Mathematica. CRC Press, Boca Raton, FL.

65. **Munch-Petersen, A. and J. Neuhard**. 1964. Studies on the acid-soluble nucleotide pool in thymine-requiring mutants of *Escherichia coli* during thymine starvation. Accumulation of deoxyadenosine triphosphate in *Escherichia coli* 15 T.A.U. Biochim.Biophys.Acta **80**:542-551.

66. **Neidhardt, F. C., J. L. Ingraham, and M. Schaechter**. 1990. Physiology of the Bacterial Cell. Sinauer Associates, Inc., Sunderland, MA.

67. **Norager, S., K. F. Jensen, O. Bjornberg, and S. Larsen**. 2002. *E. coli* dihydroorotate dehydrogenase reveals structural and functional distinctions between different classes of dihydroorotate dehydrogenases. Structure (Camb.) **10**:1211-1223.

68. **Ogata, H., S. Goto, K. Sato, W. Fujibuchi, H. Bono, and M. Kanehisa**. 1999. KEGG: Kyoto Encyclopedia of Genes and Genomes. Nucleic Acids Res. **27**:29-34.

69. **Palfey, B. A., O. Bjornberg, and K. F. Jensen**. 2001. Insight into the chemistry of flavin reduction and oxidation in *Escherichia coli* dihydroorotate dehydrogenase obtained by rapid reaction studies. Biochemistry **40**:4381-4390.

70. **Pierard, A., N. Glansdorff, and J. Yashphe**. 1972. Mutations affecting uridine monophosphate pyrophosphorylase or the *argR* gene in *Escherichia coli*. Effects on carbamoyl phosphate and pyrimidine biosynthesis and on uracil uptake. Mol.Gen.Genet. **118**:235-245.

71. **Piette, J., H. Nyunoya, C. J. Lusty, R. Cunin, G. Weyens, M. Crabeel, D. Charlier, N. Glansdorff, and A. Pierard**. 1984. DNA sequence of the *carA* gene and the control region of *carAB*: tandem promoters, respectively controlled by arginine and the pyrimidines, regulate the synthesis of carbamoyl-phosphate synthetase in *Escherichia coli* K-12. Proc.Natl.Acad.Sci.USA **81**:4134-4138.

72. **Pogliano, K., J. Pogliano, and E. Becker**. 2003. Chromosome segregation in Eubacteria. Curr.Opin.Microbiol **6**:586-593.

73. **Poulsen, P., F. Bonekamp, and K. F. Jensen**. 1984. Structure of the *Escherichia coli pyrE* operon and control of *pyrE* expression by a UTP modulated intercistronic attentuation. EMBO J. **3**:1783-1790.

74. **Purcarea, C., D. R. Evans, and G. Hervé**. 1999. Channeling of carbamoyl phosphate to the pyrimidine and arginine biosynthetic pathways in the deep sea hyperthermophilic archaeon *Pyrococcus abyssi*. J.Biol.Chem. **274**:6122-6129.

75. **Radzicka, A. and R. Wolfenden**. 1995. A proficient enzyme. Science **267**:90-93.

76. **Raghunathan, A., N. D. Price, M. Y. Galperin, K. S. Makarova, S. Purvine, A. F. Picone, T. Cherny, T. Xie, T. J. Reilly, R. Munson, Jr., R. E. Tyler, B. J. Akerley, A. L. Smith, B. O. Palsson, and E. Kolker**. 2004. In silico metabolic model and protein expression of *Haemophilus influenzae* strain Rd KW20 in rich medium. OMICS. **8**:25-41.

77. **Raushel, F. M., J. B. Thoden, and H. M. Holden**. 1999. The amidotransferase family of enzymes: molecular machines for the production and delivery of ammonia. Biochemistry **38**:7891-7899.

78. **Reed, J. L. and B. O. Palsson**. 2004. Genome-scale in silico models of *E. coli* have multiple equivalent phenotypic states: assessment of correlated reaction subsets that comprise network states. Genome Res. **14**:1797-1805.

79. **Reed, J. L., T. D. Vo, C. H. Schilling, and B. O. Palsson**. 2003. An expanded genome-scale model of *Escherichia coli* K-12 (iJR904 GSM/GPR). Genome Biol. **4**:R54.

80. **Ricard, J. and A. Cornish-Bowden**. 1987. Co-operative and allosteric enzymes: 20 years on. Eur.J.Biochem. **166**:255-272.

81. **Robin, J. P., B. Penverne, and G. Hervé**. 1989. Carbamoyl phosphate biosynthesis and partition in pyrimidine and arginine pathways of *Escherichia coli*. In situ properties of carbamoyl-phosphate synthase, ornithine transcarbamylase and aspartate transcarbamylase in permeabilized cells. Eur.J.Biochem. **183**:519-528.

82. **Rodriguez, M., T. A. Good, M. E. Wales, J. P. Hua, and J. R. Wild**. 2005. Modeling allosteric regulation of de novo pyrimidine biosynthesis in *Escherichia coli*. J Theor.Biol. **234**:299-310.

83. **Rohwer, J. M., P. W. Postma, B. N. Kholodenko, and H. V. Westerhoff**. 1998. Implications of macromolecular crowding for signal transduction and metabolite channeling. Proc.Natl.Acad.Sci.USA **95**:10547-10552.

84. **Rubino, S. D., H. Nyunoya, and C. J. Lusty**. 1986. Catalytic domains of carbamyl phosphate synthetase - glutamine-hydrolyzing site of *Escherichia coli* Carbamyl-Phosphate Synthetase. J.Biol.Chem. **261**:1320-1327.

85. **Rudolph, J. and J. Stubbe**. 1995. Investigation of the mechanism of phosphoribosylamine transfer from glutamine phosphoribosylpyrophosphate amidotransferase to glycinamide ribonucleotide synthetase. Biochemistry **34**:2241-2250.

86. **Sander, E. G. and M. J. Heeb**. 1971. Purification and properties of dihydroorotase from *Escherichia coli* B. Biochim.Biophys.Acta **227**:442-452.

87. **Scapin, G., C. Grubmeyer, and J. C. Sacchettini**. 1994. Crystal structure of orotate phosphoribosyltransferase. Biochemistry **33**:1287-1294.

88. **Scapin, G., J. C. Sacchettini, A. Dessen, M. Bhatia, and C. Grubmeyer**. 1993. Primary structure and crystallization of orotate phosphoribosyltransferase from *Salmonella typhimurium*. J.Mol.Biol. **230**:1304-1308.

89. **Schilling, C. H., M. W. Covert, I. Famili, G. M. Church, J. S. Edwards, and B. O. Palsson**. 2002. Genome-scale metabolic model of *Helicobacter pylori* 26695. J.Bacteriol. **184**:4582-4593.

90. **Schlosser, P. M. and J. E. Bailey**. 1990. An integrated modeling-experimental strategy for the analysis of metabolic pathways. Math.Biosci. **100**:87-114.

91. **Schwartz, M. and J. Neuhard**. 1975. Control of expression of the pyr genes in *Salmonella typhimurium*: effects of variations in uridine and cytidine nucleotide pools. J.Bacteriol. **121**:814-822.

92. **Segre, D., J. Zucker, J. Katz, X. Lin, P. D'Haeseleer, W. P. Rindone, P. Kharchenko, D. H. Nguyen, M. A. Wright, and G. M. Church**. 2003. From annotated genomes to metabolic flux models and kinetic parameter fitting. OMICS. **7**:301-316.

93. **Shepherdson, M. and A. B. Pardee**. 1960. Production and crystallization of aspartate transcarbamylase. J.Biol.Chem. **235**:3233-3237.

94. **Sherratt, D. J.** 2003. Bacterial chromosome dynamics. Science **301**:780-785.

95. **Shimizu, T. S. and D. Bray**. 2002. Modelling the bacterial chemotaxis receptor complex. Novartis.Found.Symp. **247**:162-177.

96. **Thoden, J. B., H. M. Holden, G. Wesenberg, F. M. Raushel, and I. Rayment**. 1997. Structure of carbamoyl phosphate synthetase - a journey of 96 Angstrom from substrate to product. Biochemistry **36**:6305-6316.

97. **Trotta, P. P., M. E. Burt, R. H. Haschemeyer, and A. Meister**. 1971. Reversible dissociation of carbamyl phosphate synthetase into a regulated synthesis subunit and a subunit required for glutamine utilization. Proc.Natl.Acad.Sci.USA **68**:2599-2603.

98. **Turnbough, C. L., Jr., K. H. Kerr, W. R. Funderburg, J. P. Donahue, and F. E. Powell**. 1987. Nucleotide sequence and characterization of the *pyrF* operon of *Escherichia coli* K12. J.Biol.Chem. **262**:10239-10245.

99. **Vilar, J. M., C. C. Guet, and S. Leibler**. 2003. Modeling network dynamics: the *lac* operon, a case study. J.Cell.Biol. **161**:471-476.

100. **Wales, M. E., M. G. Mann-Dean, and J. R. Wild**. 1989. Characterization of pyrimidine metabolism in the cellular slime mold, *Dictyostelium discoideum*. Can.J.Microbiol. **35**:432-438.

101. **Wales, M. E. and J. R. Wild**. 1999. Aspartate Transcarbamoylase, p. 196-201. *In* T. E. Craighton (ed.), Encyclopedia of Molecular Biology. Wiley, New York.

102. **Wang, G. P., S. M. Cahill, X. Liu, M. E. Girvin, and C. Grubmeyer**. 1999. Motional dynamics of the catalytic loop in OMP synthase. Biochemistry **38**:284-295.

103. **Wang, G. P., C. Lundegaard, K. F. Jensen, and C. Grubmeyer**. 1999. Kinetic mechanism of OMP synthase: a slow physical step following group transfer limits catalytic rate. Biochemistry **38**:275-283.

104. **Wang, H., N. Glansdorff, and D. Charlier**. 1998. The arginine repressor of *Escherichia coli* K-12 makes direct contacts to minor and major groove determinants of the operators1. J.Mol.Biol. **277**:805-824.

105. **Washabaugh, M. W. and K. D. Collins**. 1984. Dihydroorotase from *Escherichia coli*. Purification and characterization. J.Biol.Chem. **259**:3293-3298.

106. **Washabaugh, M. W. and K. D. Collins**. 1986. Dihydroorotase from *Escherichia coli*. Sulfhydryl group-metal ion interactions. J.Biol.Chem. **261**:5920-5929.

107. **Weber, J., F. Hoffmann, and U. Rinas**. 2002. Metabolic adaptation of *Escherichia coli* during temperature-induced recombinant protein production: 2. Redirection of metabolic fluxes. Biotechnol.Bioeng. **80**:320-330.

108. **Wild, J. R., S. J. Loughrey, and T. C. Corder**. 1989. In the presence of CTP, UTP becomes an allosteric inhibitor of aspartate transcarbamoylase. Proc.Natl.Acad.Sci.USA **86**:52-56.

109. **Williams, L. G., S. A. Bernhardt, and R. H. Davis**. 1971. Evidence for two discrete carbamyl phosphate pools in *Neurospora*. J.Biol.Chem. **246**:973-978.

110. **Wilson, H. R., C. D. Archer, J. Liu, and C. L. Turnbough, Jr.** 1992. Translational control of *pyrC* expression mediated by nucleotide sensitive selection of transcriptional start sites in *Escherichia coli*. J.Bacteriol. **174**:514-524.

111. **Wilson, H. R., P. T. Chan, and C. L. Turnbough**. 1987. Nucleotide sequence and expression of the *pyrC* gene of *Escherichia coli* K-12. J.Bacteriol. **169**:3051-3058.

112. **Wilson, H. R. and C. L. Turnbough, Jr.** 1990. Role of the purine repressor in the regulation of pyrimidine gene expression in *Escherichia coli* K-12. J.Bacteriol. **172**:3208-3213.

113. **Wolfram Research, Inc**. Mathematica. [5.1]. 2004. Wolfram Research, Inc. Champaign, IL.

114. **Wolfram, S.** 2003. The Mathematica Book. Wolfram Media, Champaign, IL.

115. **Zalkin, H.** 1985. CTP synthetase. Methods Enzymol. **113**:282-287.

VITA

MAURICIO RODRIGUEZ RODRIGUEZ
2128 TAMU, Department of Biochemistry and Biophysics
College Station, TX 77845 – USA

Education

- PhD Biochemistry, August 2005

Texas A&M University, College Station, TX, USA

- BS Bacteriology, December 1995

Pontificia Universidad Javeriana, Bogotá D.C., COLOMBIA

Experience

- Graduate Research Assistant

1998 – 2005. Texas A&M University, College Station, TX, USA

- Visiting Scientist

1998 (Jan–May). Katholieke Universiteit Leuven, Leuven, Belgium

- Research Scientist

1995 – 1998. CORPOICA, Bogotá D.C., Colombia

- Visiting Scientist

1997 (October). CIAT, Cali, Colombia

- Lecturer

1996. Pontificia Universidad Javeriana, Bogotá D.C., Colombia

- Intern / Research Thesis Student

1995. Human Genetics Institute, Bogotá D.C., Colombia

Awards and Distinctions

- Fulbright Fellowship, 1998–2001
- UNESCO Fellowship in Biotechnology, 1998

Affiliations

- President and Founder, Colombian Aggie Network. Texas A&M University. 2004.
- President, Colombian Students Association, Texas A&M University. 2002-2003.
- Secretary, Fulbright Association, Texas A&M University. 1998-1999.
- Member, Fulbright Association.
- Member, Union Javeriana.
- Member, Society for Mathematical Biology
- Member, Society for Industrial and Applied Mathematics